We thank the Editor for assessing our manuscript with respect to the referees suggestions and answer her queries below.

*You have adequately addressed the similarity between the abstract and the conclusions and indeed, included a few sentences on future developments of TM5. However, I'd also be keen that you comment here on the STE findings in relation to the NH flux. How do you propose to investigate this further? What about plans to address the low bias in $O_3$ deposition. Equally, I don't think you fully addressed the reviewer's point of "What would be the way forward to further improve CTMs?", which requires a more general response than solely focussing on TM5. Given the moderate improvement as a result of increasing resolution and given the reviewer's question above on using 3 x 2 profiles as a priori in retrievals, I would also suggest that you include your response in the conclusions section, should other readers have similar thoughts.*

We now modify the text included at the end of the paper to include some aspects mentioned above.

"Future updates to TM5-MP will most likely focus on developing an online Secondary Organic Aerosol scheme, tropospheric halogen chemistry and incorporating an updated isoprene oxidation scheme involving more intermediate species. It will also be applied in the context of an Earth System Model (EC-EARTH) for allowing future studies concerning chemistry-climate feedbacks. When computing resources allow more expensive simulations can be performed using the applying 60 vertical levels as defined in the ERA-Interim meteorological dataset, approximately doubling the resolution of the simulations presented here. An additional update to improve the STE would be to apply the second-order moments scheme (Prather, 1986), whose application has been shown to capture the seasonality and magnitude of STE exchange to a better degree (Bönisch et al., 2008). In terms of oxidative capacity, one means of reducing the tropospheric near-surface $O_3$ mixing ratios would be improve loss to land-surfaces (Hardacre et al., 2010), although mixing ratios have been shown to be insensitive to the additional loss term to oceans, which is currently missing from many CTM's (Ganzeveld et al., 2009). Our comparisons of $CH_2O$ and $SO_2$ show that there is a significant uncertainty of chemical processes that affect distributions in the pristine marine environment. For instance, the physical process of deposition seems to be under-represented possibly due to too low surface area of the surface i.e. lack of a flat surface. The significant underestimates in $SO_2$ suggest missing biogenic sources terms, therefore more understanding of biogenic emission terms is necessary."

It is not our aim to provide a review of the all of the current issues surrounding CTM models. The diverse range of CTM's available in the community means that different models include different ways of accounting for chemistry and microphysics, therefore commonality between models is not so striking and subject to individual focus as to the potential importance of missing components. This provides a range in the performance skill, with different models exhibiting different biases. What we have therefore done is provide some ideas of how to improve CTM modelling based on our findings presented here.

*I have to agree with the reviewer here. Could I please ask that you include some sensitivity experiments, looking at the impact of reducing/increasing emissions by a fixed amount that represents the uncertainty in the emission inventories? Although you argue that including such experiments would turn the manuscript into a scientific paper rather than a description and validation paper, I believe that a key part of benchmarking a model is understanding the cause of the known biases. Such experiments would add to the current manuscript, would address a major concern by this reviewer, and are well within the scope of a GMD paper.*

As discussed previously by e-mail and in contact with the Lead Editor this step in not feasible because of funding restrictions, where the main body of the work was finished during Summer 2015. Sensitivity experiments are envisaged during future research projects where this version of TM5-MP will be applied.

*Although you argue here that the turbulent vertical transport scheme itself hasn't changed between the 3x2 version and the 1x1 version of TM5, its behaviour will potentially have changed due to the difference in resolution of the input fields. Therefore, could I please ask that you include a discussion on the differences, even if small, in the modelled turbulent vertical transport? In addition, you've added information on scaling the global annual lightning emissions totals between resolutions, differences in the global and vertical distributions of lightning NOx emissions are potentially important and would be worth including in the manuscript. Differences between Tiedtke and the mass flux simulations at 1x1 resolution would also be of relevance here.*

There is currently no way of sampling turbulent fluxes in TM5 and this would require a dedicated body of work for the extraction and analysis of these fields. However, a paper on tropospheric transport in TM5 has recently been published (Koffi et al., 2016), which allows the assessment of the performance of TM5 at $1° \times 1°$, with focus on the diurnal behavior of the boundary layer and vertical transport. We now reference this paper throughout our manuscript to provide more clarity. For lightning $NO_x$ we now include a global horizontal cross-section of Lightning $NO_x$ distributions for the month of July 2006 for the $3° \times 2°$, $1° \times 1°$ and $1° \times 1°$ (Tiedtke) simulations, so the reader can see both the changes in the regional distributions and the totals to the LiNOx emissions. We also include 1-D cross sections of the differences in LiNOx emissions due to changing the convective scheme in TM5 (c.f. new FigS1).

*I think the reviewer makes a very valid point here and some indication of how the meteorological fields themselves differ should be included in the manuscript (you've already included some of that information in your responses). It need not detract from the main focus of the paper, but would rather add to it.*

The performance of the transport in TM5 using both ERA-interim and Tiedtke convective mass-fluxes has recently been published by Koffi et al. (2016), which we now reference throughout the manuscript. There are no real strong conclusions as to which convective scheme performs the best when analysis [222]Rn distributions. We now include further comments regarding ground albedo and also now include an additional diagram related to the global distribution in cloud cover between $3° \times 2°$ and $1° \times 1°$ simulations. We then use it during the discussion of the impact of resolution on monthly-mean photolysis rates.

*I think you have partly addressed the reviewer's comments here. However, one aspect which you haven't addressed is "it is not sufficient to quantify the difference between the 3° x 2° and 1° x 1° versions only for the observation locations of the manuscript." In order to fully address this comment, could I please ask you to put the comparisons at the observation locations into a global context?*

We have now included diagrams of the lower tropospheric distribution of $O_3$, $NO_2$, $CH_2O$ and $SO_2$ for the month of May 2006, indicating the regional domains where the validation of each trace species takes place. This allows the reader to see the latitudinal variability in mixing ratios at global scale.

*Again, this comment partly relates to a comment by Reviewer 1 about placing the comparisons with observations within a global context. Could I please ask you to consider including global comparisons between the two resolutions and/or using MOPITT O3 or multi-model output (e.g. ACCENT, ACCMIP) as a somewhat independent global O3 dataset?*

We have now added two additional diagrams to allow the reader to compare the global distributions of $O_3$, $NO_2$, $CH_2O$ and $SO_2$ in the $3° \times 2°$ and $1° \times 1°$ TM5-MP simulations, where we also place the regional comparisons in context on a global scale. We also refer to these diagrams during the discussions of each of the trace gas species.

*Page 24, Table 3: Add units for emissions of CO, HCHO, CH₃OH and NOx to Table caption for completeness. Other species in the table whose emissions are NOT in units of TgC/year are DMS, SO₂ and NH₃. Again, can you add emissions units to Table caption? For example, it is currently unclear whether the SO2 emissions are in terms of S or SO2.*

We now put more details regarding the units used for listing the different emissions terms in the Table header.

*Page 9, Lines 334-340: Significant differences exist between Rn profiles simulated with the Tiedtke scheme and those simulated with the convective mass fluxes from ERA-Interim. Apart from saying there are differences, can you use the observations to conclude about which simulation compares better to the observations?*

This had been performed in the recent Koffi et al. (2016) paper, which we now reference throughout the manuscript. In summary, the study was rather inconclusive as to which of the convective schemes

performs better with respect to $^{222}$Rn distributions when compared against measurements in the European domain.

*Pg 10, Line 364: Can you change the word "residual" to use "ratio" instead (and be explict about what ratio it is i.e. 3x2/1x1 or vice versa) and add this explicitly to the captions for Figure S6a and S6b?*

Now corrected.

*Pg 10, Line 377: Correct the grammar in "Olszyna et al., 1994) and the also the efficiency of the NOx recycling terms"*

Now corrected.

*Page 25, Table 4: Can you be explicit about the percentage difference in the caption i.e.(ResolutionA-ResolutionB)/Resolution A, rather than referring to it as ResA/ResB?*

We now provide the formulation used for calculating the differences.

*Pg 16, Line 648-649: The sentence "At 1º x 1º significant improvements occur as a result of the better temporal resolution of the emission sources as a result of increasing horizontal resolution." doesn't make sense. Do you mean that the temporal variability of modelled SO2 has improved as a result of increasing horizontal resolution? Or do you mean that you've altered the time profile of the so2 emissions in 1x1?*

We have now re-written the sentence thus: "At 1º x 1º significant improvements occur in the correlations as a result of the better temporal distribution of anthropogenic emission sources."

1

We thank the Editor for assessing our manuscript with respect to the referees suggestions and answer her queries below.

*You have adequately addressed the similarity between the abstract and the conclusions and indeed, included a few sentences on future developments of TM5. However, I'd also be keen that you comment here on the STE findings in relation to the NH flux. How do you propose to investigate this further? What about plans to address the low bias in $O_3$ deposition. Equally, I don't think you fully addressed the reviewer's point of "What would be the way forward to further improve CTMs?", which requires a more general response than solely focussing on TM5. Given the moderate improvement as a result of increasing resolution and given the reviewer's question above on using 3 x 2 profiles as a priori in retrievals, I would also suggest that you include your response in the conclusions section, should other readers have similar thoughts.*

We now modify the text included at the end of the paper to include some aspects mentioned above.

"Future updates to TM5-MP will most likely focus on developing an online Secondary Organic Aerosol scheme, tropospheric halogen chemistry and incorporating an updated isoprene oxidation scheme involving more intermediate species. It will also be applied in the context of an Earth System Model (EC-EARTH) for allowing future studies concerning chemistry-climate feedbacks. When computing resources allow more expensive simulations can be performed using the applying 60 vertical levels as defined in the ERA-Interim meteorological dataset, approximately doubling the resolution of the simulations presented here. An additional update to improve the STE would be to apply the second-order moments scheme (Prather, 1986), whose application has been shown to capture the seasonality and magnitude of STE exchange to a better degree (Bönisch et al., 2008). In terms of oxidative capacity, one means of reducing the tropospheric near-surface $O_3$ mixing ratios would be improve loss to land-surfaces (Hardacre et al., 2010), although mixing ratios have been shown to be insensitive to the additional loss term to oceans, which is currently missing from many CTM's (Ganzeveld et al., 2009). Our comparisons of $CH_2O$ and $SO_2$ show that there is a significant uncertainty of chemical processes that affect distributions in the pristine marine environment. For instance, the physical process of deposition seems to be under-represented possibly due to too low surface area of the surface i.e. lack of a flat surface. The significant underestimates in $SO_2$ suggest missing biogenic sources terms, therefore more understanding of biogenic emission terms is necessary."

It is not our aim to provide a review of the all of the current issues surrounding CTM models. The diverse range of CTM's available in the community means that different models include different ways of accounting for chemistry and microphysics, therefore commonality between models is not so striking and subject to individual focus as to the potential importance of missing components. This provides a range in the performance skill, with different models exhibiting different biases. What we have therefore done is provide some ideas of how to improve CTM modelling based on our findings presented here.

36

*I have to agree with the reviewer here. Could I please ask that you include some sensitivity experiments, looking at the impact of reducing/increasing emissions by a fixed amount that represents the uncertainty in the emission inventories? Although you argue that including such experiments would turn the manuscript into a scientific paper rather than a description and validation paper, I believe that a key part of benchmarking a model is understanding the cause of the known biases. Such experiments would add to the current manuscript, would address a major concern by this reviewer, and are well within the scope of a GMD paper.*

43

As discussed previously by e-mail and in contact with the Lead Editor this step in not feasible because of funding restrictions, where the main body of the work was finished during Summer 2015. Sensitivity experiments are envisaged during future research projects where this version of TM5-MP will be applied.

47

*Although you argue here that the turbulent vertical transport scheme itself hasn't changed between the 3x2 version and the 1x1 version of TM5, its behaviour will potentially have changed due to the difference in resolution of the input fields. Therefore, could I please ask that you include a discussion on the differences, even if small, in the modelled turbulent vertical transport? In addition, you've added information on scaling the global annual lightning emissions totals between resolutions, differences in the global and vertical distributions of lightning NOx emissions are potentially important and would be worth including in the manuscript. Differences between Tiedtke and the mass flux simulations at 1x1 resolution would also be of relevance here.*

56

There is currently no way of sampling turbulent fluxes in TM5 and this would require a dedicated body of work for the extraction and analysis of these fields. However, a paper on tropospheric transport in TM5 has recently been published (Koffi et al., 2016), which allows the assessment of the performance of TM5 at $1 \times 1$, with focus on the diurnal behavior of the boundary layer and vertical transport. We now reference this paper throughout our manuscript to provide more clarity. For lightning $NO_x$ we now include a global horizontal cross-section of Lightning $NO_x$ distributions for the month of July 2006 for the $3 \times 2$, $1 \times 1$ and $1 \times 1$ (Tiedtke) simulations, so the reader can see both the changes in the regional distributions and the totals to the LiNOx emissions. We also include 1-D cross sections of the differences in LiNOx emissions due to changing the convective scheme in TM5 (c.f. new FigS1).

66

*I think the reviewer makes a very valid point here and some indication of how the meteorological fields themselves differ should be included in the manuscript (you've already included some of that information in your responses). It need not detract from the main focus of the paper, but would rather add to it.*

The performance of the transport in TM5 using both ERA-interim and Tiedtke convective mass-fluxes has recently been published by Koffi et al. (2016), which we now reference throughout the manuscript. There are no real strong conclusions as to which convective scheme performs the best when analysis $^{222}$Rn distributions. We now include further comments regarding ground albedo and also now include an additional diagram related to the global distribution in cloud cover between 3 x 2 and 1 x 1 simulations. We then use it during the discussion of the impact of resolution on monthly-mean photolysis rates.

*I think you have partly addressed the reviewer's comments here. However, one aspect which you haven't addressed is "it is not sufficient to quantify the difference between the 3° x 2° and 1° x 1° versions only for the observation locations of the manuscript." In order to fully address this comment, could I please ask you to put the comparisons at the observation locations into a global context?*

We have now included diagrams of the lower tropospheric distribution of $O_3$, $NO_2$, $CH_2O$ and $SO_2$ for the month of May 2006, indicating the regional domains where the validation of each trace species takes place. This allows the reader to see the latitudinal variability in mixing ratios at global scale.

*Again, this comment partly relates to a comment by Reviewer 1 about placing the comparisons with observations within a global context. Could I please ask you to consider including global comparisons between the two resolutions and/or using MOPITT O3 or multi-model output (e.g. ACCENT, ACCMIP) as a somewhat independent global O3 dataset?*

We have now added two additional diagrams to allow the reader to compare the global distributions of $O_3$, $NO_2$, $CH_2O$ and $SO_2$ in the 3° x 2° and 1° x 1° TM5-MP simulations, where we also place the regional comparisons in context on a global scale. We also refer to these diagrams during the discussions of each of the trace gas species.

*Page 24, Table 3: Add units for emissions of CO, HCHO, $CH_3OH$ and NOx to Table caption for completeness. Other species in the table whose emissions are NOT in units of TgC/year are DMS, $SO_2$ and $NH_3$. Again, can you add emissions units to Table caption? For example, it is currently unclear whether the SO2 emissions are in terms of S or SO2.*

We now put more details regarding the units used for listing the different emissions terms in the Table header.

*Page 9, Lines 334-340: Significant differences exist between Rn profiles simulated with the Tiedtke scheme and those simulated with the convective mass fluxes from ERA-Interim. Apart from saying there are differences, can you use the observations to conclude about which simulation compares better to the observations?*

This had been performed in the recent Koffi et al. (2016) paper, which we now reference throughout the manuscript. In summary, the study was rather inconclusive as to which of the convective schemes performs better with respect to $^{222}$Rn distributions when compared against measurements in the European domain.

103 *Pg 10, Line 364: Can you change the word "residual" to use "ratio" instead (and be explict about what ratio it*
104 *is i.e. 3x2/1x1 or vice versa) and add this explicitly to the captions for Figure S6a and S6b?*

105 Now corrected.

106 *Pg 10, Line 377: Correct the grammar in "Olszyna et al., 1994) and the also the efficiency of the NOx*
107 *recycling terms"*

108 Now corrected.

109 *Page 25, Table 4: Can you be explicit about the percentage difference in the caption i.e.(ResolutionA-*
110 *ResolutionB)/Resolution A, rather than referring to it as ResA/ResB?*

111 We now provide the formulation used for calculating the differences.

112 *Pg 16, Line 648-649: The sentence "At 1° x 1° significant improvements occur as a result of the better temporal*
113 *resolution of the emission sources as a result of increasing horizontal resolution." doesn't make sense. Do you*
114 *mean that the temporal variability of modelled SO2 has improved as a result of increasing horizontal*
115 *resolution? Or do you mean that you've altered the time profile of the so2 emissions in 1x1?*

116 We have now re-written the sentence thus: "At 1° x 1° significant improvements occur in the correlations as a
117 result of the better temporal distribution of anthropogenic emission sources."

118

119

**The high-resolution version of TM5-MP for optimised satellite retrievals: Description and Validation.**

**J. E. Williams**[1], **K. F. Boersma**[1,2], **P. Le Sager**[1], **W. W. Verstraeten**[1,2,*]

[1] {KNMI, De Bilt, The Netherlands}
[2] {Meteorology and Air Quality Group, Wageningen University, Wageningen, The Netherlands}
[*] now at: KMI, Ukkel, Brussels, Belgium

**Abstract**

We provide a comprehensive description of the high-resolution version of the TM5-MP global Chemistry-Transport Model, which is to be employed for deriving highly resolved vertical profiles of nitrogen dioxide ($NO_2$), formaldehyde ($CH_2O$), and sulphur dioxide ($SO_2$) for use in satellite retrievals from platforms such as the Ozone Monitoring Instrument (OMI) and the Sentinel-5 Precursor, the TROPOspheric Monitoring Instrument (tropOMI). Comparing simulations conducted at horizontal resolutions of 3º x 2º and 1º x 1º reveals differences of $\pm20\%$ exist in the global seasonal distribution of $^{222}Rn$, being larger near specific coastal locations and tropical oceans. For tropospheric ozone ($O_3$), analysis of the chemical budget terms shows that the impact on globally integrated photolysis rates is rather low, in spite of the higher spatial variability of meteorological data fields from ERA-Interim at $1° \times 1°$. Surface concentrations of $O_3$ in high-$NO_x$ regions decrease between 5-10% at $1° \times 1°$ due to a reduction in $NO_x$ recycling terms and an increase in the associated titration term of $O_3$ by NO. At $1° \times 1°$, the net global stratosphere-troposphere exchange of $O_3$ decreases by ~7%, with an associated shift in the hemispheric gradient. By comparing NO, $NO_2$, $HNO_3$ and PAN profiles against measurement composites, we show that TM5-MP captures the vertical distribution of $NO_x$ and long-lived $NO_x$ reservoirs at background locations, again with modest changes at $1° \times 1°$. Comparing monthly mean distributions in lightning NOx we show that applying ERA-interim convective mass fluxes We show that surface mixing ratios in both NO and $NO_2$ are generally underestimated in both low and high $NO_x$ scenarios. For Europe, a negative bias exists for [NO] at the surface across the whole domain, with lower biases at $1° \times 1°$ at only ~20% of sites. For $NO_2$, biases are more variable, with lower (higher) biases at $1° \times 1°$ occurring at ~35% (~20%) of sites, with the remainder showing little change. For $CH_2O$, the impact of higher resolution on the chemical budget terms is rather modest, with changes less than 5%. The simulated vertical distribution of $CH_2O$ agrees reasonably well with measurements in pristine locations, although column-integrated values are generally underestimated relative to satellite measurements in polluted regions. For $SO_2$, the performance at $1° \times 1°$ is principally governed by the quality of the emission inventory, with limited improvements in the site specific biases with most showing no significant improvement. For the vertical column, improvements near strong source regions occur which reduce the biases in the integrated column.

## 1.    Introduction

One application of Chemistry Transport Models (CTM) is to provide accurate vertical and horizontal global distributions of trace gases such as ozone ($O_3$), nitrogen dioxide ($NO_2$), sulphur dioxide ($SO_2$) and formaldehyde ($CH_2O$) that are used as *a-priori* best-guesses in the retrievals of tropospheric abundances from instruments mounted on Earth-orbiting satellites such as the Tropospheric Emission Sounder (TES; Worden et al., 2007) Global Ozone Monitoring Experiment (GOME), SCanning Imaging Absorption spectroMeter for Atmospheric CHartographY (SCIAMACHY; De Smedt et al., 2008), the Ozone Monitoring Instrument (OMI; Boersma et al., 2011), and GOME-2 (Valks et al., 2011). To date, although high-resolution regional models have been employed for selected regions such as the US and Europe (e.g. Russell et al., 2011; Zhou et al., 2012; Vinken et al., 2014), at the global scale the CTMs resolutions employed are still rather coarse (between 1.1-4.0º latitude and 1.1-6º longitude), resulting in 'footprints' which aggregate hundreds of kilometers in area. This has limitations as the resulting total columns are sensitive to topography, surface albedo and the shape of the *a-priori* vertical profiles themselves. Using rather coarse resolution leads to substantial errors in the retrievals (e.g. Boersma et al., 2007; Heckel et al., 2011; Russell et al., 2011) and imposes limitations towards capturing the regional scale variability in short-lived trace gas abundances observed from high-resolution satellite instruments such as OMI.

This lack of spatial detail is particularly relevant for situations where strong spatio-temporal variability in the vertical distribution of $NO_2$, $SO_2$, and $CH_2O$ can be expected. Examples include shipping lanes in the relatively unpolluted marine boundary layer (e.g. Vinken et al., 2014) and coal-fired power plant $SO_2$ pollution (e.g. Fioletov et al., 2015). Moreover, during the day the local lifetime and mixing ratios of trace gases such as nitric oxide (NO) and $NO_2$ are critically dependent on a host of variables e.g. temperature, surface albedo, cloud cover (via photolysis), chemical conversion (i.e. $NO/NO_2$ ratio) and the extent of mixing by convective upwelling (i.e. land type) and advective transport. Thus, the information provided for the retrievals is affected by the coarsening of the high-resolution meteorological data used to drive the CTM. Recently, Heckel et al. (2011) demonstrated that there is an associated uncertainty of ~2 using a-priori data from a global CTM rather than a regional CTM, principally due to loss of spatial information. Two other studies focusing on the impact of horizontal resolution on the retrieval of vertical column densities of $NO_2$ suggested that errors of up to ~50% exist (Yamaji et al., 2014; Lin et al., 2014). This problem becomes accentuated for the next generation of Earth-orbiting satellites such as the Tropospheric Monitoring Instrument (tropOMI), which has a smaller footprint compared to its predecessors (Veefkind et al., 2012). Applications of TM5 include the retrieval of $NO_2$, $CH_2O$, and $SO_2$ column densities from OMI and tropOMI (e.g. van Geffen et al., 2016), where studies related to the influence of horizontal resolution have been limited principally to $NO_2$.

The dominant tropospheric loss terms for $CH_2O$ are photolysis and scavenging into cloud droplets (wet deposition; Jacob, 2000). Thus the atmospheric lifetime of $CH_2O$ is highly sensitive to the extent of cloud cover and the vertical profiles of the photolysis rates. A dominant application of $CH_2O$ retrievals is to provide constraints on tropical and sub-tropical isoprene emission fluxes (e.g. Palmer et al., 2006; Stavrakou et al., 2009; Marais et al., 2012). The resulting emission estimates are highly sensitive to the stoichiometric yield of $CH_2O$ from isoprene oxidation, the chemical lifetime of $CH_2O$ and spatial differences in land cover. Other applications include estimating emissions released during Biomass Burning (BB) episodes (Gonzi et al., 2011),

whose spatial location is also smeared via coarsening in TM5-MP. For $SO_2$, which predominantly originates from point sources, an adequate spatial distribution of such sources is crucial for estimating accurate biases in existing emission inventories.

In this paper we provide a comprehensive description of the global, high-resolution 1º x 1º version of the TM5 CTM tailored for the application of satellite retrievals (hereafter referred to as TM5-MP). In Sect. 2 we give details related to the modifications which have been made to the TM5 model compared to previous versions, the emission inventories employed, updates that have been made to the modified CB05 chemical mechanism, the stratospheric boundary conditions, the photolysis scheme, the heterogeneous conversion and the overall model structure. In Sect. 3 we analyse the impact on convective and advective transport of trace species from the BL of both increased horizontal resolution and use of ERA-interim convective mass-fluxes, as derived using radon ($^{222}$Rn) distributions. In Sect. 4 we investigate the effects on regional and global photolysis frequencies and in Sect. In Sects. 5-9 we examine the differences introduced for both in the vertical and horizontal distributions of tropospheric $O_3$, $NO_x$ and, Lightning induced $NO_x$, N-containing species (i.e. nitric acid (HNO3), peroxy-acetyl-nitrate (PAN) and lumped organic nitrates (ORGNTR)) at higher resolution)), $CH_2O$ and $SO_2$, where we make comparisons against both surface and aircraft measurements to investigate effects. In Sect. 6 we examine impact on the global $CH_2O$ budget and integrated columns, and validate mixing ratios. Finally, in Sect. 7 we show the subsequent improvement in the distribution of $SO_2$ at 1º x 1º. In Sect. 810, we present our conclusions.

## 2   Description of TM5-MP

Previous versions of TM5 (TM5-chem-v3.0, Huijnen et al., 2010) included a two-way nested zooming option as described by Krol et al. (2005). This option allowed high-resolution simulations to be performed over any pre-defined regional domain, with boundary conditions being determined by the global simulation at coarser resolution. Typically, global simulations at 3º x 2º with zoom regions at 1º x 1º were performed to alleviate the long runtime of a global 1º x 1º run. In the new version of TM5 (hereafter referred to as TM5-MP; the massively parallel version), the usage of Message Parsing Interface (MPI) has been totally rewritten. Zoom regions are no longer available, but data sets are distributed along longitudes and latitudes, instead of model levels and tracers. The advantages of that overhaul towards domain decomposition are a smaller memory requirement and the possibility to use more processors making global 1º x 1º simulations feasible in terms of runtime and affordable in terms of computing resources. A TM5-MP global 3º x 2º (1º x 1º) run is ~6 (~ 20) times faster than the previous version of TM5 (Huijnen et al., 2010) for similar resources. The following model description pertains to both 3º x 2º and 1º x 1º simulations discussed in this manuscript.

Here we provide a comprehensive description of the modifications and updates introduced into TM5-MP compared to TM5 v3.0 (Huijnen et al., 2010). The model is driven using the ERA-interim meteorological re-analysis (Dee et al., 2011) and updated every 3 hours, with interpolation of fields for the intermediate time periods. Although TM5-MP can adopt all 60 vertical levels provided by the ECMWF ERA-Interim reanalysis, we employ 34 vertical levels for this study with higher resolution in the troposphere and Upper Troposphere-Lower Stratosphere (UTLS). Convective mass-fluxes and detrainment rates are taken from ERA-interim

236  dataset to describe the updraft velocities from the Boundary Layer (BL) into the free troposphere, which
237  replaces the parameterization of Tiedtke (1989) used in previous versions. The vertical diffusion in the free
238  troposphere is calculated according to Louis (1979), and in the BL by the approach of Holtslag and Boville
239  (1993). Diurnal variability in the BL height is determined using the parameterization of Vogelezang and
240  Holtslag (1996). We use the first-order moments scheme with an iterative time-step to prevent too much mass
241  being transported out of any particular grid-cell during the time-step according to the preservation of the
242  Courant-Friedrichs-Lewy (CFL) criterium (Bregman et al., 2003), which is especially relevant when reducing
243  the size of grid-cells as done here.

244  The gas-phase chemistry in TM5-MP is described by an expanded version of the modified CB05 chemical
245  mechanism (hereafter mCB05; Williams et al., 2013). We have placed emphasis on updating and expanding
246  the fast $NO_x$ chemistry to account for an accurate partitioning of nitrogen for higher $NO_x$ regimes than those
247  occurring at coarser horizontal resolutions. All reaction rate data is now taken from the latest IUPAC
248  recommendations (sited at http://iupac.pole-ether.fr/; last access June 2016) using updated formulations for
249  third-body collisions, where the rate data for fast $NO_x$ and $CH_2O$ chemistry is given in Table 1. This includes
250  the recent update to the formation rate of $HNO_3$ determined by Möllner et al. (2010). The most relevant
251  modifications are: (i) The yield of $CH_2O$, methanol ($CH_3OH$) and the hydro-peroxy radical ($HO_2$) from the
252  self-termination of the methyl-peroxy radical ($CH_3O_2$) is increased according to Yarwood et al. (2005), (ii) the
253  direct formation of $CH_2O$ from the reaction of $CH_3O_2 + HO_2$ is added using the temperature dependent
254  branching ratio defined in Atkinson et al. (2004), (iii) the production of $HNO_3$ during the oxidation of di-
255  methyl sulphide (DMS) by the $NO_3$ is now included, (iv) explicit organic peroxy radicals have been introduced
256  as products from the oxidation of propene ($C_3H_6$) and propane ($C_3H_8$) by OH, which are lost by either the
257  reaction with nitric oxide (NO) or $HO_2$ allowing the in-situ chemical formation of acetone ($CH_3COCH_3$) and
258  higher aldehydes (ALD2), respectively, following the stoichiometry given in Emmons et al. (2010), (v) a
259  second product channel for $N_2O_5$ photolysis is added producing NO, (vi) the formation and photo-dissociation
260  of HONO has been included, (vi) the formation and transport of methyl peroxy nitrate ($CH_3O_2NO_2$) is also
261  included (Browne et al., 2011), and (vii) modifications to the gas-phase chemistry involving $NH_3$ have been
262  introduced following the stoichiometry given in Hauglestaine et al. (2014). This version of the modified CB05
263  chemical mechanism is hereafter referred to as mCB05v2.

264  The calculation of height resolved photolysis rates ($J$ values) is performed using a tailored version of the
265  Modified Band Approach (MBA). The implementation and performance of this parameterization in TM5 has
266  been fully described in Williams et al. (2012). For the calculation of the height-resolved actinic fluxes at the
267  seven specific wavelengths used for calculating the $J$ values (these being 205.1nm, 287.9nm, 302.0nm,
268  311.0nm, 326.5nm, 385.0nm and 610.0nm), the 2-stream radiative transfer solver of Zdunkowski et al. (1980)
269  is embedded into TM5-MP. Details regarding the parameterizations used to account for the scattering and
270  absorption introduced by gaseous molecules, aerosols and clouds the reader is referred to Williams et al.
271  (2012). For aerosols, the climatology of Shettle and Fenn (1979) is included. The calculation of the effective
272  radius ($r_{eff}$) of cloud droplets is now performed using the approach of Martin et al. (1994), where different
273  parameter values are used for over the land and ocean using cloud condensation nuclei concentrations of 40
274  and 900, respectively. Due to potentially erroneous values at low horizontal resolution, we weight the final $r_{eff}$
275  value using the land fraction in each grid-cell. We apply limits between 4-16um on the resulting $r_{eff}$ values.

276    This improves the representation of the scattering component due to cloud droplets used for the calculation of

277    the actinic flux in the lower troposphere (LT; not shown). For the scattering effects from cloud droplets, we

278    subsequently downsize the physical $r_{eff}$ by ~0.5-2µm to account for the relationship between the optical and

279    physical $r_{eff}$ values.

280    For aerosols, an aerosol scheme is available for use within TM5-MP (aan den Brugh et al., 2010), but we

281    choose not to use it for the purpose of satellite retrievals due to the extra computational expense needed when

282    performing high resolution simulations that would potentially hinder operational use. We acknowledge that the

283    description of aerosols in this study is rather crude and increasing scattering could have an impact under

284    instances of low cloud coverage. For the application of TM5-MP towards satellite retrieval, it is preferable to

285    use any advancements in computational performance on further increases in the horizontal resolution

286    employed. Therefore it is not currently envisaged that a full description of aerosol processes will be included

287    during operational satellite retrievals.

288    However, heterogeneous conversion processes still need the description of the total reactive Surface Area

289    Density (SAD) from aerosols. In TM5-MP this is assumed as the cumulative value of contributions from

290    sulphate, nitrate, ammonium and methane sulphonic acid as calculated by the EQuilibrium Simplified Aerosol

291    Model (EQSAM) approach (Metzer et al., 2002), thus the secondary organic aerosol component is not

292    included. The distribution of these aerosol species is calculated online and coupled to the respective gaseous

293    precursors. The density of each aerosol type (1.7 g/cm$^3$) and $r_{eff}$ (of between 0.18-0.2µm) is prescribed as in

294    Huijnen et al. (2014). Swelling at higher relative humidities (> 70%) is crudely accounted for by increasing $r_{eff}$

295    between 0.25-0.27µm. The contributions due to sea-salt, black carbon and organic carbon towards

296    heterogeneous loss are not accounted for. Temperature dependent gas-phase diffusion co-efficients ($D_g$) are

297    used in the derivation of the pseudo first-order heterogeneous rate constants based on the theory of Schwartz

298    (1986).

299    For $N_2O_5$, the uptake coefficient (γ) is calculated using the parameterization of Evans and Jacob (2005),

300    therefore dependent on both temperature and relative humidity. Once a surface reaction with $H_2O$ occurs two

301    molecules of $HNO_3$ are formed. No uptake on cirrus particles is included for $HNO_3$, which can lead to de-

302    nitrification of the upper troposphere (Lawrence and Crutzen, 1998; von Kuhlmann and Lawrence, 2006). For

303    $HO_2$ we adopt a fixed $\gamma_{HO2}$= 0.06 across all aerosol types as taken from Abbatt et al. (2012) and for $NO_3$ we

304    adopt a fixed $\gamma_{NO3} = 10^{-3}$ as recommended by Jacob (2000). For $HO_2$, heterogeneous conversion forms 0.5

305    molecules of Hydrogen Peroxide ($H_2O_2$), whereas for $NO_3$ it forms one molecule of $HNO_3$ is formed,

306    following Emmons et al. (2010). For the SAD associated with cloud droplets we use the $r_{eff}$ values that are

307    calculated by Martin et al. (1994) thus maintaining consistency between the size of the cloud droplets used for

308    the scattering component in the calculation of $J$ values and heterogeneous loss rates on the clouds. By using the

309    ECMWF cloud fraction for each respective grid-cell, we assume that instantaneous mixing throughout the grid-

310    cell does not occur in order to avoid exaggerated conversion rates on cloud surfaces.

311    As TM5-MP contains no explicit stratospheric chemistry, we apply constraints above the tropopause to ensure

312    realistic Stratosphere-Troposphere Exchange (STE) of $O_3$ and for constraining the incoming radiation reaching

313    the troposphere needed for the MBA (Williams et al., 2012). For stratospheric $O_3$, we use total column values

314    derived from the assimilation of satellite observations as provided in the improved version of the Multi-Sensor

Re-analysis (MSR, van der A., 2010), which is vertically distributed according to the climatology of Fortuin and Kelder (1998). Three distinct zonal bands are used for nudging the stratospheric $O_3$ fields, these being 30 S-30 N, 30-66 S/N and > 66 S/N, where nudging occurs at pressure levels <45hPa, <95hPa and <120hPa, with relaxation times of 2.5 days, 3 days and 4 days, respectively.

For stratospheric $CH_4$ we use the monthly 2D climatological fields provided by Grooß and Russell (2005), with the nudging heights and relaxation times being identical to those used for stratospheric $O_3$. For stratospheric CO and $HNO_3$ we constrain mixing ratios by using monthly mean ratios of $CO/O_3$ (Dupuy et al., 2004) and $HNO_3/O_3$ (Jégou et al., 2008; Urban et al., 2009) based on the latitudinal climatologies derived from ODIN observations using data for 2003/2004 (CO) and 2001-2009 ($HNO_3$). In order to avoid jumps in the nudging constraints between months, we gradually change between ratios using the total monthly difference/number of days in the month. These ratios are applied using the monthly mean stratospheric $O_3$ distribution in TM5-MP, which is constrained by the MSR dataset (van der A et al., 2010). For both species, model fields are nudged at 5.5hPa, 10hPa and 28hPa using relaxation times of 5, 10 and 60 days, respectively. Previous versions of TM5 used a $HNO_3$ climatology from the UARS MLS instrument and applied nudging constraints at 10hPa only (Huijnen et al., 2010).

For our study ~~concerned with~~on the impact of horizontal resolution on the performance of TM5-MP, we present ~~12 month~~ simulations for the year 2006, which has been used for previous benchmarking studies (Huijnen et al., 2010; Williams et al., 2012). We use a one year spin-up from the same initial conditions, where the initial conditions are representative of the state-of-the-atmosphere for January 2005 taken from a previous simulation (see Zeng et al., 2015). The model is run using 34 levels, as it will be used operationally for satellite retrievals, where details of the pressure levels being given in Huijnen et al., 2010.

## 2.2 Emission inventories

All emission inventories applied in TM5-MP are yearly specific meaning that the year-to-year variability in emission fluxes due to changes in anthropogenic activity, biogenic activity and burning extent are taken into account. For the anthropogenic emission of $NO_x$, CO, $SO_2$, $NH_3$ and Non-Methane Volatile Organic Compounds (NMVOC), we adopt the MACCity emission estimates described in Granier et al. (2011). The lack of sector-specific information complicates the use of daily cycles for e.g. ~~the road transport component.~~the road transport component, where a bi-sinusoidal distribution could be applied peaking in the morning and late afternoon to represent variability in traffic volume. Aircraft emissions are included only for NO, using a homogenous hourly flux estimate not related to regional flight times. For volcanic $SO_2$ emissions, the estimated emission flux has been scaled up to 10 Tg S $yr^{-1}$ based on Halmer et al. (2002). For the biogenic component, where available we use the CLM-MEGANv2.1 emission inventories produced for the Southern Hemispheric Multi-model Intercomparison Project (SHMIP) as described in Zeng et al. (2015), with the missing trace species (e.g. ethane, propane, higher organics) coming from alternative MEGAN simulations as outlined in Sindelarova et al. (2014). A diurnal cycle is imposed on the isoprene emissions and introduced into the first ~50m between 20ºS-20ºN~~.~~, whereas for other latitudes a continuous daily flux is applied. The BB emissions are taken from the monthly estimates provided by the GFEDv3 inventory (van der Werf et al., 2010)

and latitude dependent injection heights and a tropical burning cycle are implemented following Huijnen et al. (2010). All emission inventories are provided on a 0.5º x 0.5º resolution and subsequently coarsened onto the horizontal resolution employed in any simulation. ~~For lightning NO$_x$ we use the parameterization which uses convective precipitation fields (Meijer et al., 2001) and constrain the annual global emission term at ~6 Tg N yr$^{-1}$. This uses the convective flux values meaning that re-scaling of the nudging term was necessary in order to achieve similar total lightning NO$_x$ across simulations.~~ In TM5-MP all NO$_x$ emissions are introduced as NO, rather than speciating a fraction ~~which is~~ emitted directly as NO$_2$ (Carslaw and Beevers, 2005). Global NO$_x$ emissions for the year 2006 total 49 Tg N yr$^{-1}$ (including lightning). Other notable species include CO (1081 Tg CO yr$^{-1}$), SO$_2$ (117 Tg S yr$^{-1}$), CH$_2$O (13.5 Tg C yr$^{-1}$) and isoprene (510 Tg C yr$^{-1}$). An overview of the global and zonal emissions terms used in the simulations analysed here are given in Table 3.

For lightning NO$_x$ we use the parameterization which uses convective precipitation fields (Meijer et al., 2001) and constrain the annual global emission term at ~6 Tg N yr$^{-1}$. This uses the convective flux values meaning that re-scaling of the nudging term was necessary in order to achieve similar total lightning NO$_x$ emissions across simulations. An example of the resulting horizontal distributions in lightning NO$_x$ at ~400hPa for the tropics for both horizontal resolutions is shown in the top panel of Fig. S1a in the supplementary material. Although the spatial variability increases at 1º x 1º, the global distribution remains essentially the same, where the constraints on annual lightning NO$_x$ emissions homogenize the total emission flux between resolutions. One other factor affecting the vertical distribution of lightning NO$_x$ emissions is the convective parameterization which is used. The lower panels of Fig. S1a show that, at this altitude, the Tiedke (1989) approach increases the NO$_x$ emissions at this level by ~14%, accompanied by a significant re-distribution between regions (c.f. SH below 30ºS and an significant increase in the tropical component in the Tiedke simulation). However this is altitude dependent, where the absolute differences in the vertical distribution in the monthly NO$_x$ emissions for a selection of latitudes are shown in Fig. S1b. Here comparisons are shown both over the continents (e.g. 50.5ºN) and the oceans (e.g. 59.5ºS). Although the differences in the integrated monthly global emission NO$_x$ flux is only around ~1-2%, the temporal and vertical distribution can be quite different between convective schemes. Profiles show that in the upper troposphere ERA-interim consistently results in higher NO$_x$ emissions around 300hPa, especially for July.

Latitudinal constraints on CH$_4$ global distributions are applied using the methodology given in Banda et al. (2015) with a 3-day relaxation time. We also introduce similar constraints based on the appropriate surface measurements for H$_2$ in order to account for the latitudinal gradient and variability across seasons, which replaces the fixed global value of 550ppb used in previous versions. Finally, for Radon (Rn[222]) emissions we apply the estimates of Schery (2004), whose global distribution is given in Zhang et al. (2011).

**2.3 Observations**

Although the performance of mCB05 in TM5 v3.0 has been validated for selected NMVOC, O$_3$, CH$_2$O, CO and NOy in both hemispheres (Williams et al., 2013; 2014; Fisher et al., 2015; Zeng et al., 2015), the significant changes made to both the chemical scheme and the rate parameters in mCB05v2 necessitate independent validation at both 3º x 2º and 1º x 1º. We choose a range of ground-based and airborne

393    measurements taken at diverse locations during the year 2006 representing different chemical regimes. Here

394    we briefly describe the observations utilised for this purpose.

395    For validation of simulated surface concentrations we use measurements of gaseous $O_3$, NO, $NO_2$, $HNO_3$ and

396    $SO_2$ available from the European Monitoring and Evaluation program (EMEP, www.emep.int), where we

397    exploit measurements taken at various background sites in Norway, Finland, The Netherlands, Belgium,

398    Poland, the Czech republic, Germany, Great Britain, Spain, Slovakia, Italy and Portugal. The number of sites

399    used for comparisons of trace species other than $O_3$ is smaller due to data availability.  For the model

400    composites we extract data from 3 hourly instantaneous output in order to assemble both the weekly and

401    monthly mean values from the simulations. For the weekly comparisons of $NO_2$ and $SO_2$ we use values

402    extracted at 13:00 local time, close to the overpass time of the OMI instrument (e.g. Boersma et al, 2008). The

403    selected stations allow validation of the seasonality for both rural regions (FI37) and urban regions (NL09),

404    where we include identical stations where possible for both species. For $HNO_3$ we assemble the weekly values

405    from the daily averages.

406    Measured [$O_3$] in the EMEP network are obtained using UV monitors (Aas et al. 2001). For all species, spatial

407    interpolation of model data is performed accounting for the height of the measurement station and by

408    weighting using the distance of the station from the surrounding grid-cells. The wide range of measurement

409    sites chosen ensures that both background and polluted cases are assessed.

410    For validating the vertical distribution of relevant trace species such as $O_3$, $SO_2$ and $CH_2O$, we use

411    measurements by the DC-8 aircraft during the Intercontinental Chemical Transport Experiment B (INTEX-B;

412    Singh et al., 2009) that took place between March and May 2006. Observations of a host of co-located

413    nitrogen-containing species are available (namely NO, $NO_2$, PAN and $HNO_3$). These flights were conducted

414    over a wide region, and we use all three months of measurements.  Each month sampled a different region

415    representing different meteorological conditions and local emission sources, namely: the Gulf of Mexico (90-

416    100ºW, 15-30ºN), the remote Pacific (176-140ºW, 20-45ºN) and to the south and west of Alaska over the

417    ocean (160-135ºW, 20-60ºN). Measurements cover altitudes up to 10.5km, and we bin the values with respect

418    to pressure using 50 hPa bins or less in the LT. We interpolated three-hourly output against measurements for

419    each respective day, similar to the comparisons performed in previous evaluations of TM5 (e.g. Huijnen et al.,

420    2010), but we segregate our comparisons into the three distinct regions. For details relating to the location of

421    each flight the reader is referred to the campaign overview of Singh et al. (2009).

422    For tropospheric $O_3$, we supplement the INTEX-B comparisons with measurements taken over more polluted

423    regions as part of the Measurement of Ozone, water vapour, carbon monoxide and nitrogen oxides by Airbus

424    In-service aircraft initiative (MOZAIC; Thouret et al., 1998). We aggregate the measurements as seasonal

425    means for December-January-February (DJF) and June-July-August (JJA) in order to provide a robust number

426    of samples for each location. Here we choose to use profiles representative of the Northern mid-latitudes,

427    namely: London (0.2ºW, 51.2ºN), Vienna (16.5ºE, 48.1ºN), Washington (77.5ºW, 38.9ºN), Portland (122.6ºW,

428    45.6ºN), Shanghai (121.8ºE, 31.2ºN) and Tokyo (140.4ºE, 35.8ºN).

429    We also make comparisons of $O_3$, NO, $NO_2$, selected N-reservoir species, $SO_2$ and $CH_2O$ profiles using

430    measurements made aboard the NOAA WP-3D aircraft as part of the Second Texas Air Quality Study

431    (TexAQS II; Parrish et al, 2009), which was conducted over the Texas sea-board during September and

432    October 2006. This allows the assessment of TM5-MP over a region with higher NMVOC emissions and

industrial activity. These measurements were typically sampled at altitudes below 500hPa, therefore no measurements in the UTLS are available from this campaign.

**3 The Effect on Atmospheric Transport**

Here we analyse the differences in convective transport out of the BL by analysing the vertical and horizontal distribution of $^{222}$Rn, which is a diagnostic typically used for assessing the differences in transport in CTMs (e.g. Jacob et al., 1997). $^{222}$Rn is emitted at a steady rate and exhibits a half-life of ~3.8 days, which is long enough to be transported from the BL into the FT due to chemical passivity, with loss via wet scavenging and dry deposition being negligible. Therefore, it acts as an ideal tracer to assess differences in convective transport from the surface out of the BL. The representation of BL dynamics for TM5-MP has recently been assessed at 1º x 1º using $^{222}$Rn distributions for both the Tiedtke (1989) scheme and when adopting convective mass transport values from the ERA-Interim meteorological data (Koffi et al, 2016).

Figure 1 shows seasonal mean horizontal global distributions of $^{222}$Rn for DJF and JJA in the 1º x 1º simulation averaged between 800 and 900hPa (i.e. sampling the LT). Also shown are the associated percentage differences against the re-binned 3º x 2º $^{222}$Rn distribution, allowing a direct comparison. Resolution dependent differences result from the cumulative effects of the use of higher resolution mass-fluxes from the ERA-interim meteorological data for describing convective activity and the more accurate temporal distribution of regional $^{222}$Rn emissions at 1º x 1º. In general it can be seen that seasonal differences of ±20% exist, typically with increases over continents and decreases over oceans in the 1º x 1º simulations. ~~Maximal~~Maximum differences of >60% occur near selected coastal regions (California, West Africa, Madagascar) or in outflow regions such as off South America and Africa, where differences exhibit a strong seasonal dependency. This is due to the large differences in convective strength due to the variability in heating rates, and thus temperatures, between land and ocean (e.g. Sutton et al., 2007).

A comparison of the ratio of the monthly mean $^{222}$Rn profiles (1º x 1º /3º x 2º) extracted above selected European cities for January (black) and July (blue) 2006 are shown in Fig. ~~S1~~S3 in the Supplementary Material. The typical tropospheric profile of $^{222}$Rn exhibits an exponential decay from the LT to the FT (not shown). In order to homogenise the emission flux in the comparison, we coarsen the 1º x 1º data onto the 3º x 2º grid by averaging the six individual values into a representative mean column. The extent of the changes in the vertical distribution of $^{222}$Rn is somewhat site specific meaning an in depth analysis is beyond the scope of this paper. In summary, the 1º x 1º simulation generally provides stronger convective activity for January, with the main impact occurring below ~~700hpa~~700hPa (e.g. London and Paris). The changes in $^{222}$Rn in the LT range between 2 and 10% (i.e. ratios of 0.9 to 1.1), implying both weaker and stronger convective transport depending on changes in location (e.g. orography and land type). ~~In that the~~The impact at Berlin is larger than ~~at~~ e.g. Barcelona ~~also~~which shows that, surprisingly, the inclusion of a large ocean fraction (with weaker convective mixing) in the 3º x 2º cell does not seem to introduce dominating effects. Recently Koffi et al. (2016) have shown that comparisons of $^{222}$Rn at coastal sites in Europe at 1º x 1º exhibit significant discrepancies compared to more continental stations. For July the changes in the vertical distribution extend into the FT up to 500hPa, although changes in the upper FT have a significant component due to changes in long-range transport. The magnitude of the changes are similar to those exhibited during January, although

473   maybe of the opposite sign (e.g. Rome). Thus the influence on e.g. $NO_2$, $CH_2O$ and $SO_2$ *a-priori* vertical

474   profiles will be non-negligible and diverse.

475   For the tropical cities located in regions where convective mixing is stronger, the corresponding differences

476   between resolutions can reach ± 20%, especially near the surface (e.g. Caracas and Karachi). There is a site-

477   specific seasonal dependency in the magnitude of the changes related to the regional land characteristics (e.g.

478   Lagos versus Kuala Lumpar).) and the extent of ocean within any particular grid-cell. Thus, differences in *a-*

479   *priori* vertical profiles of trace gases forusing a resolution of 1° x 1° can be considerable compared to those

480   provided at a 3° x 2° resolution.

481   We also show comparisonsratios of profiles from 1° x 1° simulations using the convective scheme of

482   TiedkeTiedtke (1989) against those using the convective mass-fluxes from the ERA-interim meteorological

483   dataset for Europe (Fig. S3S4), defined as ERA(1° x 1°)/Tiedtke (1° x 1°). For this comparison no daily

484   averaging is employed with $^{222}Rn$ profiles extracted from 3 hourly instantaneous sampling, with the profiles

485   shown being interpolated directly above urban conurbations (with high trace gas emissions). The

486   residualsratios, which are defined as show that the significant differences exist, with the convective mass-

487   fluxes from ERA-interim being somewhat weaker than those calculated online using TiedkeTiedtke (1989)

488   (i.e) the ratio is typically less than 1, especially during July. In the recent study by Koffi et al. (2016)

489   performed at 1° x 1° for the European domain, there was no appreciable improvement in the correlation co-

490   efficients when distributions of $^{222}Rn$ were compared against measurements resulting in no strong conclusion

491   towards which of the parameterizations results in better atmospheric transport.

492

493   **4 The Impact on tropospheric photolysis frequencies**

494

495   The changes in the spatio-temporal distribution of cloud cover and surface albedo have the potential to alter the

496   penetration depth and upwelling of photolysing light, and thus photochemical production and destruction

497   terms. tropospheric clouds and surface albedo have the potential to alter the incident flux of photolysing light

498   reaching the surface, and thus photochemical production and destruction terms. When present, clouds dominate

499   the integrated optical density in the tropospheric column. TM5-MP uses a random overlap method for

500   determining the impact of clouds on actinic flux, which is weighted by cloud cover (Williams et al., 2012).

501   Comparing seasonal mean cloud coverage for DJF and JJA (Fig. S5), we show that there are significant

502   increases in the fractional cloud cover (*fcc*) at 1° x 1° resulting in *fcc* values ranging between 0.1-0.8 (c.f. 0.1-

503   0.5 for 3° x 2°). Moreover, the definition of tropical equatorial cloud systems becomes much more defined and

504   there are significant differences in the cloud distributions around the west coast of Southern America. For DJF,

505   the largest changes occur at high latitudes over the tundra and oceans, but correspond with low intensity

506   incident radiation due to the polar winter. For the SH, the seasonal *fcc* increases significantly, which will

507   potentially impose effects on Antarctic oxidative capacity (see Sect. 5). For JJA, most increases in *fcc* do not

508   occur directly above high $NO_x$ sources but rather over the oceans. This limits the impact on the lifetime of

509   chemical pre-cursors (e.g. $NO_2$) as discussed in Sect. 6. Examining similar plots for surface albedo (not shown)

510   reveals that maximum differences (increases at 1° x 1°) again occur in the polar regions under low temperatures

511   related to sea-ice and snow coverage typically during polar winters. For mid-latitudes and tropics, although

512   differences in the absolute albedo value can be significant (±50%) values are typically below 0.1, which will

contribute to the perturbations in the final J value tropospheric profiles as discussed below. The monthly mean comparisons in surface J values provided in Fig. S4 show that any differences in instantaneous cloud cover are moderated to the order of a few percent when looking at longer periods.

The similarity in the monthly mean photolysis frequencies for $O_3$ and $NO_2$ across resolutions (hereafter denoted $J_{O3}$ and $J_{NO2}$, respectively) are shown in Fig. S4S6 of the Supplementary Material. Comparisons of the monthly mean $J_{O3}$ and $J_{NO2}$ values are shown at five different locations identical to those shown in Williams et al. (2012). For $J_{O3}$ the impact of increasing resolution is limited to a few percent in the monthly mean values. At, even for regions which have high surface albedo. At the global scale this leads to a reduction of ~2% in the total mass of $O_3$ photolysed (not shown). For $J_{NO2}$, the corresponding differences become more appreciable, with 1º x 1º exhibiting ~5-10% higher values at high Northern latitudes (associated with locations with high-$NO_x$ regimes). Focusing on $J_{NO2}$ and comparing seasonal mean values near the surface shows that very similar large-scale spatial patterns occur for both simulations at the global scale (c.f. Fig. S7). The highest $J_{NO2}$ values occur over the tropical oceans and high altitude regions (e.g. Nepal), with a latitudinal shift related to seasonal changes in daylight hours. Although more regional fine-structure can be seen at 1º x 1º (e.g. the high-$NO_x$ scenario). South-Western US and South-West China for DJF), these seasonal averages show that the small perturbations in $J_{NO2}$ shown in Fig. S6 extend to the global scale, leading to only modest changes in the tropospheric lifetime of $NO_2$ (see Sect. 6).

Focusing on $J_{NO2}$ and comparing seasonal mean values near the surface shows that very similar spatial patterns occur for both simulations at global scale (c.f. Fig. S5). The highest $J_{NO2}$ values occur over the tropical oceans and high altitude regions (e.g. Nepal). Although more regional fine-structure can be seen at 1º x 1º (e.g. South-Western US for DJF), these seasonal averages show that the small perturbations shown in Fig. S3 extend to the global scale leading to a reduction of ~5% at 1º x 1º.

Comparisons of monthly mean vertical profiles of $J_{O3}$ and $J_{NO2}$ extractedas sampled over the location of selected tropical cities are shown in the Figs. S6aS8a and b, respectively, in the Supplementary Material. Here no averaging is performed towards an identical horizontal resolution, therefore values are representative of the $J$ values directly above the selected urban centres. The $J_{O3}$ profiles are affected to a larger extent than the $J_{NO2}$ profiles, due to the characteristic absorption spectra of each species, which makes $J_{O3}$ more sensitive to the additional scattering introduced due to clouds. Profiles over Dubai act as a proxy for clear-sky conditions, where values of unity exist in the residual of $J_{O3}$ and $J_{NO2}$ calculated through most of the column. The small difference at the surface is due to changes in the surface albedo between resolutions, with Dubai being situated on the coast meaning that a sharp horizontal gradient exists in surface albedo. For other cities, the largest perturbations occur away from the surface (e.g. Jakarta, Nairobi and Lagos) around the altitude where tropospheric clouds are most abundant. There are typically changes of between ±5-10% in the monthly mean profiles. The changes in $J_{NO2}$ reflect those simulated for $J_{O3}$, with somewhat smaller perturbations.

**5 Implications for oxidative capacity and tropospheric $O_3$**

The partitioning of reactive N between the short- and long-lived chemical N-reservoirs included in TM5-MP depends on the oxidative capacity simulated for the troposphere via competition between the various different radicals (i.e. OH, $CH_3C(O)O_2$, $NO_3$ and $CH_3O_2$). Therefore, changes to the distribution and resident mixing

ratios of tropospheric $O_3$ subsequently impose changes ~~on~~in the fractional composition of the $NO_y$ budget (~~e.g.~~ Olszyna et al., 1994) and ~~the~~ also the efficiency of the $NO_x$ recycling terms by altering the chain length (Lelieveld et al., 2004). In this section we analyse the global and zonal chemical budget terms for tropospheric $O_3$ to highlight the inter-hemispheric differences which occur (i.e. under low and high-$NO_x$ environments). An overview of the resulting near-surface global distribution of tropospheric $O_3$ for May 2006 is shown in Figure 3, which also includes the location of the regional comparisons presented below in a larger global context. In general, the pattern of minimum and maximum mixing ratios in $O_3$ occur in similar locations, with the long-range transport component being more clearly defined in the 1° x 1° simulation. There is a distinct latitudinal gradient in $O_3$ mixing ratios imposed by the global distribution of $NO_x$ emissions.

Table 4 provides the zonally segregated chemical budget terms for tropospheric $O_3$, from which the global component due to STE can be determined by closing the budget terms following the methodology given in Stevenson et al. (2006). The chemical tropopause calculated for 3º x 2º is applied for the analysis of 1° x 1° budget terms to ensure that a valid comparison is performed, (i.e. the same mass of air is accounted for). For computational efficiency the budget terms are aggregated in 10º latitudinal bins for each vertical level and summed across all longitudes providing the cumulative latitudinal terms.

The most significant change with resolution concerns STE. By using a dedicated tagged stratospheric $O_3$ tracer (which only undergoes photo-chemical destruction and deposition in the troposphere; hereafter denoted as $O_3S$) changes in the zonal mean STE can be determined. The stratospheric burden of $O_3$ (~~$BO_3S$~~$BO_3$ (strat)) exhibits a strong hemispheric gradient with much more downwelling occurring in the NH peaking during boreal springtime. At the global scale the STE exchange is 579 Tg $O_3$ yr$^{-1}$, which agrees well with the multi-model mean for STE of 556±154 Tg $O_3$ yr$^{-1}$ in Stevenson et al. (2006), with observational estimates being ~550±140 Tg $O_3$ yr$^{-1}$ (Olsen et al., 2001). The ~7% reduction of STE at 1° x 1° is encouraging considering that previous studies using TM5 have concluded that STE in TM5 at 3º x 2º was biased high compared to STE inferred from TES and MLS satellite observations (Verstraeten et al. (2015)). The increase in STE in the SH, with an associated decrease in the NH (see below), implies that there is a shift in circulation patterns at 1° x 1° even though ~~$BO_3S$~~$BO_3$ (strat) remains essentially unchanged. Previous studies have shown that in order to resolve the correct spatial and temporal Stratosphere-Troposphere flux, high resolution is required both in the horizontal and the vertical gridding (e.g. Meloen et al., 2002). The NH STE diagnosed with TM5-MP is an order of magnitude smaller than estimates derived in a CTM study also conducted at a 1° x 1° resolution (Tang et al, 2011; ~200 Tg$O_3$ yr$^{-1}$), which identified deep convection as important for STE. Here we use a different vertical grid and meteorological dataset to drive TM5-MP, both of which affect the ability towards capturing an accurate STE flux (Meloen et al., 2002). For the 1° x 1° simulation using the Tiedtke scheme, there is a further reduction in the STE component of 21 Tg $O_3$ yr$^{-1}$, resulting in an STE component almost identical to the multi-model mean in Stevenson et al. (2006).

The zonal seasonal means of the fraction of $O_3S$ to $O_3$ ($O_3S/O_3$) for both simulations are shown in Fig. 2 for DJF and JJA. There is a clear seasonal zonal shift in the fractional contribution due to the $O_3$ transported downwards from the Stratosphere exhibiting a longer lifetime in the winter hemisphere reflecting a lower photochemical destruction rate. At 1° x 1° the largest increase in STE occurs in the Southern Hemisphere (SH) during JJA. Here ~20-25% of tropospheric $O_3$ is transported down from the Stratosphere. Comparing the 0.2 contour for the NH mid-troposphere shows significant changes, extending further down towards the surface

during boreal wintertime leading to the higher total mass of $O_3S$ in the troposphere. The extent of nudging towards the MSR climatology is essentially constant across simulations (c.f. Table 4). Interestingly, less $O_3S$ reaches the surface in the tropics at 1º x 1º due to the enhanced chemical destruction term in the Free Troposphere. Approximately 10% of the global deposition term for $O_3$ is associated with $O_3$ that originates from the Stratospheric at 1º x 1º (c.f. ~5% at 3º x 2º). For the NH, this contributes to the simulated increase in deposition of ~9%.

For tropospheric $O_3$ there are similarities that occur between the NH, tropics and SH (i.e.) high and low-$NO_x$ scenarios, resulting in a cumulative decrease in $O_3$ production of ~2-4% across zones. For the chemical loss terms there is a modest decrease of ~3% (~12%) in the NH (SH) reflective of the changes discussed for $J_{O3}$, which acts as the primary destruction term. Therefore, in the SH the significant differences shown for *fcc* do not significantly impose a lower photochemical destruction term on the annual tropospheric $O_3$ budget. There is a zonal gradient in the tropospheric burden of $O_3$ ($BO_3$) following the zonal gradient in $NO_x$ emissions. (c.f. Fig. 3). Comparing terms shows that $BO_3$ decreases at 1º x 1º by a few percent at the global scale (~7 Tg $O_3$) making a rather small impact on oxidative capacity. This is of the same order of magnitude as that found in previous studies concerned with horizontal resolution (e.g. Wild and Prather, 2006). Interestingly, changes in the deposition flux of $O_3$ are rather small, even though there is a larger amount of variability in the land surfaces and better-resolved land-sea contrast at 1º x 1º, although differences in regional deposition fluxes can be more significant. Multi-model inter-comparisons of surface deposition terms across models have shown previous versions of TM5 to be aat the low end of the model spread in terms of $O_3$ (Hardacre et al., 2015), suggesting that the surface deposition flux to e.g. should be increased by ~10% in TM5-MP towards the multi-model mean value. This can be partly attributed to the large uncertainty which exists related to the loss of $O_3$ to the ocean (Hardacre et al., 2015).

Figure 34 shows comparisons of simulated and observed mass mixing ratios of surface $O_3$ at EMEP sites across Europe ([www.emep.int](www.emep.int); Aas et al. 2001), with countriesstations chosen so to cover a range of latitudes. Previous comparisons using mCB05 have revealed high biases in surface $O_3$, especially during boreal summertime (Williams et al., 2013). These high biases originate from cumulative effects associated with the accuracy of the emission inventories, the convective and turbulent mixing component, the underestimation of the scattering and absorption of photolysing light due to aerosols and the chemical mechanism that is employed. For the emission component it should be noted that even at 1º x 1º coarsening is performed, where emission inventories are typically supplied at 0.5º x 0.5º resolution. The seasonal cycle in surface $O_3$ is captured to a large degree, and the high bias exhibited by the model is generally reduced by ~2-5 ppb (or ~20%) at 1º x 1º. This is associated with perturbations in the $NO_x$ recycling terms, chemical titration by NO, changes to the turbulent diffusion and convective mixing out of the BL. In that the improvement in biases is largest during boreal summertime is associated with the shorter chain length of the $NO_x$ recycling term during boreal wintertime (c.f. Fig 2). However, there is still a significant monthly mean bias in both simulations when compared against observations throughout the year, especially for locations impacted by a large anthropogenic $NO_x$ source. This is partly due to the low $NO/NO_2$ ratio as discussed in Sect. 46 below.

Comparing vertical profiles from composites assembled from the MOZAIC measurements for DJF and JJA (Figs. S7aS9a and S7bS8b, respectively), INTEX-B (Singh et al, 2009; Fig. S8S10) and TexAQS II (Parrish et al, 2009; Fig. S9) showsS11) show consistently that differences are small between simulations across regions,

and typically mimic those which occur at the surface. There is a general positive bias of ~20-40% in mixing ratios exhibited across all comparisons, although the variability in the vertical gradients across regions is ~~capture~~captured rather well. Such positive biases have consequences for both the $NO_x$ recycling terms and $HNO_3$ formation discussed in the sections below.


## ~~4~~6 Implications for the distribution of NO and $NO_2$

Table 5 provides the zonally segregated annual $NO_x$ recycling terms involving the main peroxy-radicals and the direct titration term involving NO for the 1º x 1º simulation. The conversion rate of NO back into $NO_2$ decreases by ~2-3% across zones as a consequence of an associated increase in the titration term and re-partitioning of N into long-lived reservoir species (see below). For the titration term involving NO, although the globally integrated flux remains relatively constant, there is contrasting behaviour for the two most important zones (TR, NH), which exhibit a lower and higher titration term, respectively. It has been shown that for regions such as Europe the increased titration results in lower surface $O_3$ mixing ratios (c.f. Fig. ~~3~~4), improving the boreal summertime high bias at the surface.

Important model uncertainties include the quality of the MACCity $NO_x$ emission inventory, the lifetime of $NO_2$ simulated in TM5 ~~and the recycling term via the chemical titration of O₃. Figures 4 and 5~~, BL mixing and the $NO_x$ recycling term via the chemical titration of $O_3$. Figure 3 provides an illustration of the global distribution in surface $NO_2$ during May 2006 for both the 3º x 2º and 1º x 1º simulations, where the short-lifetime means that the maximum mixing ratios occur directly near the strong source regions. Most $NO_x$ is anthropogenic in origin, therefore there is strong latitudinal gradient between the NH and SH, with ship-tracks also visible. The regions where validation occurs are also superimposed in the figure, including the extent of the EMEP domain over which $NO_2$ weekly comparisons are made. Figures 5 and 6 shows comparisons of weekly [NO] and [$NO_2$] surface measurements against the corresponding composites from both ~~of the~~ simulations, sampled at 13:00 local time which is close to the ~~time of~~local overpass time for both OMI and tropOMI. Although the number of EMEP sites conducting $NO_x$ measurements is smaller than those measuring $O_3$, we choose stations located throughout Europe in both high and low $NO_x$ regimes. To supplement these comparisons we provide the seasonal mean biases for DJF and JJA from both simulations in Tables 6 and 7, respectively, calculated using weekly binned data from all EMEP sites~~, which~~ that measure hourly [NO] and [$NO_2$~~] levels.~~]. Here we perform an analysis across sites rather than focusing on the behaviour at selected individual locations.

For the determination of [$NO_2$], the reduction of NO on a Molybdenum convertor takes place with subsequent detection by chemi-luminescense, with an associated detection limit of ~0.4ppb. Previous studies have shown that some bias can result due the oxidation of nitrogen reservoirs such as PAN (Dunlea et al., 2007; Steinbacher et al., 2007). In TM5-MP all $NO_x$ emissions are introduced as NO, although a fraction for road transport is known to be emitted directly as $NO_2$ (e.g. Carslaw and Beevers, 2005). Many studies have been performed comparing satellite $NO_2$ columns with model values, implying that inadequacies in emission inventories are somewhat region specific (e.g. Zyrichidou et al., 2015; Pope et al., 2015).

Table 6 shows a negative bias of a few $\mu$g m$^{-3}$ in TM5-MP in seasonal surface [NO] in Europe. This is a cumulative effect of the accuracy of the MACC $NO_x$ emission estimates, an overestimate in daytime vertical

673    mixing (Koffi et al., 2016) (enhanced dilution) and, to a lesser extent, too high surface [O$_3$]

674    (~~enhancing~~increasing the oxidation rate of NO to NO$_2$). As anthropogenic emissions are the principle source of

675    NO, there is no significant seasonal cycle in the monthly emission estimates in the NH. Seasonal differences in

676    convective mixing (i.e. lower BL heights) do cause somewhat higher surface [NO] during DJF~~, which for~~

677    ~~approximately equal emission terms. This is often~~ captured ~~in~~by TM5-MP~~.~~, although under night-time

678    conditions TM5-MP has been shown to overestimate nocturnal BL heights (Koffi et al., 2016). For ~80% of

679    the EMEP sites we do not observe any significant change in the quality of the comparisons. For ~20% of sites,

680    simulations of [NO] at 1° x 1° introduce significant improvements over those at 3° x 2° and there is an

681    improvement regarding the extent of seasonal variability (Fig. 4).

682    Table 7 shows that for [NO$_2$] the biases are more variable being typically in the range of ±0-6 µg m$^{-3}$, with both

683    positive and negative biases occurring across sites. Both the conversion efficiency from NO, loss to reservoir

684    compounds (e.g. HNO$_3$), photo-dissociation rate, convective mixing and emission estimates contribute to these

685    biases. The seasonal biases show improvements at 1° x 1° for ~35% of the EMEP sites, accompanied with

686    degradations at ~20% of the sites. The ~~maximal~~maximum biases in [NO$_2$] at 1° x 1° can be approximately

687    double those for [NO]. For the corresponding NO/NO$_2$ ratio, there will generally be an under prediction in the

688    model due to the negative biases shown for the [NO] comparisons. Analyzing the corresponding seasonal

689    correlation co-efficients (not shown) shows in ~25% of the cases there is little seasonal correlation between the

690    weekly [NO$_2$] in TM5-MP and the measurements regardless of resolution for both seasons (Pearson's *r* in the

691    range -0.3 to 0.3). In ~30% of cases there is actually a degradation in *r* between resolutions, the changes

692    somewhat reflect those seen in the seasonal biases i.e. simultaneous changes to both the meteorology and local

693    emission fluxes do not necessarily improve the performance of the model. Comparing 1° x 1° values both with

694    and without the Tiedtke convection scheme shows that for the most convective regions (e.g. south of 45°N)

695    increases in *r* generally occur during JJA when employing the ERA-interim mass-fluxes. Conversely for e.g.

696    Finland the correlation becomes worse.

697    Beyond Europe, we compared monthly mean TM5-MP vertical distributions of NO and NO$_2$ between March

698    and May 2006 against measurements taken during the INTEX-B campaign in Fig. ~~6~~7. In general differences

699    between 1° x 1° and 3° x 2° simulations are the order of a few percent, with NO$_2$ biased low in the LT by ~70-

700    80%. This is partially associated with the take-off and landing of the aircraft from polluted airfields, where

701    point sources of high anthropogenic emissions cannot be resolved ~~at 1° x 1°.~~even at 1° x 1°. For March, there is

702    a strong signature from biomass burning plumes in the middle troposphere which is not captured using the

703    monthly burning estimates. For the FT, TM5-MP captures the observed gradient to reasonable degree. In the

704    UT there is a consistent high bias for NO and an associated low bias for NO$_2$ suggesting that the conversion

705    term is too low and the NO$_x$ cycle is out of synch at these cold temperatures despite the addition of new

706    reservoir species (i.e. CH$_3$O$_2$NO$_2$~~).~~) and application of new rate data.

707    One important gauge as to whether the chemical mechanism can capture the correct recycling efficiency of NO

708    into NO$_2$ is to examine their ratio, which is presented in the third column of Fig. ~~6~~7. In the LT (< 900 hPa)

709    NO/NO$_2$ ratios of 0.1-0.2 exist ~~which TM5-MP represents~~that are captured quite well by TM5-MP, with

710    negligible differences between 3° x 2° and 1° x 1 ° simulations. For the FT, TM5-MP consistently overestimates

711    the ratio in spite of a high bias in O$_3$ (c.f. Fig. ~~3) suggesting an exaggerated photo-dissociation rate or low bias~~

712    ~~in HO$_2$.~~4) which is imposed by the overestimates in NO$_2$. This implies the chemical conversion is too slow and,

assuming representative $J_{NO2}$ values, indicates a low bias in HO$_2$ or an under-estimation in the mixing ratios of other long-lived and short-lived NOy compounds (see Sect. 7).

Finally in Fig. 78 we show the corresponding comparisons against measurements taken during the TexAQS II campaign (Parrish et al, 2009) for both September and October 2006. ThereAs for the EMEP comparisons shown in Figs. 5 and 6, there is a significant underestimation in NO and NO$_2$, mixing ratios, with both model profiles being outside the 1-σ variability in the observational mean of the measured mixing ratios.. This is clearly related to the emission estimates for this region being underestimated in the current emission inventories (e.g. Kim et al., 2011). For the resulting NO/NO$_2$ ratio, TM5-MP captures the correct ratio in the lowest few hundred meters of the BL, but overestimates the ratio at higher altitudes. In this case, the high NO and NO$_2$ mixing ratios at the top of the BL imply that TM5-MP under-represents the NO$_2$ fraction, regardless of the increased recycling term related to the titration of O$_3$ (c.f. Table 2). as for more pristine environments, although there is marked improvement in the ratios simulated for October.

## 57. Changes in the NOy budget

### 57.1 Long-lived reservoirs

The resolution dependent changes in the temporal distribution of [NO$_2$], and associated differences in NMVOC chemical pre-cursor emissions have the potential to alter the partitioning of reactive NO$_x$ between the three main chemical reservoirs included in mCB05v2 (i.e. HNO$_3$, PAN and ORGNTR). The differences in both the deposition efficiency and tropospheric lifetimes between trace species at 1° x 1° suggests that the fraction of NO$_x$ that can be transported out of source regions could change significantly. Here we briefly examine the zonally integrated nitrogen budget terms between simulations to quantify the effect of applying a higher spatial resolution. The seasonal distribution of these three dominant reservoir species at 1° x 1° and their individual contributions to total NOy are shown in Figures S10 to S13Figs. S12-S15 for DJF and JJA, respectively. Here we define NO$_y$ as the cumulative total of NO, NO$_2$, NO$_3$, HNO$_3$, PAN, CH$_3$O$_2$NO$_2$, HONO, 2*N$_2$O$_5$, lumped organic nitrates (ORGNTR) and HNO$_4$. It should be noted that methyl-nitrate is not in this version of TM5-MP. These figures are provided as reference for the reader to aid understanding of the discussion below.

Table S1 in the Supplementary Material provides a zonal decomposition of the tropospheric chemical budget terms for HNO$_3$, PAN and ORGNTR. For HNO$_3$, even though the recent kinetic rate parameters increase (decrease) the chemical production term at the surface (UTLS) compared to older rate data (e.g. Seltzer et al., 2015), changes in the integrated column term are small. The changes at 1° x 1° are somewhat latitude dependant (corresponding to low and high NO$_x$ regimes), with only small increases occurring in the NH and associated decreases in the tropics related to lower [OH] (i.e. chemical production). Loss by cumulative deposition terms only changes by a few percent, due to wet scavenging being so efficient for HNO$_3$ any associated change in the Surface Area Density (SAD) of cloud droplets introduced by changes in the liquid water product

For PAN, both the production and destruction terms decrease marginally by ~1-3% across all zones, meaning the transport of NO$_x$ out of the main source regions remains relatively robust. The total mass of N cycled through PAN is ~four times that of HNO$_3$,sequestrated as HNO$_3$, although the lifetime of PAN is shorter due

the efficient thermal decomposition. The changes in the production term due to temporal increases in $NO_2$ near high $NO_x$ source regions (c.f. Fig. ~~5~~3) are partially offset by a reduction in the mixing ratios of the acetyl-peroxy radical ($C_2O_3$ in Table 1) due to e.g. increased dry deposition of organic precursors at 1° x 1°. Although the chemical budget terms only exhibit small changes, it can be expected that the global distribution of PAN is somewhat different due the changes in the convective and advective mixing due to the application of higher resolution meteorological data~~.~~ (c.f. Sect. 3).

For ORGNTR, there is a 5% reduction in the annual production term at 1° x 1°, with an associated decrease in the loss by deposition. Both the largest production ~~term~~ and ~~decrease, thus,~~ destruction terms occur in the tropics related to the strongest source of ORGNTR being biogenic pre-cursors in mCB05v2. Thus at 1° x 1°, this intermediate trace species becomes less important as a $NO_x$ reservoir~~.~~.

Finally, the one additional intermediate not shown is $CH_3O_2NO_2$, which is ~~primary~~primarily a stable vehicle for transporting $NO_x$ from the surface up to the UTLS, where at cold temperatures it accounts for a significant fraction of $NO_2$ speciation along with $HNO_4$ (Browne et al., 2011). At the global scale three times as much nitrogen cycles through $CH_3O_2NO_2$ compared to PAN, although the thermal stability is low at temperatures > 255°K thus resident mixing ratios are typically small. This results in ~~maximal~~maximum mixing ratios occurring in the cold upper troposphere (up to ~0.2 ppb) and subsequently dissociates primarily by thermal decomposition (photolytic destruction accounting for <0.1% of all destruction). At 1° x 1° there is a few percent decrease in the chemical production term as a result of lower $CH_3O_2$ mixing ratios and more variability in the temporal temperature distribution.

Comparisons of weekly [$HNO_3$] at the surface in Europe are shown in ~~Figure 8~~Fig. 9 against measurements from the EMEP network. It has recently been determined that $HNO_3$ measurements are also sensitive to ambient night-time [$N_2O_5$], which could result in a positive bias in the observations (Phillips et al., 2013). In general, the modelled seasonal cycle is not evident in the measurements, which exhibit a rather homogeneous variation in mixing ratios throughout the year typically ~~leading to,~~ thus being somewhat decoupled from variability in photochemical activity. Comparisons show an underestimation in TM5-MP during March and an overestimation during JJA. No such seasonal pattern is observed for [$NO_2$] (c.f. Fig. ~~5~~6), thus seasonal [OH] variability due to variations in photo-chemical activity and [$H_2O_{(g)}$] ~~is a~~and/or an incorrect wash-out term which could both act as likely ~~cause~~causes. The impact of resolution on [$HNO_3$] is rather muted for most weeks resulting in no significant changes to the seasonal biases (not given), as constrained by the improvements in surface [$NO_2$] (c.f. Fig. ~~5~~6). The heterogeneous scavenging of $HNO_3$ into ammonium nitrate can act as a moderator toward gaseous $HNO_3$ ~~and, although.~~ Although this heterogeneous conversion process is included in TM5-MP~~, generally produces~~ as described by the EQSAM approach, low concentrations of e.g. ammonium nitrate (not shown~~).~~) typically result. Thus, gaseous [$HNO_3$] remains too high due to too little conversion into particles and subsequent deposition.

For other regions outside Europe, we make comparisons of vertical profiles of $HNO_3$ and PAN between March and ~~October~~September 2006 against those measured during INTEX-B (Figure ~~9~~10) and ~~Texas (Figure S14~~TexAQSII (Fig. S16). PAN is a good marker for transport in the free-troposphere due to the relatively long-lifetime at colder temperatures. For all regions the vertical gradients for both species are captured quite well, although some fine-structure is lost due to the vertical resolution of TM5-MP. ~~This implies that the underestimation in NO_2 (Fig. 6) in not due to lack of transport away from source regions and therefore should~~

be more attributed to local underestimations in emission fluxes and insufficient pre-cursor emissions. This implies that the underestimation in $NO_2$ simulated in the UTLS (Fig. 7) is not due to insufficient transport of $NO_2$ away from source regions, but rather should be attributed to either missing chemistry or insufficient transport down from the stratosphere. Finally, for more polluted regions, the vertical gradient of $HNO_3$ is rather less steep than that observed, with significant low biases in the lower troposphere related to the low bias in $NO_2$ shown in Fig. 8. The impact of the 1° x 1° resolution only results in a marginal improvement in the LT for $HNO_3$ (again similar to $NO_2$). For PAN the vertical profile in TM5-MP agrees remarkably well, although somewhat anti-correlated around 900hPa in both simulations and the rapid decrease in the lowest kilometre not being captured sufficiently. This overestimation would likely be larger if the emission estimates were increased as required to consolidate the $NO_2$ comparisons for the same campaign.

Finally, we present the corresponding comparisons for September 2006 for $HNO_3$ and PAN measured during the TexAQS II campaign (Parrish et al., 2009) as Figure S14 in the Supplementary Material. For $HNO_3$, although the vertical gradient is captured quite well, there is a significant low bias related to the low bias in $NO_2$ shown in Fig. 7, with the 1° x 1° showing a marginal improvement in the LT for $HNO_3$. For PAN the vertical profile in TM5-MP is somewhat anti-correlated around 900hPa in both simulations, with the rapid decrease at the surface not being captured by either simulation and the bias being larger for 1° x 1°.


5

## 7.2 Short-lived reservoirs

Here we briefly discuss the perturbations introduced for the short-lived N-reservoirs, namely HONO, $HNO_4$ and $N_2O_5$, where the chemical budget terms for all three species are provided in Table S2 in the Supplementary Material. For HONO it should be noted that many tropospheric CTMs have difficulty in simulating observed mixing ratios (e.g. Goncalves et al, 2012) suggesting missing (heterogeneous) source terms. The global production for HONO is an order of magnitude less than that for the other short-lived N-reservoirs. At 1° x 1° there is ~10% more chemical production of HONO in high $NO_x$ regions and no appreciable effect in the low $NO_x$ regions. Thus the impact of increased resolution on HONO production is rather small, which is surprising considering the higher NO mixing ratios that occur in high $NO_x$ regions (c.f. Fig 5). The muted response is due to competing oxidative processes, which effectively lower the OH available for forming HONO. For $HNO_4$, approximately the same mass of N cycles through this species as for PAN, although the shorter lifetime means that it is more important at regional scale. Again, the impact of resolution on this species is small, where decreases in $[HO_2]$ result in no significant net change in production for the NH. The most significant changes occur for the global production and heterogeneous conversion of $N_2O_5$, with enhanced chemical production of ~12% at the global scale, increasing the heterogeneous sink term by ~6%, although the changes in the total mass of N converted are small. In general, this is due to an increase in the production of the $NO_3$ radical by ~10% at 1° x 1° (not shown) resulting in enhanced $N_2O_5$ mixing ratios.

## 8 Implications for tropospheric $CH_2O$ retrieval

The implications of applying a higher resolution CTM for the global distribution of CH$_2$O are rather modest. Fig. S17 shows the near-surface global distributions of CH$_2$O for May 2006, where maximum mixing ratios occur near forested regions due to the link with isoprene oxidation (e.g. Palmer et al., 2006). The tropospheric lifetime of CH$_2$O is of the order of a few days, meaning that transport merges differences between simulations apart from in low emission areas. Also shown are the locations where regional validation occurs. In Table 8, we show zonally integrated chemical production and destruction terms for CH$_2$O, which suggests changes of the order of a few percent at the global scale. The most notable difference is the increase in the cumulative deposition term of ~4% at 1º x 1º, thus reducing the atmospheric lifetime of CH$_2$O in TM5-MP. Again, this low impact shows that the increase in the temporal variability of the meteorological data at 1º x 1º, and thus the local variability of cloud SAD, only changes the net deposition term by a few percent. Even though the temporal distribution of the surface mixing ratios shows more variability at 1º x 1º due to the better representation of regional pre-cursor sources terms (e.g.) isoprene and terpene, only moderate improvements occur to the simulated profiles and total columns due to changes in transport. For instance, when analysing individual production terms (not given) for the tropics, decreases are related to small changes in the dominating chemical source terms (e.g. oxidation of CH$_3$OOH; a reduction of ~3-5 Tg CH$_2$O yr$^{-1}$). For the chemical destruction term, the relative insensitivity of the photolysis of CH$_2$O towards resolution (similar to J$_{O3}$; c.f. Fig S4) results in small net decreases in line with changes in the chemical production term.

Figure ~~10~~11 compares monthly mean tropospheric profiles of CH$_2$O measured during INTEX-B (Singh et al., 2009) with those from both TM5-MP simulations for March to May 2006. In general, there is a fair representation of the vertical gradient of CH$_2$O by TM5-MP for all months shown, although surface mixing ratios are typically too high suggesting loss by deposition to the ocean is underestimated (potentially related to underestimations in surface area due to lack of 3D wave structure) or that the chemical production term is too efficient. Moreover, there appears to be a missing (chemical) source term in the UTLS in TM5-MP leading to a ~ 30-50% (~0.05 ppb) low bias above 600hPa, ~~therefore~~i.e. there is no significant improvement to the underestimation in the SH CH$_2$O column in TM5-MP ~~occurs~~when compared to ~~previous versions~~mCB05 (Zeng et al, 2015~~)~~.). Comparing profiles shows that the changes in the vertical distribution of CH$_2$O at 1º x 1º are minimal in the chemical background compared to 3º x 2º, with the main differences originating from more efficient transport out of source regions (c.f. March). These findings are further confirmed by the comparisons of TM5-MP against TexAQS II measurements for September and October 2006 (~~Figure S15).~~Fig. S18).

**~~7~~9 Implications for tropospheric SO$_2$ retrieval**

The global distribution of near-surface SO$_2$ mixing ratios for both the 3º x 2º and 1º x 1º simulations are shown in the bottom panels of Fig. S17, where the distribution shows the land-based point sources as applied from the MACCity emission inventory. The high mixing ratios of SO$_2$ correlate with the location of strong anthropogenic emission sources due to the relatively short atmospheric lifetime of SO$_2$ (varying between ~2 days during winter and ~19 hours during summer (Lee et al, 2011)), being rapidly oxidized to sulphate (SO$_4^=$). Although the regional distributions are similar, the 1º x 1º simulation is able to differentiate point sources to a much better degree, which enhances the ability of deriving more accurate emission fluxes. The *in-situ* chemical

872 production term of $SO_2$ from the oxidation of oceanic di-methyl sulphide (DMS) is low thus there are very low

873 $SO_2$ mixing ratios in the chemical background. Also shown are the regions used for validating the $SO_2$ surface

874 concentrations and vertical profiles (insets in FigS17; see below).

875 In Figure ~~11~~12, we compare weekly [$SO_2$] for 2006 at a number of EMEP sites in Austria (AT02, forested),

876 The Netherlands (NL09, rural), Great Britain (GB43, rural) and Spain (ES10, rural), with most sites being

877 positioned away from strong point sources. For $SO_2$ in Europe, the main emission source is anthropogenic (e.g.

878 ~~from the energy sector) and subsequently oxidised to sulphate predominantly in the aqueous phase, with the~~

879 ~~tropospheric lifetime varying between ~2 days during winter and ~19 hours during summer (Lee et al,~~

880 ~~2011).~~from the energy sector). High [$SO_2$] has been observed throughout the EMEP network in e.g. The

881 Netherlands and Spain, which is significantly higher than that measured in Central Europe (Tørseth et al.,

882 2012). Although the measurement uncertainty is somewhat site specific due to the different

883 ~~methodology~~methodologies employed, it is typically around ~1.3 ug/m$^3$ (e.g. Hamad et al., 2010). Comparing

884 weekly averages shows that for most sites shown there is a significant low bias at 3° x 2°, indicating

885 inaccuracies in the MACC emission inventory and the effect of coarsening to the model resolution. At 1° x 1°

886 significant improvements occur in the correlations as a result of the better temporal ~~resolution~~distribution of

887 ~~the~~anthropogenic emission sources ~~as a result of increasing horizontal resolution~~.

888 Table 9 provides an overview of the seasonal biases for all of the EMEP sites that measure hourly [$SO_2$], with

889 the biases calculated for the overpass time of tropOMI aggregated on a weekly basis. Improvements occur at 1°

890 x 1° for ~20% of the sites during both seasons, with the majority (~50%) of sites showing no significant

891 improvement (< 5%). In such instances the local [$SO_2$] is determined more by long-range transport (thus

892 sensitive to wash-out) rather than a local emission source, where strong mitigation practises have been

893 implemented in Europe over the last few decades reducing resident [$SO_2$] significantly (Tørseth et al., 2012).

894 For some sites there is a notable increase in biases at 1° x 1° (20% DJF, 25% JJA) indicating that too strong

895 local emission sources occur in the MACC inventories (e.g. ES13 and GR01). For others (e.g. ES08 and NL07)

896 significantly low biases occur suggesting the opposite problem.

897 Finally, for the vertical profiles, we make comparisons against monthly mean composites assembled from

898 measurements taken during INTEX-B (Fig. ~~S14~~S19) and TexAQS II (Fig. ~~12~~13) as for the other trace gas

899 species. For the more pristine locations there are typically low biases at 3° x 2° for all months, especially at the

900 surface during March indicating a significant underestimation in the emission fluxes of $SO_2$. Increasing to 1° x

901 1° only provides an improved correlation for March, due to the transport in the FT being described better as

902 shown for $NO_2$ in Fig. ~~6~~7. For April, the comparison shows a significant underestimation in the column for

903 both simulations, where corresponding comparisons of the vertical profiles of ~~di-methyl sulphide~~DMS, which

904 acts as a key source of $SO_2$ in the Equatorial Pacific (Alonza Gray et al., 2011), ~~also show significant low~~

905 ~~biases~~agree quite well (not shown). This points to an appreciable biogenic source term that is currently missing

906 from the inventories as proposed for organic nitrates (Williams et al., 2014). For May again no significant

907 improvement occurs at 1° x 1°, although both simulations capture the peak in $SO_2$ mixing ratios at the top of

908 the BL. More relevant for satellite based retrievals is the observed column near strong anthropogenic source

909 regions as shown in Fig. 13 over Texas during September ~~~~and October 2006. Here a clear improvement occurs

910 at 1° x 1°, with the low bias in the BL being reduced significantly although the integrated column is still too

low. Again this is due to the underestimation in the source emission fluxes in the anthropogenic emission inventory employed.

## ~~8~~10 Conclusions

In this paper we have provided a comprehensive description of the high-resolution 1° x 1° version of TM5, which is to be used for the purpose of providing *a-priori* columns for the satellite retrieval of trace gas columns of $NO_2$, $CH_2O$ and $SO_2$. By performing identical simulations at a horizontal resolution of 3° x 2° and 1° x 1°, and comparing the resulting global distributions of trace gas species, photolysis frequencies and chemical budget terms, we quantify and validate both the near-surface and vertical distributions for the evaluation year of 2006.

Comparing the seasonal distribution in $^{222}$Rn between resolutions we show ~~that~~ differences in the vertical distribution of up to ±20% ~~exist~~ at the global scale, with significantly larger ~~differences~~impacts for specific coastal regions and tropical oceans. In order to assess the changes in convective activity above strong $NO_x$ sources, we show that differences of between ~2-10% (~10-20%) exist for the Northern mid-latitudes (tropics) at higher resolution, with both weaker and stronger upwelling occurring depending on the region and the season. ~~The differences are site specific being somewhat affected by local orography.~~The magnitude of the changes are site specific being affected by local orography. We have also made comparisons using a 1° x 1° simulation applying the Tiedtke (1989) convection scheme, showing that ERA-interim mass-fluxes result in less transport of $^{222}$Rn out of the boundary layer, where it has been shown that the use of ERA-interim mass-fluxes introduces inconclusive improvements in surface $^{222}$Rn distributions (Koffi et al., 2016). ~~The~~Although the impact of resolution on daily photolysis rates maybe appreciable, analysing global monthly mean $J_{O3}$ and $J_{NO2}$ surface values over a range of conditions ~~is~~shows that effects are limited to ~2% and ~5-10%, respectively. ~~This is surprising considering the larger variability~~One contributing factor to this rather muted impact is that the changes in ~~cloud cover and~~surface albedo that ~~occurs~~occur at 1° x 1°~~.~~ are largest at the poles during winter, which has no impact on photo-chemistry due to the absence of photolysing light (not shown). For cloud cover, a dominant term for determining total optical depth, there are significant increases at 1° x 1° are over the oceans, although generally related to instances of low photochemical activity. Examining the resulting changes in $J_{O3}$ and $J_{NO2}$ which occur throughout the tropospheric column reveals that significant differences of >10% can occur at the top of the BL at tropical locations. Such modest changes associated with this dominant loss term result in the change in the integrated chemical budget terms for tropospheric $O_3$ and $NO_2$ to be rather low.

Analysing the chemical budget terms for tropospheric $O_3$ shows (i) a reduction in the stratosphere-troposphere exchange flux of ~7% to 597 Tg $O_3$ yr$^{-1}$, (ii) a repartitioning of the contribution from stratospheric ~~downwelling~~down-welling in both the Northern and Southern hemispheres, (iii) no significant change in the tropospheric burden of $O_3$ and (iv) modest changes in the integrated chemical production and destruction terms. Comparing simulated mixing ratios against surface measurements in Europe shows that the positive bias present in TM5 decreases by ~20% at 1° x 1° between 2-5 ppb/month. This positive bias persists throughout the vertical column across diverse global regions regardless of the local $NO_x$ emissions, although the vertical gradient in tropospheric $O_3$ through the tropospheric column is captured quite well.

For NO and NO$_2$ increasing horizontal resolution results in only modest differences in the zonal mean recycling terms and the loss of O$_3$ by chemical titration. Comparisons against surface measurements in Europe shows that there is a consistent negative bias in weekly [NO] of a few µg m$^{-3}$ associated with both too high surface O$_3$ (enhanced NO titration) and the inaccuracy of the NO$_x$ emission inventories. For NO$_2$, the biases in the weekly concentrations are larger and can be both positive and negative. Increasing horizontal resolution has little effect on reducing the NO biases, but results in improvements for NO$_2$ at ~35% of the available sites, with ~45% of sites showing limited changes. Examining correlation co-efficients shows that although there is typically a higher correlation at 1° x 1°, many sites still exhibit very low correlation or anti-correlation for some seasons. For the tropospheric column the improvement in the comparisons is only by a few percent, with a significant underestimation in both NO and NO$_2$ throughout the tropospheric column. Analysing the NO/NO$_2$ ratio and comparing against observations shows that although partitioning is captured in the BL there is a significant overestimation in the upper troposphere.

Finally for CH$_2$O and SO$_2$, which can also be retrieved from satellite measurements, the effect of increased resolution is rather modest due to compensating changes towards the chemical budget terms. When compared against observations there is a persistent low bias for tropospheric CH$_2$O due to missing production terms especially on the Free Troposphere. For SO$_2$ comparison with surface observations in Europe shows lower biases at 20% of sites due to more accurate local emission fluxes, whereas for the majority of cases (~50%) there is no significant change. Comparing vertical profiles shows a significant underestimation in the tropospheric column likely associated with either missing precursors or an underestimation in the direct emission terms.

Future updates will most likely focus on developing an online Secondary Organic Aerosol scheme, tropospheric halogen chemistry and incorporating an updated isoprene oxidation scheme, which will be built using TM5-MP as the core.

Future updates to TM5-MP will most likely focus on developing an online Secondary Organic Aerosol scheme, tropospheric halogen chemistry and incorporating an updated isoprene oxidation scheme involving more intermediate species. It will also be applied in the context of an Earth System Model (EC-EARTH) for allowing future studies concerning chemistry-climate feedbacks. When computing resources allow more expensive simulations can be performed using the applying 60 vertical levels as defined in the ERA-Interim meteorological dataset, approximately doubling the resolution of the simulations presented here. An additional update to improve the STE would be to apply the second-order moments scheme (Prather, 1986), whose application has been shown to capture the seasonality and magnitude of STE exchange to a better degree (Bönisch et al., 2008). In terms of oxidative capacity, one means of reducing the tropospheric near-surface O$_3$ mixing ratios would be improve loss to land-surfaces (Hardacre et al., 2010), although mixing ratios have been shown to be insensitive to the additional loss term to oceans, which is currently missing from many CTM's (Ganzeveld et al., 2009). Our comparisons of CH$_2$O and SO$_2$ show that there is a significant uncertainty of chemical processes that affect distributions in the pristine marine environment. For instance, the physical process of deposition seems to be under-represented possibly due to too low surface area of the surface i.e. lack of a flat surface. The significant underestimates in SO$_2$ suggest missing biogenic sources terms, therefore more understanding of biogenic emission terms is necessary.

**Code Availability**

The TM5-MP code can be downloaded from the SVN server hosted at KNMI, The Netherlands. A request to generate a new user account for access can be made by e-mailing sager@knmi.nl. Any new user groups need to agree to the protocol set out for use, where it is expected that any developments are accessible to all users after publication of results. Attendance at 9-monthly TM5 international meetings is encouraged to avoid duplicity and conflict of interests.

1003 Table 1: Details of the reaction rate data applied for $NO_x$ and nitrogen reservoirs. The $k_0$ terms are multiplied by
1004 the relevant air density to calculate the correct forward and backward rate constants. The reaction data and
1005 stiochiometery are taken from Atkinson et al. (2004) accommodating the latest evaluation at http://iupac.pole-
1006 ether.fr.

| Reactants | Products | Rate parameters |
|---|---|---|
| $NO + O_3$ | $NO_2$ | $3.0 \times 10^{-12} *\exp(-1500/T)$ |
| $NO_2 + O_3$ | $NO_3$ | $1.4 \times 10^{-13} *\exp(-2470/T)$ |
| $NO + HO_2$ | $NO_2 + OH$ | $3.3 \times 10^{-12} *\exp(270/T)$ |
| $NO + CH_3O_2$ | $CH_2O + HO_2 + NO_2$ | $2.8 \times 10^{-12} *\exp(300/T)$ |
| $OH + NO_2$ | $HNO_3$ | $k_0 = 3.2 \times 10^{-30}*(300/T)^{4.5}$ $k_\infty = 3.0 \times 10^{-11}$ |
| $NO + NO_3$ | $NO_2 + NO_2$ | $1.8 \times 10^{-11} *\exp(110/T)$ |
| $NO_2 + NO_3$ | $N_2O_5$ | $k_0 = 8.0 \times 10^{-27}*(300/T)^{3.5}$ $k_\infty = 3.0 \times 10^{-11}*(300/T)^{1.0}$ |
| $N_2O_5 + M$ | $NO_2 + NO_3$ | $k_0 = 1.3 \times 10^{-3}*(300/T)^{3.5}*$ $\exp(-11000/T)$ $k_\infty = 9.7 \times 10^{14}*(300/T)^{-0.1}*$ $\exp(-11080/T)$ |
| $HO_2 + NO_2$ | $HNO_4$ | $k_0 = 1.4 \times 10^{-31}*(300/T)^{3.1}$ $k_\infty = 4.0 \times 10^{-12}$ |
| $HNO_4 + M$ | $HO_2 + NO_2$ | $k_0 = 4.1 \times 10^{-5}*\exp(-10650/T)$ $k_\infty = 6.0 \times 10^{15}*\exp(-11170/T)$ |
| $OH + HNO_4$ | $NO_2$ | $1.3 \times 10^{-12} *\exp(380/T)$ |
| $OH + NO + M$ | $HONO$ | $k_0 = 7.0 \times 10^{-31}*(300/T)^{4.4}$ $k_\infty = 3.6 \times 10^{-11}*(300/T)^{0.1}$ |
| $HONO + h$ | $OH + NO$ | |
| $OH + HONO$ | $NO_2$ | $2.5 \times 10^{-12} *\exp(260/T)$ |
| $NO_2 + CH_3C(O)O_2$ | $PAN$ | $k_0 = 3.28 \times 10^{-28}*(300/T)^{6.87}$ $k_\infty = 1.125 \times 10^{-11}*(300/T)^{1.105}$ |
| $PAN$ | $NO_2 + CH_3C(O)O_2$ | $k_0 = 1.1 \times 10^{-5}*\exp(-10100/T)$ $k_\infty = 1.9 \times 10^{17}*\exp(-14100/T)$ |

Formatted: Indent: Left: 0 cm

| | | |
|---|---|---|
| PAN + h | CH$_3$C(O)O$_2$ + NO$_2$ | |
| | CH$_3$O$_2$ + NO$_3$ | |
| CH$_3$O$_2$ + NO$_2$ | CH$_3$O$_2$NO$_2$ | $k_0$= 2.5 x 10$^{-30}$*(300/T) |
| | | $k_\infty$= 1.8 x 10$^{-11}$ |
| CH$_3$O$_2$NO$_2$ | CH$_3$O$_2$ + NO$_2$ | $k_0$= 9.0 x 10$^{-5}$*exp(-9690/T) |
| | | $k_\infty$= 1.1 x 10$^{16}$*exp(-10560/T) |
| NO$_3$ + HO$_2$ | HNO$_3$ | 4.0 x 10$^{-12}$ |

1007
1008

1009 Table 2: Details of updates made to the reaction data and stoichiometry of the modified CB05 chemical
1010 mechanism for other reactions. Data is taken from the following: [1] Atkinson et al. (2004) accommodating the
1011 latest evaluation at http://iupac.pole-ether.fr, [2] branching ratio (R) equal to $1/(1+498.*exp(-1160./T))$, [3]
1012 Yarwood et al. (2005), [4] Sander et al. (2011), [5], Atkinson et al. (2006), [6] Emmons et al. (2010), [7]
1013 Hauglustaine et al. (2014), [8] rate assumed equal to $NH_2$ analogue, [9] assumed to be equal to $HNO_4$ after
1014 Browne et al. (2011) and E is an estimated value.
1015

| Reactants | Products | Rate expression | Ref. |
|---|---|---|---|
| $CH_3O_2 + HO_2$ | $CH_3OOH$ | $3.8 \times 10^{-13}*exp(750/T)*R$ | [1],[2] |
| $CH_3O_2 + HO_2$ | $CH_2O$ | $3.8 \times 10^{-13}*exp(750/T)$ $*(1-R)$ | [1],[2] |
| $CH_3O_2 + CH_3O_2$ | $1.37CH_2O + 0.74HO_2 + 0.63CH_3OH$ | $9.5 \times 10^{-14}*exp(390/T)$ | [3],[4] |
| $OH + C_3H_8$ | $i\text{-}C_3H_7O_2$ | $7.6 \times 10^{-12}*exp(-585/T)$ | [5],[6] |
| $NO + IC_3H_7O_2$ | $0.82CH_3COCH_3 + HO_2 + 0.27ALD2 + NO_2$ | $4.2 \times 10^{-12}*exp(180/T)$ | [6] |
| $HO_2 + IC_3H_7O_2$ | $ROOH$ | $7.5 \times 10^{-13}*exp(700/T)$ | [6] |
| $OH + C_3H_6$ | $C_3H_6O_2$ | $k_0= 8.0 \times 10^{-27}*(-300/T)^{3.5}$ $k_\infty=3.0 \times 10^{-11}*(-300/T)^{1.0}$ | [5],[6] |
| $NO_3 + C_5H_8$ | $0.2ISPD + XO_2 + 0.8HO_2 + 0.8ORGNTR + 0.8ALD2 + 2.4 PAR + 0.2 NO_2$ | $2.95 \times 10^{-12}*exp(465/T)$ | [5] |
| $NO + C_3H_6O_2$ | $ALD2 + CH_2O + HO_2 + NO_2$ | $4.2 \times 10^{-12}*exp(180/T)$ | [6] |
| $HO_2 + C_3H_6O_2$ | $ROOH$ | $7.5 \times 10^{-13}*exp(700/T)$ | [6] |
| $NO_3 + DMS$ | $SO_2 + HNO_3$ | $1.9 \times 10^{-13}*exp(520/T)$ | [1] |
| $NH_2 + OH$ | | $3.4 \times 10^{-11}$ | [E] |
| $NH_2 + HO_2$ | $NH_3$ | $3.4 \times 10^{-11}$ | [4],[7] |
| $NH_2 + O_3$ | $NH_2O_2$ | $4.3 \times 10^{-12}*exp(-930/T)$ | [4],[7] |
| $NH_2 + O_2$ | $NO$ | $6.0 \times 10^{-21}$ | [1],[7] |
| $NH_2O_2 + NO$ | $NH_2 + NO_2$ | $4.0 \times 10^{-12}*exp(450/T)$ | [7],[8] |
| $NH_2O_2 + O_3$ | $NH_2$ | $4.3 \times 10^{-12}*exp(-930/T)$ | [7],[8] |
| $NH_2O_2 + HO_2$ | $NH_2$ | $3.4 \times 10^{-11}$ | [8] |
| $CH_3O_2NO_2 + h$ | $CH_3O_2 + NO_2$ | | [9] |

| | | |
|---|---|---|
| $CH_3O_2NO_2 + h$ | $CH_2O + HO_2 + NO_3$ | [9] |
| $HO_2 + aero$ | $0.5H_2O_2$ | |
| $NO_3 + aero$ | $HNO_3$ | [6] |

1016
1017

1018 Table 3: The zonally segregated emission totals introduced into TM5-MP for the year 2006. All
1019 organic hydrocarbons are given in Tg C yr$^{-1}$, except for CO, (Tg CO yr$^{-1}$), $CH_2O$ (Tg CH$_2$O yr$^{-1}$) and
1020 CH$_3$OH and all(Tg CH$_3$OH yr$^{-1}$). All $NO_x$ emissions are introduced as NO (Tg N yr$^{-1}$). For SO$_2$
1021 emission totals are given as Tg SO$_2$ yr$^{-1}$ and for NH$_3$ as Tg NH$_3$ yr$^{-1}$. No direct emissions occur for
1022 HNO$_3$, PAN, ORGNTR, HONO, N$_2$O$_5$, NO$_2$, CH$_3$O$_2$NO$_2$ or O$_3$.
1023

| Species Tg Yr$^{-1}$ | Global | 30-90°S | 30S-30°N | 30-90°N |
|---|---|---|---|---|
| CO | 1081.0 | 24.4 | 755.1 | 301.27 |
| NO$_x$ (as N) | 49.0 | 1.5 | 24.0 | 23.6 |
| SO$_2$ | 117.0 | 3.0 | 49.2 | 64.3 |
| DMS (as S) | 19.2 | 6.7 | 9.3 | 3.2 |
| NH$_3$ | 56.6 | 3.1 | 27.9 | 25.6 |
| CH$_2$O | 13.5 | 0.3 | 10.5 | 2.7 |
| PAR | 34.1 | 0.7 | 18.5 | 14.9 |
| OLE | 22.4 | 0.9 | 16.6 | 4.9 |
| ALD2 | 13.4 | 0.4 | 11.2 | 1.8 |
| CH$_3$CHCHO | 2.2 | 0.0 | 1.2 | 1.0 |
| CH$_3$OH | 100.7 | 3.3 | 82.5 | 14.9 |
| CH$_3$CH$_2$OH | 70.4 | 2.8 | 52.6 | 15.1 |
| C$_2$H$_4$ | 25.9 | 1.0 | 19.0 | 5.9 |
| C$_2$H$_6$ | 6.1 | 0.3 | 5.3 | 1.5 |
| C$_3$H$_8$ | 5.6 | 0.4 | 3.6 | 1.6 |
| C$_3$H$_6$ | 19.6 | 0.9 | 14.8 | 3.9 |
| CH$_3$COCH$_3$ | 27.4 | 0.8 | 22.0 | 4.6 |
| HCOOH | 1.8 | 0.0 | 1.5 | 0.3 |
| CH$_3$COOH | 7.1 | 0.1 | 6.0 | 1.0 |
| C$_5$H$_8$ | 510.0 | 23.2 | 441.9 | 45.0 |
| C$_{10}$H$_{16}$ | 85.4 | 2.3 | 70.2 | 12.9 |

1024
1025

1026
1027 Table 4: The tropospheric chemical budget terms and burden for $O_3$ during 2006 for the 1° x 1°
1028 simulation, with all quantities being given in Tg $O_3$ yr$^{-1}$. The associated percentage changes are given
1029 when comparing against the 3° x 2° simulation (equal to (1° x 1°)-( 3° x 2°)/3° x 2°). The definition of
1030 the chemical tropopause and the calculation of the STE are calculated using the methodology outlined
1031 in Stevenson et al. (2006). The stratospheric nudging term refers to total change in the mass of $O_3$ in
1032 the stratospheric column when constraining zonal distributions towards observational values from the
1033 MSR (Huijnen et al., 2010). The contribution to each term from the SH extra-tropics/tropics/NH
1034 extra-tropics regions (defined as 90-30°S/30°S-30°N/30-90°N) are provided.
1035

| Term | Global | % | SH | % | Tropics | % | NH | % |
|---|---|---|---|---|---|---|---|---|
| Net STE | 579 | -6.7 | 166 | 3.9 | 396 | -7.5 | —16 | 240 |
| Strat. Nudging | 1440 | -0.7 | -224 | 2.8 | 1615 | - | 49 | 5.8 |
| Trop.Chem.Prod | 5532 | -1.9 | 389 | -2.2 | 3938 | -3.5 | 1206 | -2.2 |
| Trop.Chem.Loss | 5162 | -2.4 | 440 | -1.0 | 3869 | -2.5 | 853 | -2.8 |
| $BO_3$ | 378 | -2.0 | 72 | 1.7 | 203 | -2.3 | 104 | -3.4 |
| Strat $BO_3$ | 80 | -2.0 | 23 | 9.1 | 38 | -6.5 | 24 | -2.0 |
| | | | | | | | | |
| Deposition | 949 | 0.8 | 115 | 0.6 | 465 | - | 369 | 1.9 |
| $O_3S$ Deposition | 97 | 5.0 | 19 | 7.5 | 37 | -1.2 | 42 | 10.0 |

1036
1037
1038 Table 5: The annual NO to $NO_2$ re-cycling terms involving peroxy-radicals given in Tg N yr$^{-1}$ for
1039 2006 at 1° x 1° resolution. In mCB05v2 $XO_2$ represents lumped alkyl-peroxy radicals (Yarwood et al,
1040 2005). The NO + $RO_2$ term is an aggregate of numerous specific peroxy-radical conversion terms in
1041 the modified CB05 mechanism (Williams et al., 2013; Tables 1 and 2). Also provided are the
1042 approximate percentage differences when comparing with 3° x 2° (equal to (1° x 1°)-( 3° x 2°)/3° x 2°).
1043 The chemical tropopause is defined using the methodology outlined in Stevenson et al. (2006).

| Reaction | Global | % | SH | % | Tropics | % | NH | % |
|---|---|---|---|---|---|---|---|---|
| NO + $HO_2$ | 1058 | -1.2 | 79 | -1.2 | 740 | -1.9 | 239 | 1044 |
| NO + $CH_3O_2$ | 407 | -2.2 | 31 | -2.6 | 294 | -2.8 | 82 | 1047 |
| NO + $XO_2$ | 147 | -2.1 | 7 | -3.6 | 111 | -2.6 | 29 | 1048 |
| NO + $RO_2$ | 9.4 | -4.4 | 0.4 | -2.6 | 6.3 | -4.4 | 2.7 | 1049 |
| | | | | | | | | |
| NO + $O_3$ | 5403 | 0.1 | 518 | 7.5 | 2933 | -3.9 | 1953 | 1051 |

1052
1053

Table 6: The seasonal mean absolute biases as calculated using weekly [NO] values ($\mu$g m$^{-3}$). The weekly means are composed from daily measurements taken at 13:00 for DJF and JJA (given as the difference in the measurements-model). Values are shown for both the 3° x 2° and 1° x 1° simulations for all stations with available data. Those with differences < 5% are considered to exhibit no discernible change in the bias.

| EMEP Station | Lat | Lon | DJF 3° x 2° | DJF 1° x 1° | JJA 3° x 2° | JJA 1° x 1° |
|---|---|---|---|---|---|---|
| CH01 | 46.32 | 7.59 | -0.01 | -0.01 | 0.00 | -0.01 |
| CZ03 | 49.35 | 15.50 | -4.05 | -3.30 | -1.61 | -1.35 |
| DE43 | 47.48 | 11.10 | -2.37 | -2.36 | -0.47 | -0.48 |
| DK05 | 54.44 | 10.44 | -2.51 | -2.61 | -1.29 | -1.51 |
| ES07 | 58.23 | 21.49 | -3.80 | -3.84 | -1.45 | -1.48 |
| ES08 | 43.26 | -4.51 | -2.08 | -2.09 | -1.00 | -1.01 |
| ES09 | 41.16 | -3.80 | -0.93 | -0.93 | -1.07 | -1.07 |
| ES10 | 38.28 | 3.19 | -1.14 | -1.24 | -0.75 | -0.88 |
| ES11 | 39.50 | -6.55 | -1.07 | -1.07 | -0.44 | -0.45 |
| ES12 | 41.17 | -1.60 | -1.34 | -1.34 | -0.95 | -0.95 |
| ES13 | 41.24 | -5.52 | -2.50 | -1.90 | -0.74 | -0.62 |
| ES14 | 39.31 | 0.43 | -2.21 | -2.20 | -1.27 | -1.27 |
| ES15 | 43.13 | -4.21 | -1.62 | -1.61 | -0.99 | -1.00 |
| ES16 | 43.37 | -7.41 | -2.39 | -2.39 | -1.11 | -1.11 |
| FR13 | 46.39 | 0.11 | -1.90 | -1.94 | -0.52 | -0.52 |
| FR15 | 55.18 | 0.45 | -3.09 | -3.04 | -1.51 | -1.58 |
| GB02 | 50.35 | -3.12 | -1.23 | -1.23 | -0.93 | -0.92 |
| GB13 | 54.20 | -3.42 | -1.28 | -1.32 | -0.58 | -0.55 |
| GB14 | 52.30 | -0.48 | -3.03 | -3.04 | -0.98 | -0.98 |
| GB31 | 53.23 | -3.11 | -1.74 | -1.74 | -0.90 | -0.91 |
| GB37 | 50.47 | -1.45 | -3.09 | -3.08 | -1.22 | -1.21 |
| GB38 | 51.13 | 0.10 | -2.87 | -2.78 | -1.92 | -1.72 |
| GB44 | 51.17 | -3.20 | -1.65 | -1.45 | -0.27 | -0.67 |
| GB45 | 52.17 | 0.17 | -1.80 | 0.11 | 0.20 | 0.19 |
| GB51 | 52.33 | 0.46 | -3.68 | -3.42 | -1.29 | -1.17 |
| NL91 | 52.18 | 4.30 | -4.47 | -3.51 | -1.98 | -1.86 |

1062   Table 7: As for Table 5 except for NO$_2$.
1063

| EMEP Station | Lat | Lon | DJF 3° x 2° | DJF 1° x 1° | JJA 3° x 2° | JJA 1° x 1° |
|---|---|---|---|---|---|---|
| BE32 | 50.30 | 4.59 | 10.56 | 1.27 | 1.69 | -2.13 |
| CH01 | 46.32 | 7.59 | -0.04 | -0.03 | -0.02 | -0.01 |
| CZ03 | 49.35 | 15.50 | -4.04 | 0.03 | -1.62 | 0.34 |
| DE43 | 47.48 | 11.10 | -2.37 | -2.36 | -0.49 | -0.48 |
| DK05 | 54.44 | 10.44 | 6.07 | 5.56 | 1.04 | -0.02 |
| ES07 | 58.23 | 21.49 | -1.13 | -1.79 | -0.96 | -1.15 |
| ES08 | 43.26 | -4.51 | -2.01 | -2.10 | -0.93 | -1.01 |
| ES09 | 41.16 | -3.80 | -0.95 | -0.94 | -1.07 | -1.07 |
| ES10 | 42.19 | 3.19 | 2.18 | 1.46 | 0.92 | -0.01 |
| ES11 | 38.28 | -6.55 | -1.08 | -1.08 | -0.44 | -0.44 |
| ES12 | 39.50 | -1.60 | -1.36 | -1.35 | -0.95 | -0.95 |
| ES13 | 41.17 | -5.52 | -2.51 | -0.29 | -0.74 | 0.19 |
| ES14 | 41.24 | 0.43 | -2.22 | -2.21 | -1.27 | -1.26 |
| ES15 | 39.31 | -4.21 | -1.64 | -1.63 | -0.99 | -0.99 |
| ES16 | 43.13 | -7.41 | -2.40 | -2.39 | -1.11 | -1.11 |
| FI09 | 59.46 | 21.22 | 0.79 | -0.91 | -0.10 | -0.53 |
| FI37 | 60.31 | 27.41 | 10.04 | 9.60 | 1.70 | 0.92 |
| FI96 | 62.35 | 24.11 | 0.40 | 0.34 | 0.31 | 0.17 |
| FR13 | 43.37~~68.00~~ | 24.09~~0.11~~ | -1.96 | -1.95 | -0.54 | -0.54 |
| FR15 | 46.39~~43.37~~ | 0.11~~45~~ | -3.84 | -3.91 | -1.78 | -1.81 |
| GB02 | 55.18~~46.39~~ | 0.45~~-3.12~~ | 3.12 | 3.42 | 0.82 | 0.54 |
| GB13 | 50.35~~55.18~~ | -3.12~~42~~ | -2.17 | -2.13 | -1.00 | -0.98 |
| GB14 | 54.20~~50.35~~ | -3.42~~0.48~~ | 5.02 | 3.93 | 1.17 | 1.50 |
| GB31 | 52.30~~54.20~~ | -0.48~~3.11~~ | -1.71 | -1.71 | -0.90 | -0.90 |
| GB37 | 53.23~~52.30~~ | -3.11~~1.45~~ | -3.10 | -3.08 | -1.25 | -1.25 |
| GB38 | 50.47~~53.23~~ | -1.45~~0.10~~ | -4.05 | -4.03 | -2.20 | -2.19 |
| GB44 | 51.13~~50.47~~ | 0.10~~-3.20~~ | 6.21 | 6.69 | 0.61 | 1.42 |
| GB45 | 52.17~~51.13~~ | -3.20~~0.17~~ | 6.28 | 6.00 | 3.48 | 1.94 |
| GB51 | 52.17~~33~~ | -0.17~~46~~ | 12.56 | 16.60 | 4.11 | 4.50 |
| GR01 | 41.45 | 42.49 | 0.50 | 2.07 | 0.40 | 1.05 |
| NL09 | 53.2 | 6.16 | -3.21 | -1.63 | -1.18 | -0.19 |
| NL10 | 51.32 | 5.51 | 3.48 | 3.52 | 0.92 | -0.29 |
| NL91 | 52.18 | 4.30 | 11.81 | 6.42 | 1.48 | -0.81 |

1064
1065

1066

1067  Table 8: The tropospheric chemical budget for the CH$_2$O given in Tg CH$_2$O yr$^{-1}$ during 2006 for the 1°
1068  x 1° simulation. Percentage differences are shown against the corresponding 3° x 2° simulation.
1069

| Budget Term | Global | % | SH | % | Tropics | % | NH | % |
|---|---|---|---|---|---|---|---|---|
| CH$_2$O CP | 1919 | -1.1 | 147 | -0.3 | 1491 | -1.0 | 281 | -2.0 |
| CH$_2$O CD | 1739 | -1.6 | 134 | -0.5 | 1349 | -1.1 | 256 | -2.3 |
| CH$_2$O Dep. | 193 | 3.1 | 15 | 2.0 | 149 | 3.9 | 29 | - |

1070
1071  Table 9: The seasonal mean biases of daily [SO$_2$] (µg m$^{-3}$) at 13:00 for DJF and JJA, when taking the
1072  difference between measurements-model values. Values are shown for both the 3° x 2° and 1° x 1°
1073  simulations. Those with differences < 5% are considered to exhibit no discernible change in the bias.
1074

| EMEP Station | Lat | Lon | DJF 3° x 2° | DJF 1° x 1° | JJA 3° x 2° | JJA 1° x 1° |
|---|---|---|---|---|---|---|
| AT02 | 47.46 | 16.46 | -3.34 | -3.15 | -0.89 | -0.53 |
| AT05 | 46.40 | 12.58 | -0.42 | -0.41 | -0.14 | -0.14 |
| AT48 | 47.50 | 14.26 | -0.64 | -0.63 | -0.14 | -0.15 |
| CZ03 | 49.35 | 15.50 | -3.52 | 3.65 | -0.69 | 0.64 |
| ES07 | 58.2337.14 | 21.49-3.32 | 1.22 | 0.73 | 0.38 | 0.31 |
| ES08 | 43.26 | -4.51 | -2.98 | -3.21 | -1.19 | -1.58 |
| ES09 | 41.16 | -3.80 | -0.62 | -0.61 | -0.42 | -0.42 |
| ES10 | 42.19 | 3.19 | 2.37 | 2.45 | 1.93 | 1.53 |
| ES11 | 38.28 | -6.55 | -0.63 | -0.61 | -0.70 | -0.70 |
| ES12 | 39.50 | -1.60 | -0.47 | -0.45 | -0.32 | -0.32 |
| ES13 | 41.17 | -5.52 | -0.81 | 2.71 | -0.78 | 0.55 |
| ES14 | 41.24 | 0.43 | -0.70 | -0.67 | -0.47 | -0.47 |
| ES15 | 39.31 | -4.21 | -0.40 | -0.37 | -0.45 | -0.46 |
| ES16 | 43.13 | -7.41 | -3.84 | -3.82 | -1.66 | -1.66 |
| GB37 | 52.30 | -3.11 | -2.92 | -2.91 | -1.72 | -1.72 |
| GB38 | 53.23 | -1.45 | 2.93 | 2.75 | 0.39 | 1.33 |
| GB43 | 51.14 | -4.42 | -1.49 | 4.77 | -2.03 | -0.63 |
| GB45 | 52.17 | -0.17 | 3.87 | 7.20 | 1.01 | 1.77 |
| GR01 | 38.22 | 23.50 | 1.70 | 2.77 | 0.74 | 1.50 |
| NL07 | 52.50 | 6.34 | 2.58 | -1.67 | 0.46 | -1.03 |
| NL08 | 52.70 | 5.12 | 1.77 | 1.56 | -0.14 | -0.30 |
| NL09 | 53.2 | 6.16 | 2.53 | 2.16 | 0.47 | 0.27 |

1075

Formatted: Right: 1 cm

Formatted: Right: -0.19 cm
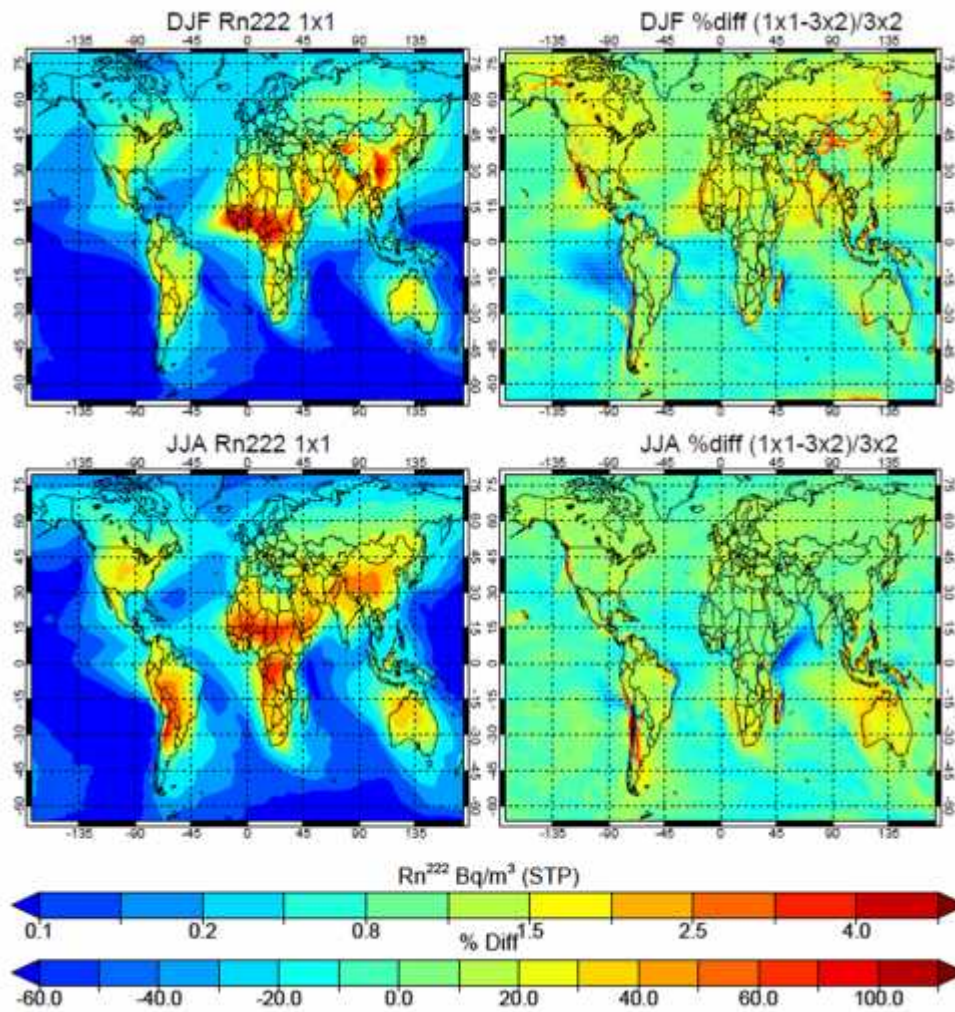
Figure 1: The seasonal distributions of $Rn^{222}$ averaged between 800 and 900hPa for DJF (top) and JJA (bottom) for the 3º x 2º (left) and 1º x 1º (right) simulation, with the associated percentage differences when compared against the 3º x 2º simulation.

1076
1077
1078
1079
1080
1081
1082
1083

Formatted: Justified
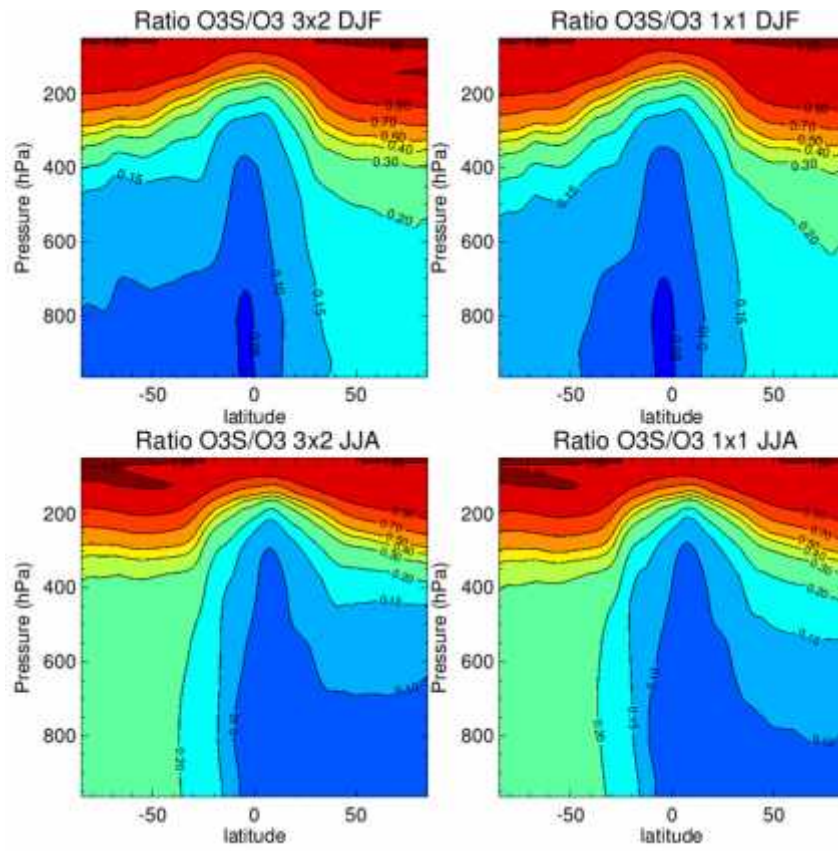
1084
1085    Figure 2: Zonal mean seasonal distribution of the TM5-MP $O_3S/O_3$ ratio for the 3º x 2º (left) and
1086    1º x 1º (right) simulations.
1087

1088



1089

1090
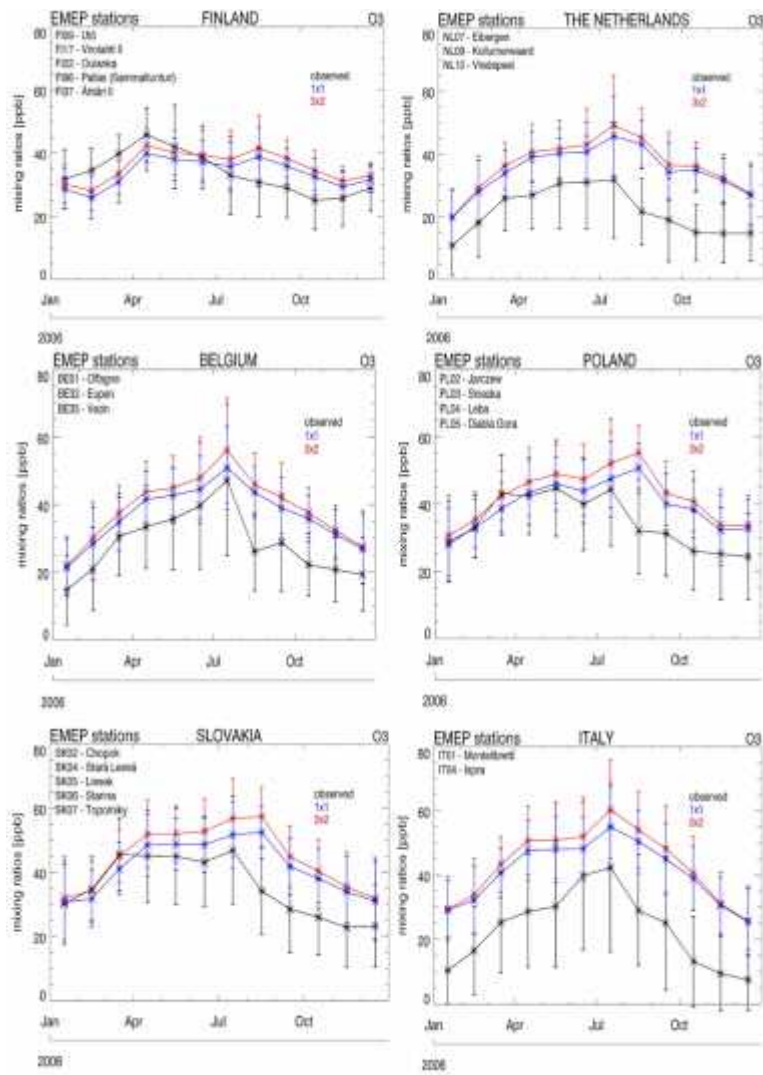
1091
1092
1093 Figure 3
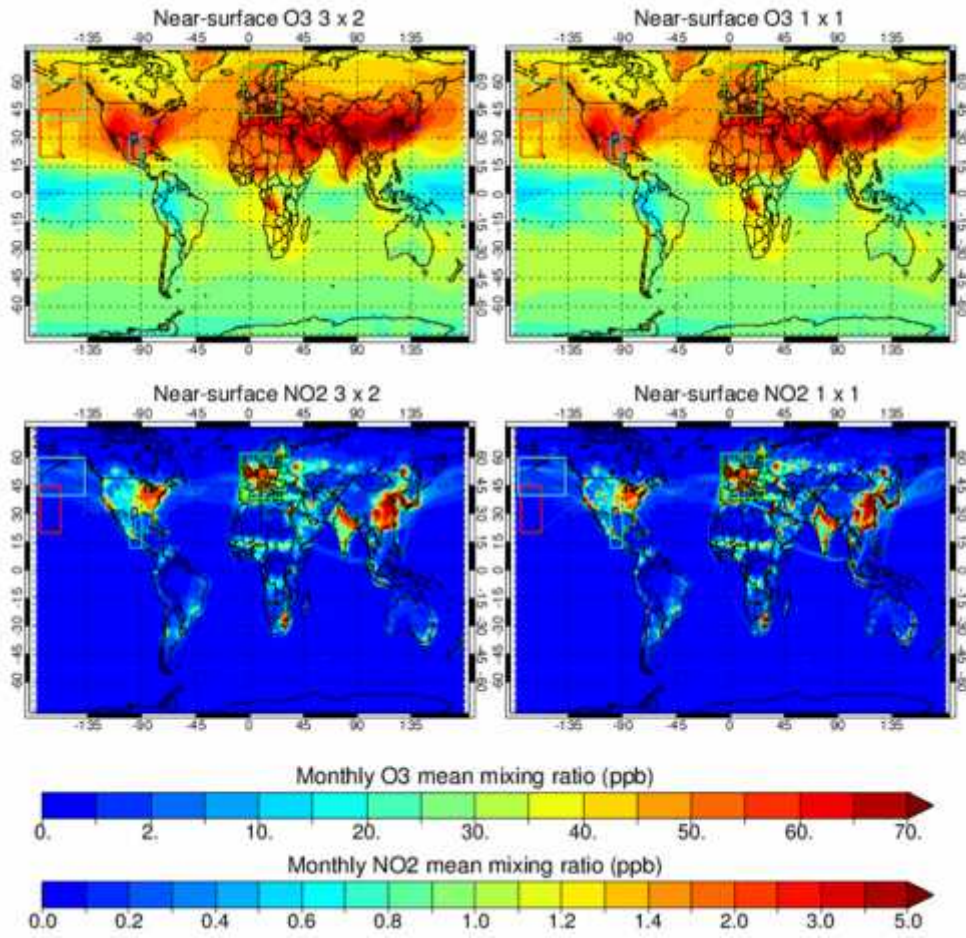
Figure 3: The near-surface distribution in tropospheric $O_3$ (top) and $NO_2$ (bottom) for May 2006 from the $3° \times 2°$ (left) and $1° \times 1°$ (right) TM5-MP simulations. The blue points represent the location of the MOZAIC airports used for comparisons. Also shown are the locations of the INTEXB and Texas-AQSII measurement campaigns, and the extent of the EMEP network in the European domain, used for the validation of the resulting $O_3$ and $NO_2$ distributions.
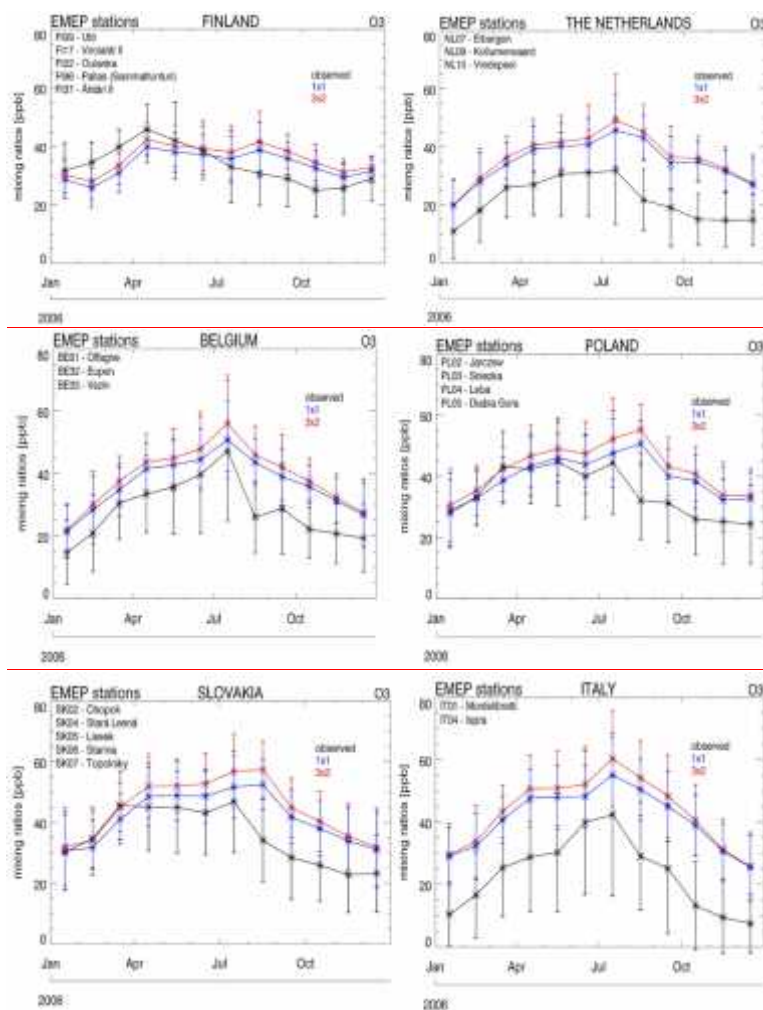
Figure 4: Comparisons of the seasonal variability in TM5-MP mass mixing ratios for surface $O_3$ against composites of measurements taken across the EMEP monitoring network for 2006. Both the co-located TM5-MP 3º x 2º and 1º x 1º monthly mean values are shown, along with the 1-$\sigma$ variability for Finland, The Netherlands, Belgium, Poland, Slovakia and Italy. Individual stations that are aggregated are given in the panels.

Formatted: Indent: Left: 1.25 cm, Right: 2 cm

1116
1117



1118

1119
1120
1121
1122
1123
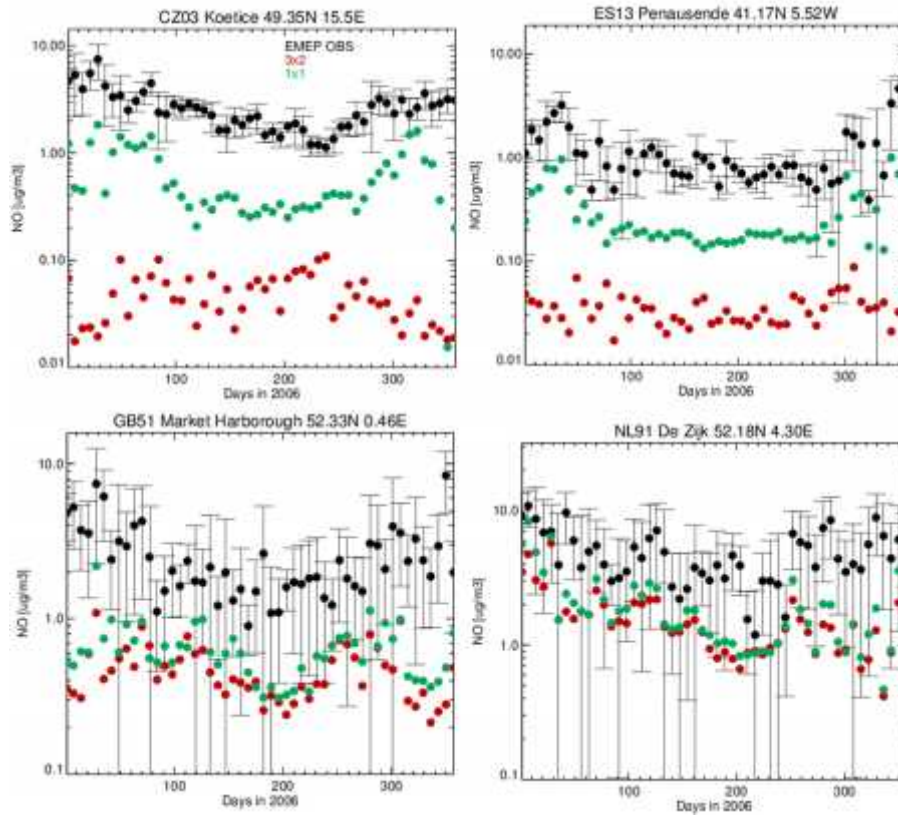
Figure 45: Comparison of TM5-MP weekly [NO] sampled at 13:00 UT each day during 2006 with observed [NO] (µg m$^{-3}$). The selected sites shown are in the Czech Republic (top left), Spain (top right), Great Britain (bottom left) and The Netherlands (bottom right).

1124
1125
1126
1127
1128
1129
1130

Formatted: Indent: Left: 0 cm, Right: 0 cm, Tab stops: Not at 10.75 cm + 14.5 cm
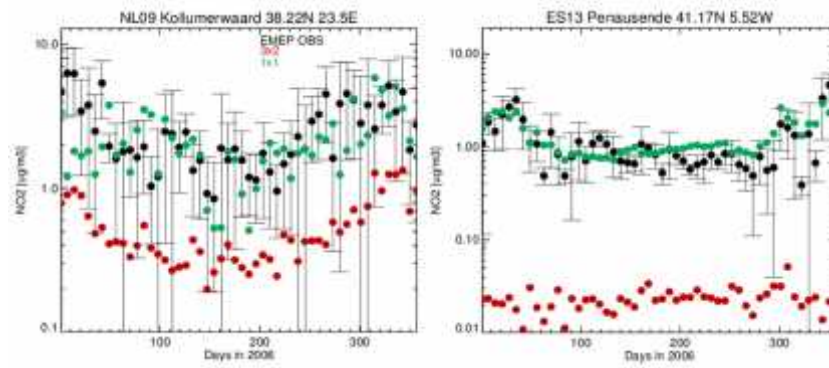
Figure 56: Comparison of weekly TM5-MP [NO$_2$] sampled at 13:00 UT each day during 2006 with observed [NO$_2$] (µg m$^{-3}$). The selected sites shown are in The Netherlands (left) and Spain (right).
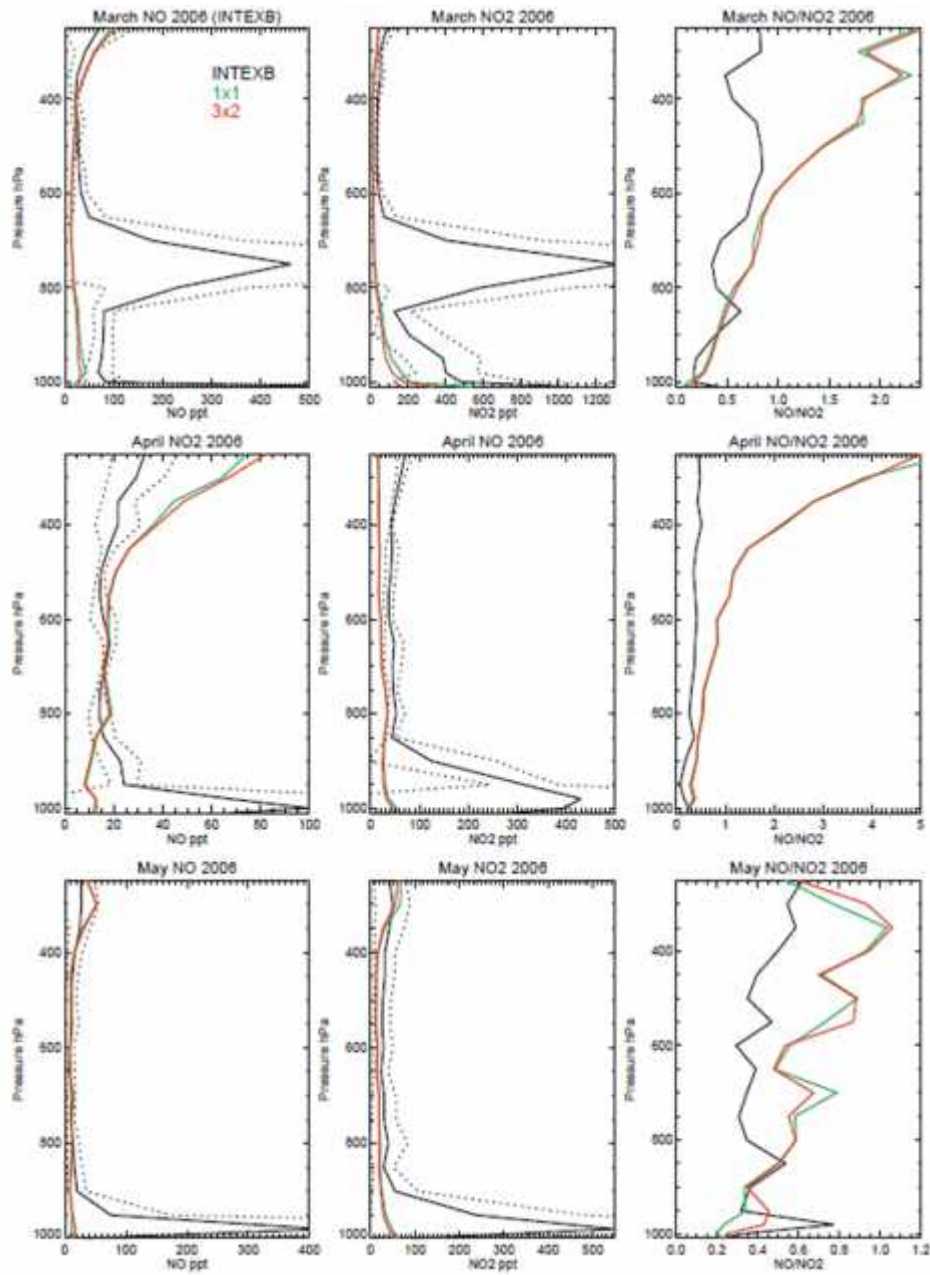
Figure 67: Monthly mean comparisons of NO (left), $NO_2$ (middle) and the resulting $NO/NO_2$ ratio (right) from INTEX-B measurements and TM5-MP simulations. The dotted line represents the 1-$\sigma$ deviation in the mean of the measurements. For details of the locations for each month the reader is referred to Singh et al. (2009).

Figure 78: Monthly mean comparisons of NO (left), $NO_2$ (middle) and the resulting $NO/NO_2$ ratio (right) from the TexAQSII campaign during September and October 2006 and TM5-MP simulations. The dotted line represents the 1-σ deviation in the mean of the measurements. For details of the locations for each month the reader is referred to Parrish et al. (2009).
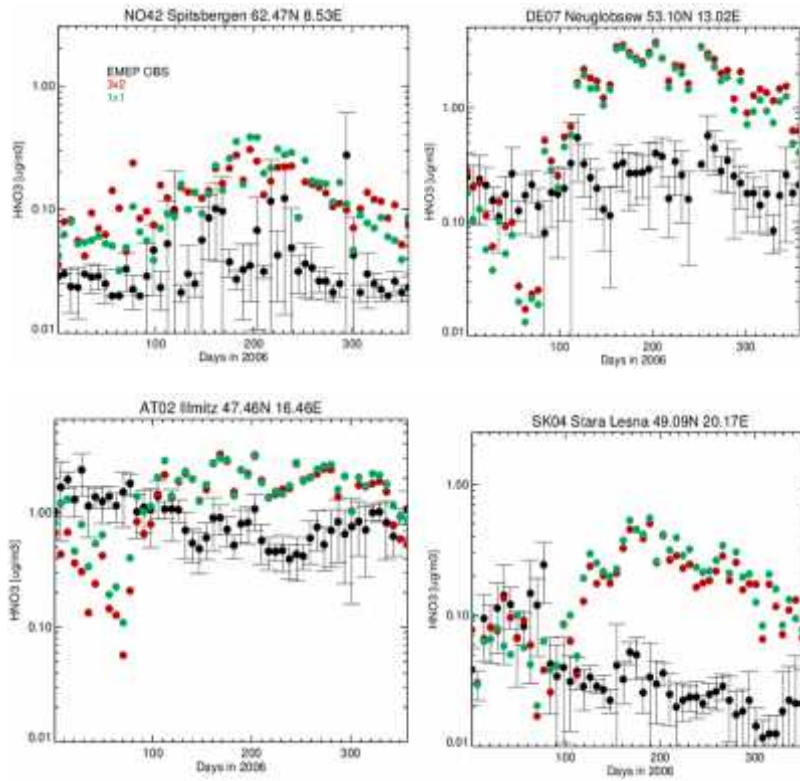
Figure 89: Comparison of weekly [HNO$_3$] (µg m$^{-3}$) from both 3° x 2° and 1° x 1° simulations at 4 selected EMEP sites for 2006. The 1-σ deviation in the weekly observations are shown as error bars. The selected sites shown are in Norway (top left), Germany (top right), Austria (bottom left) and Slovakia (bottom right).

Formatted: Indent: Left: 1.5 cm

March HNO3 2006

March PAN 2006

April HNO3 2006

April PAN 2006

May HNO3 2006

May PAN 2006

1165
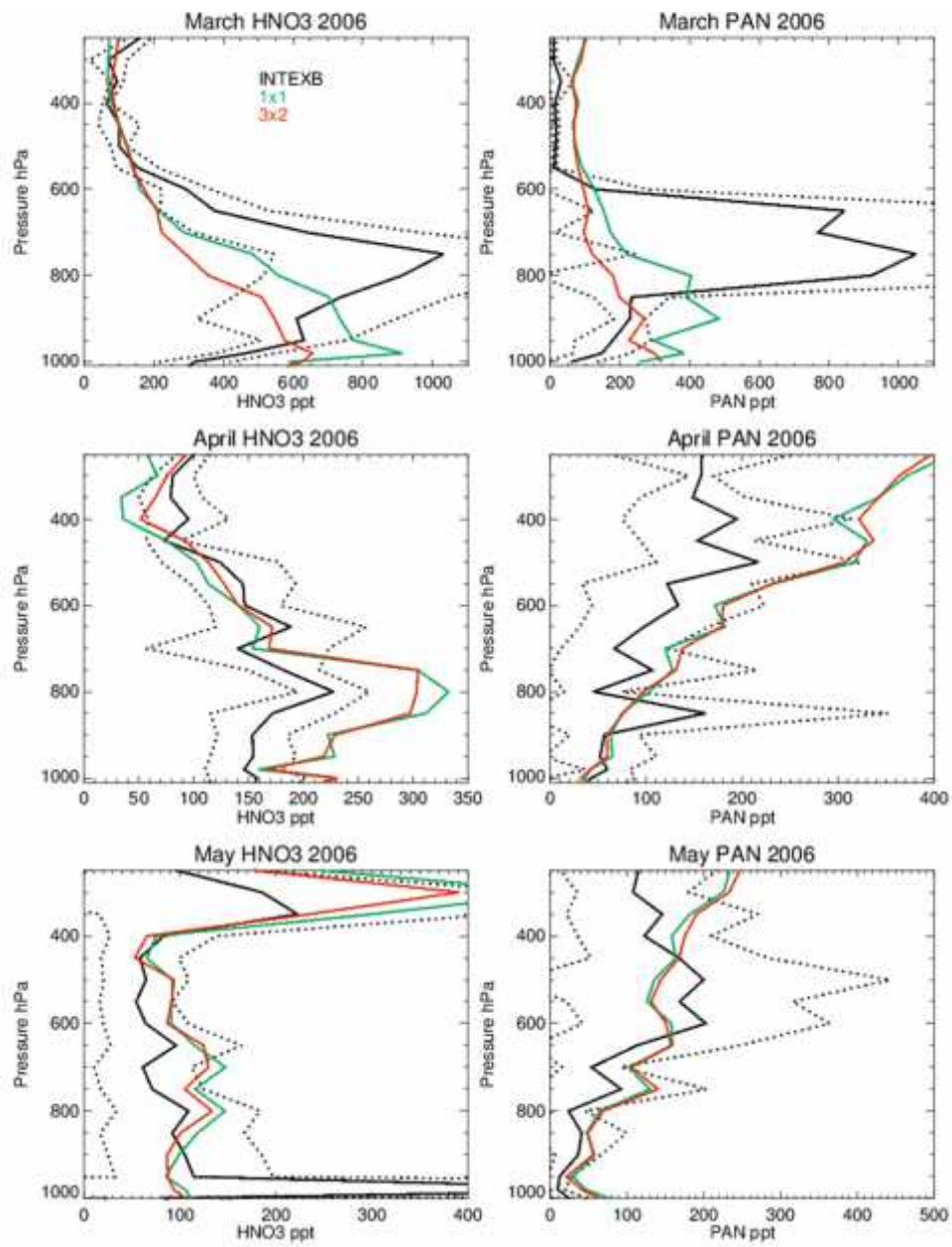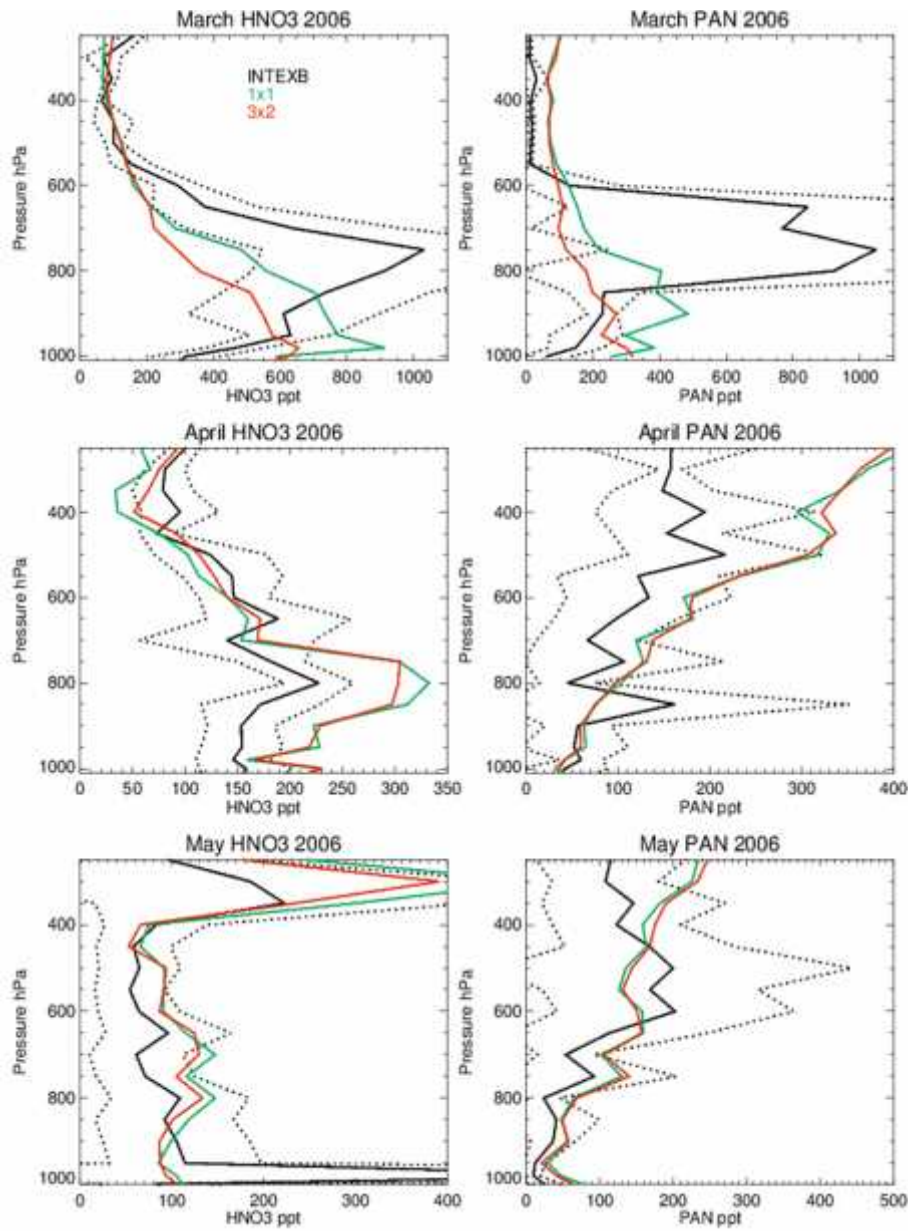
Figure 910: Monthly mean comparisons of $HNO_3$ (left) and PAN (right) from the INTEX-B measurements and TM5-MP simulations. The dotted line represents the 1-$\sigma$ deviation in the mean of the measurements. For details of the locations for each month the reader is referred to Singh et al. (2009).

Formatted: Justified, Indent: Left: -0.75 cm

Formatted: Indent: Left: 0.25 cm, Right: 1.11 cm

March CH2O 2006 (INTEXB)

April CH2O 2006 (INTEXB)

May CH2O 2006 (INTEXB)

1174
1175
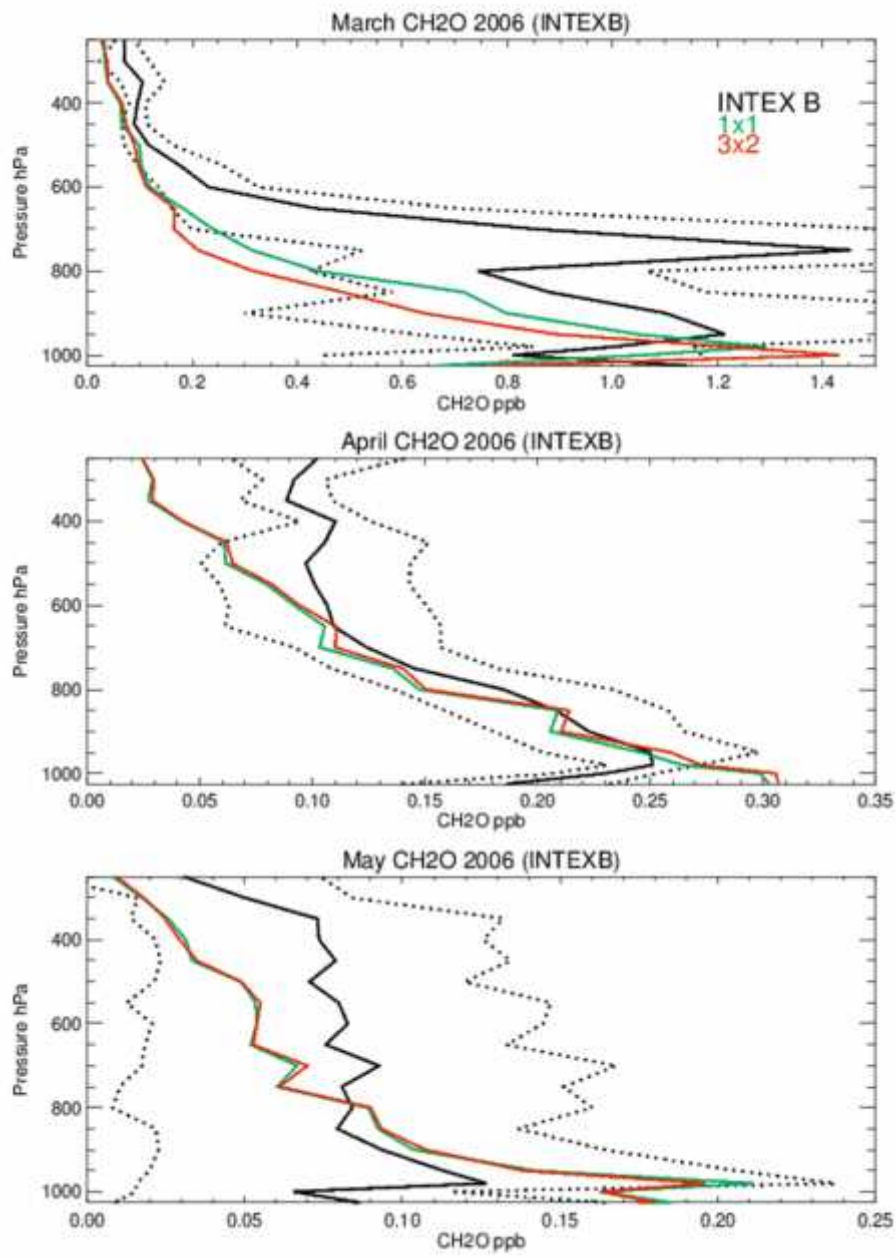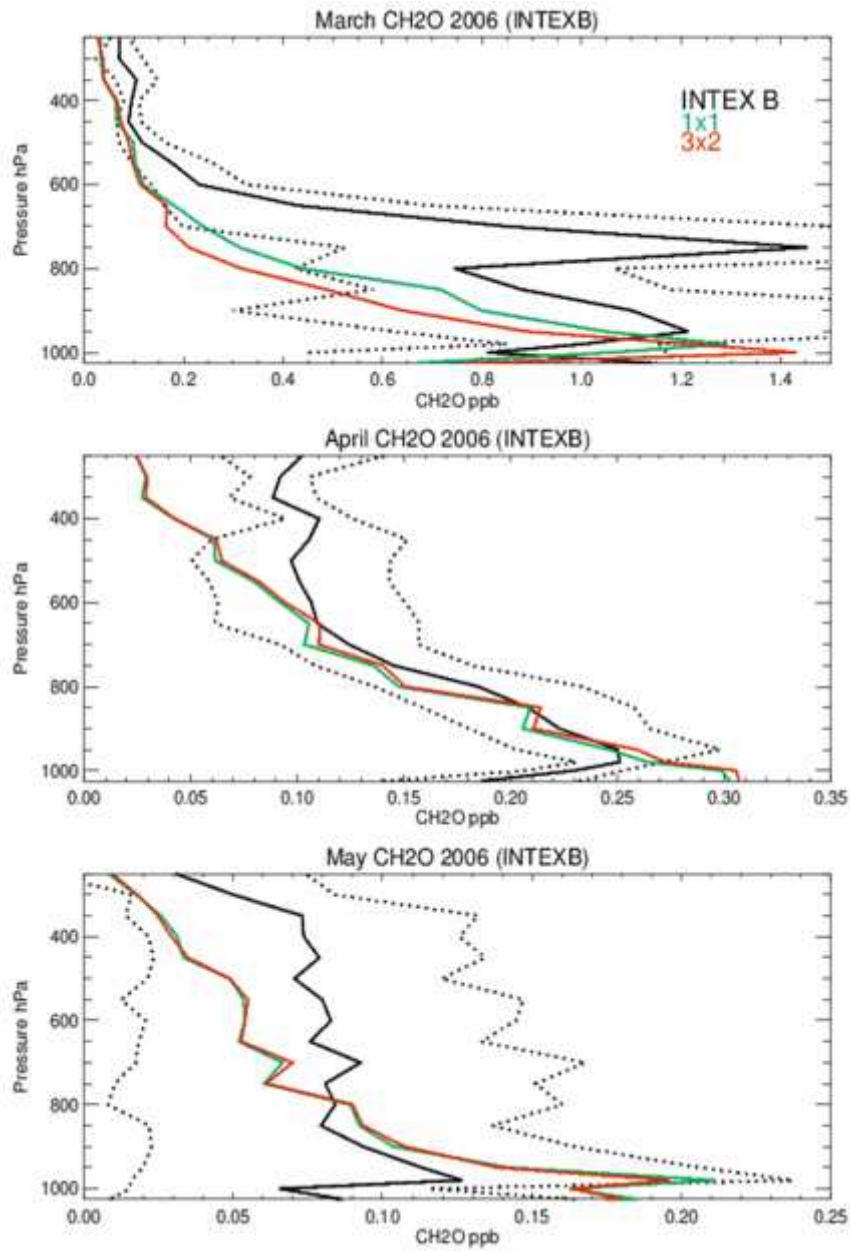
Figure 1011: Comparisons of the vertical distribution of CH₂O from both 3° x 2° and 1° x 1° simulations against measurements made as part of the INTEX-B during 2006. The dotted line represents the 1-σ deviation in the mean of the measurements. For details on the exact location of the flights the reader is referred to Parrish et al. (2009).

51

1184
1185
1186



1187
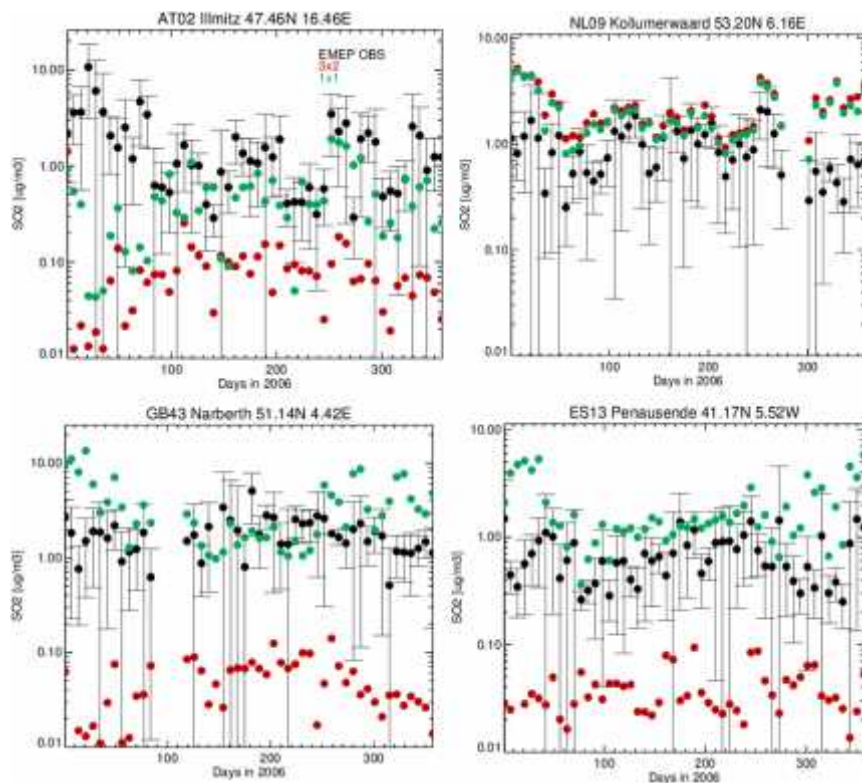
1188
1189
1190  Figure ~~11~~12: Comparison of weekly [SO$_2$] (µg m$^{-3}$) at 13:00 from both the 3º x 2º and 1º x 1º
1191  simulations at 4 selected EMEP sites for 2006. The selected sites shown are in Austria (top
1192  left), the Netherlands (top right), Great Britain (bottom left) and Spain (bottom right).
1193
1194

1195

## Sept SO2 2006 (Texas)



1196
1197

Sept SO2 2006 (Texas)

Oct SO2 2006 (Texas)
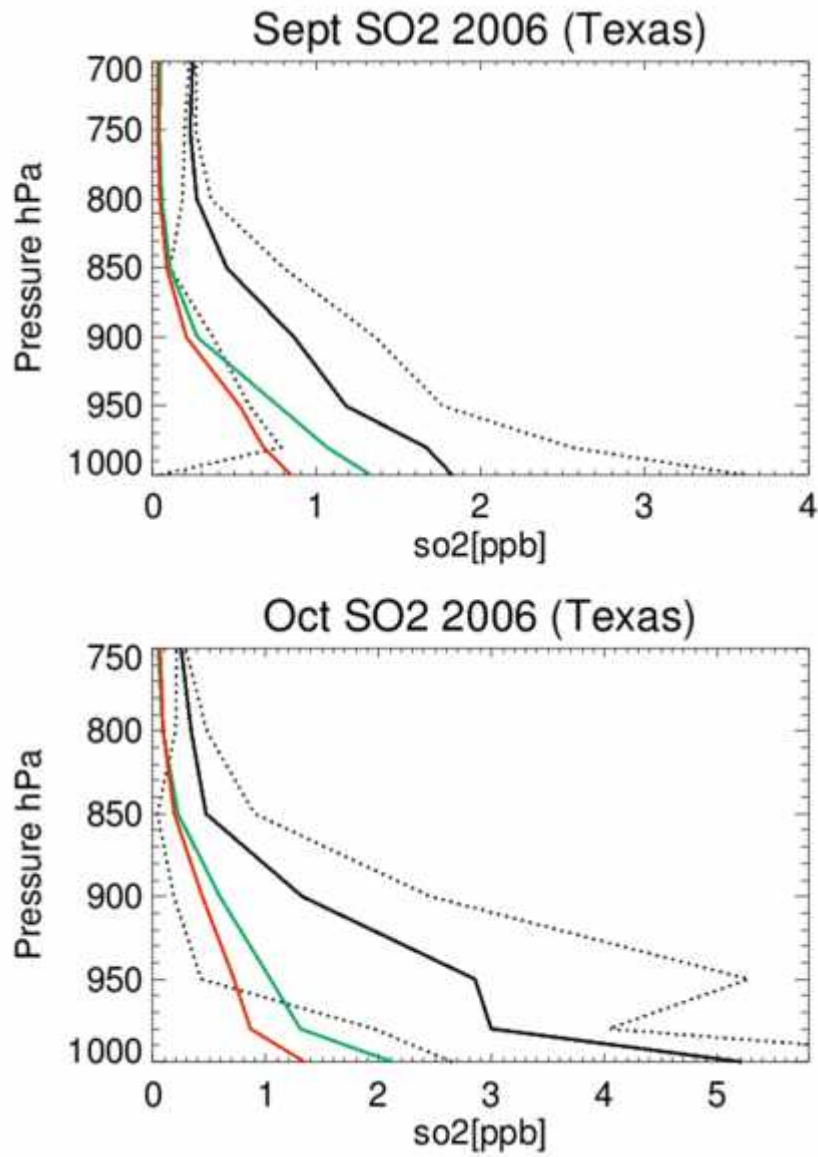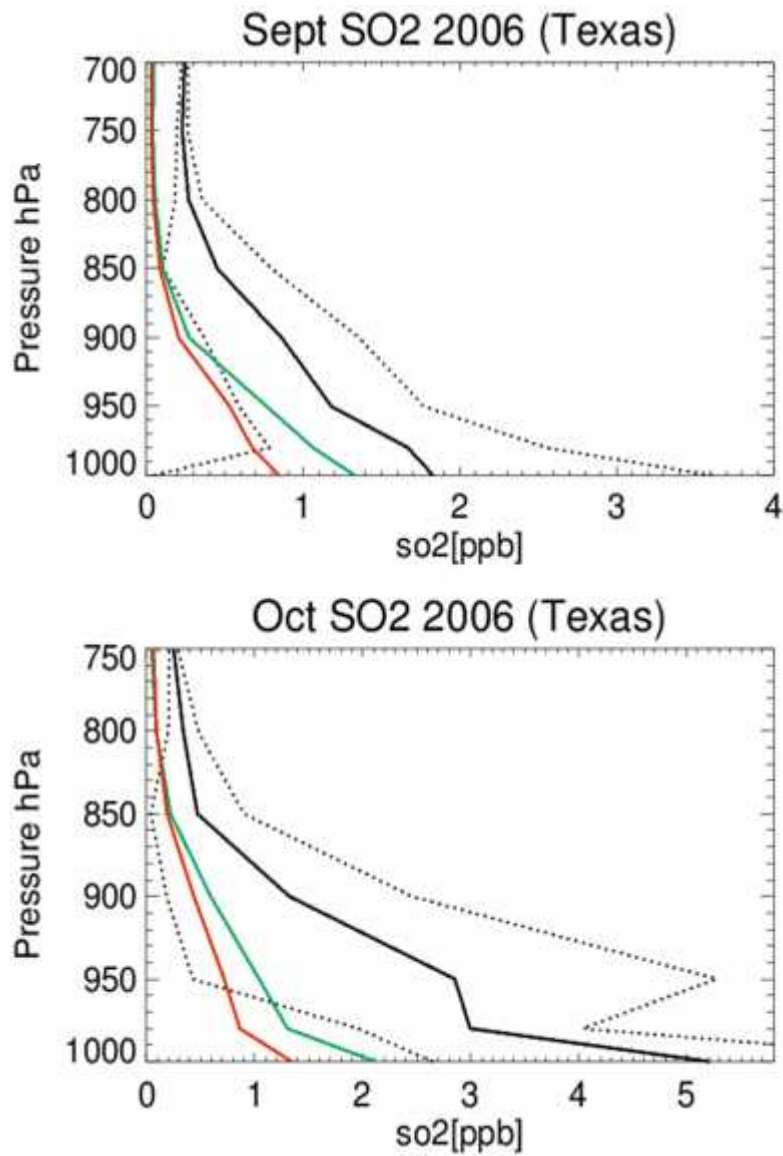
Figure ~~12~~13: Comparisons of the monthly tropospheric SO$_2$ profile assembled from data taken during September and October 2006 as part of TexAQS II. The 1-σ deviation of the mean derived from the measurements is shown as the dotted line. For details of the flight paths the reader is referred to Parrish et al. (2009).

Formatted: Indent: Left: 1.25 cm, Right: 2.25 cm

**References**

Aan de Brugh, J. M. J., Schaap, M., Vignati, E., Dentener, F., Kahnert, M., Sofiev, M., Huijnen, V., and Krol, M. C.: The European aerosol budget in 2006, Atms. Phys. Chem., 11, 1117-1139, doi:10.5194/acp-11-1117-2011, 2011.

Aas, W., Hjellbrekke, A.-G., Schaug, J., and Solberg, S.: Data quality 1999, quality assurance and field comparisons, Kjeller, Norwegian Institute for Air Research, EMEP/CCC Report 6/2001, 2001.

Abbatt, J. P. D., Lee, A. K. Y., and Thornton, J. A.: quantifying trace gas uptake to tropospheric aerosol: recent advances and remaining challenges, Chem. Soc. Rev., 41, 6555–6581, doi:10.1039/c2cs35052a, 2012.

Alonza Gray, B., Wang, Y., Gu, D., Bandy, A., Mauldin, L., Clarke, A., Alexander, B., and Davis, D. D.: Sources, transport, and sinks of $SO_2$ over the equatorial Pacific during the Pacific Atmospheric Sulfur Experiment, J. Atmos. Chem., 68, 27-53, doi: 10.1007/s10874-010-9177-7, 2011.

Atkinson, R., Baulch, D. L., Cox, R. A., Crowley, J. N., Hampson, R. F., Hynes, R. G., Jenkin, M. E., Rossi, M. J., and Tore, J., Evaluated kinetic and photochemical data for atmospheric chemistry: Volume I –gas phase reactions of $O_x$, $HO_x$, $NO_x$ and $SO_x$ species, Atmos. Chem. Phys., 4, 1461-1738, 2004.

Atkinson, R., Baulch, D. L., Cox, R. A., Crowley, J. N., Hampson, R. F., Hynes, R. G., Jenkin, M. E., Rossi, M. J., and Tore, J., Evaluated kinetic and photochemical data for atmospheric chemistry: Volume II –gas phase reactions of organic species, Atmos. Chem. Phys., 6, 3625-4055, 2006.

Bând, N., Krol., M., van Noije, T., van Weele, M., Williams J. E., Le Sager, P., Niemeier, U., Thomason, L. and Röckmann, T.: The effect of stratospheric sulfur from Mount Pinatubo on tropospheric oxidizing capacity and methane, J. Geophys. Res. Atmos., 120, doi:10.1002/2014JDO22137, 2015.

Boersma, K. F., Jacob, D. J., Eskes, H. J., Pinder, R. W., Wang, J. and van der A, R. J.: Intercomparison of SCIAMACHY and OMI tropospheric NO2 columns: observing the diurnal evolution of chemistry and emissions from space, J. Geophys. Res., 2, 113, 1-14, doi:10.1029/2007JD008816, 2008.

Boersma, K. F., Eskes, H. J., Dirksen, R. J., van der A, R. J., Veefkind, J. P., Stammes, P., Huijnen, V., Kleipool, Q. L., Sneep, M., Claas, J., Leitao, J., Richter, A., Zhou, Y. and Brunner, D.: An improved tropospheric $NO_2$ column retrieval algorithm for the Ozone Monitoring Instrument, Atmos. Meas. Tech., 4, 1905-1928, 2011.

Bönisch, H., Hoor, P., Gurk, Ch., Feng, W., Chipperfield, M., Engel, A., and Bregman, B.: Model evaluation of $CO_2$ and $SF_6$ in the extratropical UT/LS region, J. Geophys. Res., 113, D06101, doi:10.1029/2007JD008829, 2008.

Bregman, B., Segers, A., Krol, M., Meijer, E., and van Velthoven, P.: On the use of mass-conserving wind fields in chemistry-transport models, Atmos. Chem. Phys., 3, 447–457, doi:10.5194/acp-3-447-2003, 2003.

Browne, E. C., Perring, A. E., Wooldridge, P. J., Apel, E., Hall, S. R., Huey, L. G., Mao, J., Spencer, K. M., St. Clair, J. M., Weinheimer, A. J., Wisthaler, A., and Cohen, R. C.: Global and regional effects of the photochemistry of $CH_3ONO_2$: evidence from ARCTAS, Atmos. Chem. Phys., 11, 4209-4219, 2011.

1240    Carslaw, D. C. and Beevers, S. D.: Estimations of road vehicle primary $NO_2$ exhaust emission frcations using
1241    monitoring data in London, Atmos. Environ., 39(1), 167-177, 2005.

1242    De Smedt, I., Muller, J.-F., Stavrakou, T., van der A., R., Eskes, H. and Van Roozendael, M.: Twelve years of
1243    global observations of formaldehyde in the troposphere using GOME and SCIAMACHY sensors, Atmos.
1244    Chem. Phys., 8, 4947-4963, 2008.

1245    Dee, D. P., Uppala, S. M., Simmons, A. J., Berrisford, P., Poli, P., Kobayashi, S., Andrae, U., Balmaseda, M.
1246    A., Balsamo, G., Bauer, P., Bechtold, P., Beljaars, A. C. M., van de Berg, L., Bidlot, J., Bormann, N., Delsol,
1247    C., Dragani, R., Fuentes, M., Geer, A. J., Haimberger, L., Healy, S. B., Hersbach, H., Hólm, E. V., Isaksen, L.,
1248    Kållberg, P., Köhler, M., Matricardi, M., McNally, A. P., Monge-Sanz, B. M., Morcrette, J.-J., Park, B.-K.,
1249    Peubey, C., de Rosnay, P., Tavolato, C., Thépaut, J.-N. and Vitart, F.: The ERA-Interim reanalysis:
1250    configuration and performance of the data assimilation system, Q. J. Royal Met. Soc, 137, 656, 553-597, 2011.

1251    Dunlea, E. J., Herndon, S. C., Nelson, D. D., Volkamer, R. M., San Martini, F., Sheehy, P. M., Zahniser,
1252    M. S., Shorter, J. H., Wormhoudt, J. C., Lamb, B. K., Allwine, E. J., Gaffney, J. S., Marley, N. A., Grutter, M.,
1253    Marquez, C., Blanco, S., Cardenas, B., Retama, A., Ramos Villegas, C. R., Kolb, C. E., Molina, L. T., and
1254    Molina, M. J.: Evaluation of nitrogen dioxide chemiluminescence monitors in a polluted urban environment,
1255    Atmos. Chem. Phys., 7, 2691–2704, 2007, http://www.atmos-chem-phys.net/7/2691/2007/

1256    Dupuy, E., Urban, J., Ricaud, P., Le Flochmoën, E., Lautié, N., Murtagh, D., De La Noë, J., El Amraoui, L.,
1257    Eriksson, P., Forkman, P., Frisk, U., Jégou, F., Jiménez, C. and Olberg, M.: Starto-mesospheric measurements
1258    of carbon monoxide with the Odin Sub-Millimetre Radiometer: Retrieval and first results, Geophys. Res.
1259    Letts., 31, L20101, doi:10.1029/2004GL020558, 2004.

1260    Emmons, L. K., Walters, S., Hess, P. G., Lamarque, J.-F., Pfister, G. G., Fillmore, D., Granier, C., Guenther,
1261    A., Kinnison, D., Laepple, T., Orlando, J., Tie, X., Tyndall, G., Wiedinmyer, C., Baughcum, S. L., and Kloster,
1262    S.: Description and evaluation of the Model for Ozone and Related chemical Tracers, version 4 (MOZART-4),
1263    Geosci. Model Dev., 3, 43–67, doi: 10.5194/gmd-3-43-2010, 2010.

1264    Evans, M. J. and Jacob, D. J.: Impact of new laboratory studies of $N_2O_5$ hydrolysis on global model budgets of
1265    tropospheric nitrogen oxides, ozone and OH, Geophys. Res. Lett., 32, doi:10.1029/2005GL022469, 2005.

1266    Fortuin, J. P. F. and Kelder, H.: An ozone climatology based on ozonesonde and satellite measurements. J.
1267    Geophys. Res., 103, 31709–31734, 1998.

1268    Ganzeveld, L., Helmig, D., Fairall, C. W., Hare, J. and Pozzer, A.: Atmosphere-ocean ozone exchange: A
1269    global modeling study of biogeochemical, atmospheric, and waterside turbulence dependencies, Global
1270    Biogeo. Cycles, 23, GB4021, doi:10.1029/2008GB003301, 2009.

1271    Gonçalves, M., Dabdub, D., Chang, W. L., Jorba, O. and Baldasanoa, J. M.: Impact of HONO sources on the
1272    performance of mesoscale air quality models, Atmos. Environ., 54, Pages 168–176,
1273    doi:10.1016/j.atmosenv.2012.02.079, 2012.

1274    Gonzi, S., Palmer, P. I., Barkley, M., De Smedt, I. and Roozendael, M. V.: Biomass burning emission
1275    estimates inferred from satellite column measurements of HCHO: Sensitivity to co-emitted aerosol and
1276    injection height, Geophys. Res. Letts., 38, L14807, 2011.

1277 Granier, C., Bessagnet, B., Bond, T., D'Angiola, A., Denier van der Gon, H., Frost, G. J., Heil, A., Kaiser, J.
1278 W., Kinne, S., Klimont, Z., Kloster, S.-F., Lamarque, J., Liousse, C., Masui, T., Meleux, F., Mieville, A.,
1279 Ohara, T., Raut, J.-C., Riahi, K., Schultz, M. G., Smith, S. J., Thompson, A., van Aardenne, J., van der Werf,
1280 G. R., and van Vuuren, D. P.: Evolution of anthropogenic and biomass burning emissions of air pollutants at
1281 global and regional scales during the 1980–2010 period, Climate Change, 109, 163–190, doi: 10.1007/s10584-
1282 011-0154-115, 2011.

1283 Grooß, J.-U. and Russell III, J. M.: Technical note: A stratospheric climatology for $O_3$, $H_2O$, $CH_4$, $NO_x$, HCl
1284 and HF derived from HALOE measurements, Atmos. Chem. Phys., 5, 2797–2807, doi:10.5194/acp-5-2797-
1285 2005, 2005.

1286 Hardacre, C., Wild, O. and Emberson, L.: An evaluation of ozone dry deposition in global scale chemistry
1287 climate models, Atms. Chem. Phys., 15, 6419-6436, doi:10.5194/acp-15-6419-2015, 2015.

1288 Hauglustaine, D. A., Balkanski, Y. and Schulz, M.: A global model simulation of present and future nitrate
1289 aerosols and their direct radiative forcing of climate, Atms. Chem. Phys., 14, 11031-11063, doi:10.5194/acp-
1290 14-11031-2014, 2014.

1291 Heckel, A., Kim, S.-W., Frost, G. J., Richter, A., Trainer, M. and Burrows, J. P.: Influence of low spatial
1292 resolution a priori data on tropospheric NO2 satellite retreivals, Atmos. Meas. Tech., 4, 1805-1820,
1293 doi:10.5194/amt-4-1805-2011, 2011.

1294 Huijnen, V., Williams, J., van Weele, M., van Noije, T., Krol, M., Dentener, F., Segers, A., Houweling, S.,
1295 Peters, W., de Laat, J., Boersma, F., Bergamaschi, P., van Velthoven, P., Le Sager, P., Eskes, H., Alkemade,
1296 F., Scheele, R., Nédelec, P., and Pätz, H.-W., The global chemistry transport model TM5: description and
1297 evaluation of the tropospheric chemistry version 3.0, Geosci. Model Dev., 3, 445-473, 2010.

1298 Holtslag, A. A. and Boville, B. A.: Local versus non-local boundary layer diffusion in a global climate model,
1299 J. Climate, 10, 1825–1842, 1993.

1300 Huijnen, V., Williams, J. E., and Flemming, J.: Modeling global impacts of heterogeneous loss of $HO_2$ on
1301 cloud droplets, ice particles and aerosols, Atmos. Chem. Phys. Discuss., 14, 8575–8632, doi: 10.5194/acpd-14-
1302 8575-2014, 2014.

1303 Jacob, D. J., Prather, M. J., Rasch, P. J., Shia, R. L., Balkanski, Y. J., Beagley, S. R., Bergmann, D. J.,
1304 Blackshear, W. T., Brown, M., Chiba, M., Chipperfield, M. P., de Grandpré, J., Dignon, J. E., Feichter, J.,
1305 Genthon, C., W. L. Grose, W. L., Kasibhatla, P. S., Köhler, I., Kritz, M. A., Law, K., Penner, J. E., Ramonet,
1306 M., Reeves, C. E., Rotman, D. A., Stockwell, D. Z., Van Velthoven, P. F. J., Verver, G., Wild, O., Yang, H and
1307 Zimmermann, P.: Evaluation and intercomparison of global atmospheric transport models using [222]Rn and
1308 other short-lived tracers, J. Geophys. Res., 102(D5), 5953-5970, doi:10.1029/96JD02955, 1997.

1309 Jacob, J. D.: Heterogeneous chemistry and tropospheric ozone, Atmos. Environ., 34, 2131–2159, 2000.

1310 Jégou, F., Urban, J., de La Noë, J., Ricaud, P., Le Flochmoën, E., Murtagh, D. P., Eriksson, P., Jones, A.,
1311 Petelina, S., Llewellyn, E. J., Lloyd, N. D., Haley, C., Lumpe, J., Randall, C., Bevilacqua, R. M., Catoire, V.,
1312 Huret, N., Berthet, G., Renard, J. B., Strong, K., Davies, J., Mc Elroy, C. T., Goutail, F., and Pommereau, J. P.:
1313 Technical Note: Validation of Odin/SMR limb observations of ozone, comparisons with OSIRIS, POAM III,

ground-based and balloon-borne instruments, Atmos. Chem. Phys., 8, 3385–3409, doi:10.5194/acp-8-3385-2008, 2008.

Kim, S.-W., McKeen, S. A., Frost, G. J., S.-H. Lee, S.-H., M. Trainer, M., Richter, A., Angevine, W. M., Atlas, E., Bianco, L., Boersma, K. F., Brioude, J., Burrows, J. P., de Gouw, J., Fried, A., Gleason, J., Hilboll, A., Mellqvist, J., Peischl, J., Richter, D., Rivera, C., Ryerson, T., te Lintel Hekkert, S., Walega, J., Warneke, C.,Weibring, P., and Williams, E.: Evaluations of NOx and highly reactive VOC emission inventories in Texas and their implications for ozone plume simulations during the Texas Air Quality Study 2006, Atmos. Chem. Phys., 11, 11361–11386, doi:10.5194/acp-11-11361-2011, 2011.

Koffi, E. N., Bergamaschi, P., Karstens, U., Krol, M., Segers, A., Schmidt, M., Levin, I., Vermeulen, A. T., Fisher, R. E., Kazan, V., Klein Baltink, H., Lowry, D., Manca, G., Meijer, H. A. J., Moncrieff, J., Pal, S., Ramonet, M., Scheeren, H. A., and Williams, A. G.: Evaluation of the boundary layer dynamics of the TM5 model over Europe, Geosci. Model Dev., 9, 3137–3160, doi:10.5194/gmd-9-3137-2016, 2016.

Krol, M., Houweling, S., Bregman, B., van den Broek, M., Segers, A., van Velthoven, P., Peters, W., Dentener, F., and Bergamaschi, P.: The two-way nested global chemistry-transport zoom model TM5: algorithm and applications, Atmos. Chem. Phys., 5, 417–432, doi:10.5194/acp-5-417-2005, 2005.

Lawrence, M. G. and Crutzen, P. J.: The impact of cloud particle gravitational settling on soluble trace gas distributions, Tellus, 50B, 263-289, 1998.

Lee, C., Martin, R. V., van Donkelaar, A., Lee, H., Dickerson, R. R., Hains, J. C., Krotkov, N., Richter, A., Vinnikov, K. and Schwab, J. J.: $SO_2$ emissions and lifetimes: Estimates from inverse modeling using in situ and global, space-based (SCIAMACHY and OMI) observations, J. Geophys. Res., 116, D06304, doi:10.1029/2010JD014758, 2011.

Lelieveld, J., Peters, W., Dentener, F. J., and Krol, M. C.: Stability of tropospheric hydroxyl chemistry, J. Geophys. Res., 107(D23), 4715, doi:10.1029/2002JD002272, 2002.

Lin, J. T., Martin, R. V., Boersma, K. F., Sneep, M., Stammes, P., Spurr, R., Wang, P., Van Roozendael, M., Clémer, K., and Irie, H.: Retrieving tropospheric nitrogen dioxide from the Ozone Monitoring Instrument: effects of aerosols, surface reflectance anisotropy, and vertical profile of nitrogen dioxide, Atmos. Chem. Phys., 14, 1441–1461, doi:10.5194/acp- 14-1441-2014, 2014.

Lee, C., Martin, R. V., van Donkelaar, A., Lee, H., Dickerson, R. R., Hains, J. C., Krotkov, N., Richter, A., Vinnikov, K. and Schwab, J. J.: $SO_2$ emissions and lifetimes: Estimates from inverse modeling using in situ and global, space-based (SCIAMACHY and OMI) observations, J. Geophys. Res., 116, D06304, doi:10.1029/2010JD014758, 2011.

Louis, J. F.: A parametric model of vertical eddy fluxes in the atmosphere, Bound.-Layer Meteor., 17, 187–202, 1979.

Marais, E. A., Jacob, D. J., Kurosu, T. P., Chance, K., Murphy, J. C., Reeves, C., Mills, G., Casadio, S., D. B. Millet, D. B., Barkley, M. P., Paulot, F., and Mao, J.: Isoprene emissions in Africa inferred from OMI observations of formaldehyde columns, Atms. Chem. Phys., 12, 6219-6235, doi:10.5194/acp-12p6219-2012, 2012.

1351 Martin, G. M., Johnson, D. W., and Spice, A.: The measurement and parameterization of effective radius of
1352 droplets in warm stratocumulus clouds, J. Atmos. Sci., 51, 1823–1842, 1994.

1353 Meijer, E. W., van Velthoven, P. F. J., Brunner, D. W., Huntrieser, H., and Kelder, H.: Improvement and
1354 evaluation of the parameterisation of nitrogen oxide production by lightning, Phys. Chem. Earth, 26, 557–583,
1355 2001.

1356 Meloen, J., Siegmund, P., van Velthoven, P., Kelder, H., Sprenger, M., Wernli, H., Kentarchos, A., Roelofs,
1357 G., Feichter, J., Land, C., Forster, C., James, P., Stohl, A., Collins, W., and Cristofanelli, P.: Stratosphere-
1358 troposphere exchange: A model and method intercomparison, J. Geophys. Res., 108(D12), 8256,
1359 doi:1029/2002JD002274, 2002.

1360 Möllner, A. K., Valluvadasan, S., Feng, L. Sprague, M. K., Okumura, M., Milligan, D. B., Bloss, W.J., Sander,
1361 S. P., Martien, P. T., Harley, R. A.,

1362 Olsen, S. C., McLinden, C. A., and Prather, M. J.: Stratospheric $N_2O$–$NO_y$ system:  Testing uncertainties in a
1363 three-dimensional framework, J. Geophys. Res., 106, 28771–28784, 2001.

1364 Olszyna, K. J., Bailey, E. M., Simonaitis, R. and Meagher, J. F.: $O_3$ and $NO_y$ relationships at a rural site,
1365 99(D7), 14557–14563, doi:10.1029/94JD00739, 1994.

1366 Palmer, P. I., Abbot, D. S., Fu, T-M., Jacob, D. J., Chance, K., Kurosu, P., Guenther, A., Wiedinmyer, C.,
1367 Stanton, J. C., Pilling, M. J., Pressley, S. N., Lamb, B. and Sumner, A. L.: Quantifying the seasonal and
1368 interannual variability of North American isoprene emissions using satellite observations of the formaldehyde
1369 column, J. Geophys. Res., 111, D12315, doi:10.1029/2005JD006689, 2006.

1370 Parrish, D. D., Allen, D. T., Bates, T. S., Estes, M., Fehsenfeld, F. C., Feingold, G., Ferrare, R., Hardesty, R.
1371 M., Meagher, J. F., Nielsen-Gammon, J. W., Pierce, R. B., Ryerson, T. B., Seinfeld, J. H. and Williams, E. J.:
1372 Overview of the Second Texas Air Quality Study (TexAQS II) and the Gulf of Mexico Atmospheric
1373 Composition and Climate study (GoMACCS), J. Geophys. Res., 114 (D00F13), doi: 10.1029/2009JD011842,
1374 2009.

1375 Phillips, G. J., Makkonen, U., Schuster, G., Sobanski, N., Hakola, H. and Crowley, J. N.: The detection of
1376 nocturnal $N_2O_5$ as $HNO_3$ by alkali- and aqueous-denuder techniques, Atmos. Meas. Tech., 6, 231-237,
1377 doi:10.51094/amt-6-231-2013, 2013.

1378 Pope, R. J., Chipperfield, M. P., Savage, N. H., Ordóñez, C., Neal, L.S., Lee, L.A., Dhomse1, S. S., Richards,
1379 N. A. D. and Keslake, T. D.: Evaluation of a regional air quality model using satellite column $NO_2$: treatment
1380 of observation errors and model boundary conditions and emissions, Atmos. Chem. Phys., 15, 5611–5626,
1381 doi:10.5194/acp-15-5611-2015, 2015.

1382 Prather, M. J., Numerical advection by conservation of second-order moments, J. Geophys. Res., 91, 6671–
1383 6681, 1986.

1384 Russell, A. R., Perring, A. E., Valin, L. C., Bucsela, E. J., Browne, E. C., Wooldridge, P. J. and
1385 Cohen, R. C.: A high spatial resolution retrieval of $NO_2$ column densities from OMI: method and evaluation,
1386 Atmos. Chem. Phys., 11, 8543-8554, doi:10.5194/acp-11-8543-2011, 2011.

Formatted: Font color: Auto

1387 Schery, S. D.: Progress on Global Rn[222] Flux Maps and Recommendations for Future Research, in: 1st
1388 International Expert Meeting on Sources and Measurements of Natural Radionuclides Applied to Climate and
1389 Air Quality Studies (Gif-sur-Yvette, France, June 2003), edited by: Barrie, L. A. and Lee, H. N., WMO TD
1390 1201, Gif-sur-Yvette, France, 43–47, 2004.

1391 Schwartz, S. E.: Mass-transport considerations pertinent to aqueous-phase reactions of gases in liquid-water
1392 clouds, in: Chemistry of Multiphase Atmospheric Systems, edited by: Jaechske, W., Springer, Heidelberg,
1393 415–471, 1986.

1394 Seltzer, K. M., Vizuete, W. and Henderson, B. H.: Evaluation of updated nitric acid chemistry on ozone
1395 precursors and radiative effects, Atmos. Chem. Phys. Discuss., 15, 3219–3255, 2015.

1396 Shettle, E. P. and Fenn, R. W.: Models for the aerosols of the lower atmosphere and the effects of the humidity
1397 variations on their optical properties, Environ. Res. Paper, 676, AFGL-TR-79-0114, 91 pp, 1979.

1398 Sindelarova, K., Granier, C., Bouarar, I., Guenther, A., Tilmes, S., Stavrakou, T., Muller, J.-F., Kuhn, U.,
1399 Stefani, P. and Knorr, W.: Global dataset of biogenic VOC emissions calculated by the MEGAN model over
1400 the last 30 years, Atmos. Phys. Chem., 14, 9317–9341, doi:10.5194/acp-14-9317-2014, 2014.

1401 Singh, H. B., Brune, W. H., Crawford, J. H., et al.: Chemistry and transport of pollution over the Gulf of
1402 Mexico and the Pacific: spring 2006 INTEX-B campaign overview and first results, Atmos. Chem. Phys., 9,
1403 2301-2318, doi:10.5194/acp-9-2301-2009, 2009.

1404 Stavrakou, T., Müller, J.-F., De Smedt, I., Van Roozendael, M., van der Werf, G. R., Giglio, L., and Guenther,
1405 A.: Global emissions of non-methane hydrocarbons deduced from SCIAMACHY formaldehyde columns
1406 through 2003-2006, Atms. Chem. Phys., 9, 3663-3679, 2009.

1407 Steinbacher, M., Zellweger, C., Schwarzenbach, B., Bugmann, S., Buchmann, B., Ordónez, C., Prevot, A. S.
1408 H., and Hueglin, C.: Nitrogen oxides measurements at rural sites in Switzerland: bias of conventional
1409 measurement techniques, J. Geophys. Res., 112, D11307, doi:10.1029/2006JD007971, 2007.

1410 Stevenson, D. S., Dentener, F. J., Schultz, M. G., Ellingsen, K., van Noije, T. P. C., Wild, O., Zeng, G.,
1411 Amann, M., Atherton, M., Bell, N., Bergmann, D. J., Bey, I., Bulter, T., Cofala, J., Collins, W. J., Derwent, R.
1412 G., Doherty, R. M., Drevet, J., Eskes, H. J., Fiore, A. M., Gauss, M., Hauglustaine, D. A., Horowitz, L. W.,
1413 Isaksen, I. S. A., Krol, M. C., Lamarque, J.-F., Lawrence, M. G., Montanaro, V., M¨uller, J. F., Pitari, G.,
1414 Prather, M. J., Pyle, J. A., Rast, S., Rodriguez, J. M., Sanderson, M. G., Savage, N. H., Shindell, D. T.,
1415 Strahan, S. E., Sudo, K., and Szopa, S.: Multimodel ensemble simulations of present-day and near future
1416 tropospheric ozone, J. Geophys. Res., 111, D08301, doi: 10.1029/2005JD006338, 2006.

1417 Sutton, R. T., Dong, B. and Gregory, J. M.: Land/sea warming ratio in response to climate change: IPCC AR4
1418 model results and comparison with observations, Geophys. Res. Letts., 34(2), 10.1029/2006GL028164, 2007.

1419 Tang, Q., Prather, M. J. and Hsu, J.: Stratosphere-troposphere exchange ozone flux related to deep convection,
1420 Geophys. Res. Letts., 38, L03806, doi:10.1029/2010GL046039, 2011.

Thouret, V., Marenco, A., Logan, J. A., Nédélec, P., and Grouhel, C.: Comparisons of ozone measurements from the MOZAIC airborne program and the ozone sounding network at eight locations, J. Geophys. Res., 103, 25695–25720, 1998.

Tiedtke, M.: A comprehensive mass flux scheme for cumulus parameterization in large-scale models, Mon. Weather. Rev., 117(8), 1779–1800, 1989.

Tørseth, K., Aas, W., Breivik, K., Fjaeraa, A. M., Fiebig, M., Hjellbrekke, A. G., Lund-Myrhe, C., Solberg, S. and Yttri, K. E.: Introduction to the European Monitoring and Evaluation Programme (EMEP) and observed atmospheric composition change during 1972-2009, Atmospheric Chemistry and Physics, 12, 5447-5481, 2012.

Urban, J., Pommier, M., Murtagh, D. P., Santee, M. L., and Orsolini, Y. J.: Nitric acid in the stratosphere based on Odin observations from 2001 to 2009 – Part 1: A global climatology, Atmos. Chem. Phys., 9, 7031–7044, doi:10.5194/acp-9-7031-2009, 2009.

Valks, P., Pinardi, G., Richter, A., Lambert, J.-C., Hao, N., Loyola, D., Van Roozendael, M., and Emmadi, S.: Operational total and tropospheric $NO_2$ column retrieval for GOME-2, Atmos. Meas. Tech., 4, 1491-1514, doi:10.5194/amt-4-1491-2011, 2011.

van Geffen, J.H.G.M., Boersma, K. F., Eskes, H. J., Maasakkers J. D. and Veefkind, J. P., TROPOMI Algorithm Theoretical Basis Document (ATBD) tropospheric and total $NO_2$, S5P-KNMI-L2-0005-RP, 56pp, 2016.

van der A, R. J., Allaart, M. A. F., and Eskes, H. J.: Multi sensor reanalysis of total ozone, Atmos. Chem. Phys. Discuss., 10, 11401-11448, doi: 10.5194/acpd-10-11401-2010, 2010.

van der Werf, G. R., Randerson, J. T., Giglio, L., Collatz, G. J., Mu, M., Kasibhatla, P. S., Morton, D. C., DeFries, R. S., Jin, Y., and van Leeuwen, T. T.: Global fire emissions and the contribution of deforestation, savanna, forest, agriculture, and peat fires (1997–2009) Atmos. Chem. Phys., 10, 11707–11735, 2010, http://www.atmos-chem-phys.net/10/11707/2010/.

Veefkind, J.P., Aben, I., McMullan, K., Förster, H., de Vries, J., Otter, G., Claas, J., Eskes, H. J., de Haan, J. F., Kleipool, Q., van Weele, M., Hasekamp, O., Hoogeveen, R., Landgraf, J., Snel, R., Tol, P., Ingmann, P., Voors, R., Kruizinga, B., Vink, R., Visser, H. and Levelt, P. F.: TROPOMI on the ESA Sentinel-5 Precursor: A GMES mission for global observations of the atmospheric composition for climate, air quality and ozone layer applications, Remote. Sens. Environ., 120, 70-83, doi:10.1016/j.rse.2011.09.027, 2012.

Verstraeten, W. V., Neu, J. L., Williams, J. E., Bowman, K. W. and Worden, J. R.: Rapid increases in tropospheric ozone production and export from China, Nature Geosci., 8, 690-695, doi: 10.1038/ngeo2493, 2015.

Vinken, G. C. M., Boersma, K. F., Jacob, D.J. and Meijer, E. W.: Accounting for non-linear chemistry of ship plumes in the GEOS-Chem global chemistry transport model, Atms. Chem. Phys., 11, Atmos. Chem. Phys., 11707-11722, doi:10.5194/acp-11-11707-2011, 2011.

Formatted: Subscript

1456 Vinken, G. C. M., Boersma, K. F., Maasakkers, J. D., Adon, M. and Martin, R. V.: Worldwide biogenic soil
1457 NO$_x$ emissions inferred from OMI NO$_2$ observations, Atmos. Chem. Phys., 14, doi:10.5194/acp-14-10363-
1458 2014, 10363–10381, 2014.

1459 Vogelezang, D. H. P. and Holtslag, A. A. M.: Evaluation and model impacts of alternative boundary-layer
1460 height formulations, Bound.-Layer Meteor., 81, 245–269, 1996.

1461 Von Kuhlmann, R. and Lawrence, M. G.: The impact of ice uptake of nitric acid on atmospheric chemistry,
1462 Atms. Chem. Phys., 6, 225-235, 2006.

1463 Wild, O. and Prather, M. J.: Global tropospheric ozone modeling: Quantifying errors due to grid resolution, J.
1464 Geophys. Res., 111, D11305, doi:10.1029/2005JD006605, 2006.

1465 Williams, J. E., Strunk, A., Huijnen, V. and van Weele, M.: The application of the Modified Band Approach
1466 for the calculation of on-line photodissociation rate constants in TM5: implications for oxidative capacity,
1467 Geosci. Model Dev., 5, 15-35, doi:10.5194/gmd-5-15-2012,2012.

1468 Williams, J. E., van Velthoven, P. F. J., and Brenninkmeijer, C. A. M.: Quantifying the uncertainty in
1469 simulating global tropospheric composition due to the variability in global emission estimates of Biogenic
1470 Volatile Organic Compounds, Atmos. Chem. Phys., 13, 2857–2891, doi: 10.5194/acp-13-2857-2013, 2013.

1471 Williams, J. E., Le Bras, G., Kukai, A., Ziereis, H., and Brenninkmeijer, C. A. M.: The impact of the chemical
1472 production of methyl nitrate from the NO + CH$_3$O$_2$ reaction on the global distribution of alkyl nitrates, nitrogen
1473 oxides and tropospheric ozone: a global modeling study, Atmos. Chem. Phys., 14, 2363-2382, 2014.

1474 Worden, J., Liu, X., Bowman, K., Chance, K., Beer, R., Eldering, A., Gunson, M. and Worden, H., Improved
1475 tropospheric ozone profile retrievals using OMI and TES radiances, Geophys. Res. Lett., 34, L01809,
1476 doi:10.1029/2006GL027806, 2007.

1477 Yamaji, K., Ikeda, K., Irie, H., Kurokawa, J. and Ohara, T.: Influence of model grid resolution on NO$_2$ vertical
1478 column densities over East Asia, J. Air. Waste Manage. Assoc., 64(4), 436-444, 2014.

1479 Yarwood, G., Rao, S., Yocke, M., and Whitten, G.: Updates to the carbon bond chemical mechanism: CB05,
1480 Final report to the US EPA, EPA Report Number: RT-0400675, available at: www.camx.com (last access: 15
1481 January 2014), 2005.

1482 Zhang, K., Feichter, J., Kazil, J., Wan, H., Zhuo, W., Griffiths, A. D., Sartorius, H., Zahorowski, W., Ramonet,
1483 M., Schmidt, M., Yver, C., Neubert, R. E. M. and E.-G. Brunke, E.-G.: Radon activity in the lower troposphere
1484 and its impact on ionization rate: a global estimate using different radon emissions, Atmos. Chem. Phys., 11,
1485 7817–7838, doi:10.5194/acp-11-7817-201, 2011.

1486 Zeng. G., Williams, J. E., Fisher, J.A., Emmons, L. K., Jones, N. B., Morgenstern, O., Robinson, J., Smale, D.,
1487 Paton-Walsh, C. and Griffith, D. W. T.: Multi-model simulation of CO and HCHO in the Southern
1488 Hemisphere: comparison with observations and impact of biogenic emissions, Atmos. Chem. Phys., 15, 7217-
1489 7245, doi:10.5194/acp-15-7217-2015, 2015.

1490    Zdunkowski, W. G., Welsch, R. M., and Kord, G. J.: An investigation of the structure of typical 2-stream
1491    methods for the calculation of solar fluxes and heating rates in clouds, Contrib. Atms. Phys., 53, 215-238,
1492    1980.

1493    Zhou, Y., Brunner, D., Hueglin, C., Henne, S., and Staehelin, J.: Changes in OMI tropospheric NO2 columns
1494    over Europe from 2004 to 2009 and the influence of meteorological variability. Atmos Environ, 46, 482-495,
1495    2012.

1496    Zyrichidou, I.,   oukouli, M. E., Balis, D., Markakis, K., Poupkou, A., Katragkou, E., Kioutsioukis, I., Melas,
1497    D., Boersma, K. F. and van Roozendael, M.: Identification of surface NOx emission sources on a regional
1498    scale using OMI $NO_2$. Atms. Environ., 101, 82-93, 2015.

| Page 33: [1] Formatted Table | Williams, Jason (KNMI) | 13/12/2016 15:21:00 |
|---|---|---|

Formatted Table

| Page 33: [2] Formatted | Williams, Jason (KNMI) | 13/12/2016 15:21:00 |
|---|---|---|

Indent: Left: -0.19 cm

| Page 33: [3] Formatted | Williams, Jason (KNMI) | 13/12/2016 15:21:00 |
|---|---|---|

Indent: Hanging: 0.27 cm

| Page 33: [4] Formatted | Williams, Jason (KNMI) | 13/12/2016 15:21:00 |
|---|---|---|

Indent: Left: -0.19 cm

| Page 33: [5] Formatted | Williams, Jason (KNMI) | 13/12/2016 15:21:00 |
|---|---|---|

Indent: Left: -0.44 cm, First line: 0.25 cm

| Page 33: [6] Formatted | Williams, Jason (KNMI) | 13/12/2016 15:21:00 |
|---|---|---|

Indent: Left: -0.19 cm

| Page 33: [7] Formatted | Williams, Jason (KNMI) | 13/12/2016 15:21:00 |
|---|---|---|

Indent: Left: -0.21 cm

| Page 33: [8] Formatted | Williams, Jason (KNMI) | 13/12/2016 15:21:00 |
|---|---|---|

Indent: Left: -0.22 cm

| Page 33: [9] Formatted | Williams, Jason (KNMI) | 13/12/2016 15:21:00 |
|---|---|---|

Indent: Left: -0.19 cm

| Page 33: [10] Formatted | Williams, Jason (KNMI) | 13/12/2016 15:21:00 |
|---|---|---|

Indent: Left: -0.19 cm

| Page 33: [11] Formatted | Williams, Jason (KNMI) | 13/12/2016 15:21:00 |
|---|---|---|

Centered, Indent: Left: -0.19 cm, First line: 0 cm

| Page 33: [12] Formatted | Williams, Jason (KNMI) | 13/12/2016 15:21:00 |
|---|---|---|

Indent: Left: -0.44 cm

| Page 33: [13] Formatted | Williams, Jason (KNMI) | 13/12/2016 15:21:00 |
|---|---|---|

Indent: Left: -0.19 cm

| Page 33: [14] Formatted | Williams, Jason (KNMI) | 13/12/2016 15:21:00 |
|---|---|---|

Indent: Left: -0.21 cm

| Page 33: [15] Formatted | Williams, Jason (KNMI) | 13/12/2016 15:21:00 |
|---|---|---|

Indent: Left: -0.22 cm

| Page 33: [16] Formatted | Williams, Jason (KNMI) | 13/12/2016 15:21:00 |
|---|---|---|

Indent: Left: -0.19 cm

| Page 33: [17] Formatted | Williams, Jason (KNMI) | 13/12/2016 15:21:00 |
|---|---|---|

Indent: Left: -0.19 cm

| Page 33: [18] Formatted | Williams, Jason (KNMI) | 13/12/2016 15:21:00 |
|---|---|---|

Indent: Left: -0.19 cm, Right: -0.19 cm

| Page 33: [19] Formatted | Williams, Jason (KNMI) | 13/12/2016 15:21:00 |
|---|---|---|

Indent: Left: -0.46 cm, Right: -0.19 cm

| Page 33: [20] Formatted | Williams, Jason (KNMI) | 13/12/2016 15:21:00 |
|---|---|---|

Indent: Left: -0.19 cm

| Page 33: [21] Formatted | Williams, Jason (KNMI) | 13/12/2016 15:21:00 |
|---|---|---|

Indent: Left: -0.21 cm

| Page 33: [22] Formatted | Williams, Jason (KNMI) | 13/12/2016 15:21:00 |

Indent: Left: -0.22 cm

| Page 33: [23] Formatted | Williams, Jason (KNMI) | 13/12/2016 15:21:00 |

Indent: Left: -0.19 cm

| Page 33: [24] Formatted | Williams, Jason (KNMI) | 13/12/2016 15:21:00 |

Indent: Left: -0.19 cm

| Page 33: [25] Formatted | Williams, Jason (KNMI) | 13/12/2016 15:21:00 |

Indent: Left: -0.19 cm, Right: -0.19 cm

| Page 33: [26] Formatted | Williams, Jason (KNMI) | 13/12/2016 15:21:00 |

Indent: Left: -0.46 cm, Right: -0.19 cm

| Page 33: [27] Formatted | Williams, Jason (KNMI) | 13/12/2016 15:21:00 |

Indent: Left: -0.19 cm

| Page 33: [28] Formatted | Williams, Jason (KNMI) | 13/12/2016 15:21:00 |

Indent: Left: -0.21 cm

| Page 33: [29] Formatted | Williams, Jason (KNMI) | 13/12/2016 15:21:00 |

Indent: Left: -0.22 cm

| Page 33: [30] Formatted | Williams, Jason (KNMI) | 13/12/2016 15:21:00 |

Indent: Left: -0.19 cm

| Page 33: [31] Formatted | Williams, Jason (KNMI) | 13/12/2016 15:21:00 |

Indent: Left: -0.19 cm

| Page 33: [32] Formatted | Williams, Jason (KNMI) | 13/12/2016 15:21:00 |

Indent: Left: -0.19 cm, Right: -0.19 cm

| Page 33: [33] Formatted | Williams, Jason (KNMI) | 13/12/2016 15:21:00 |

Indent: Left: -0.46 cm, Right: -0.19 cm

| Page 33: [34] Formatted | Williams, Jason (KNMI) | 13/12/2016 15:21:00 |

Indent: Left: -0.19 cm

| Page 33: [35] Formatted | Williams, Jason (KNMI) | 13/12/2016 15:21:00 |

Indent: Left: -0.21 cm

| Page 33: [36] Formatted | Williams, Jason (KNMI) | 13/12/2016 15:21:00 |

Indent: Left: -0.22 cm

| Page 33: [37] Formatted | Williams, Jason (KNMI) | 13/12/2016 15:21:00 |

Indent: Left: -0.19 cm

| Page 33: [38] Formatted | Williams, Jason (KNMI) | 13/12/2016 15:21:00 |

Indent: Left: -0.19 cm

| Page 33: [39] Formatted | Williams, Jason (KNMI) | 13/12/2016 15:21:00 |

Indent: Left: -0.19 cm, Right: -0.19 cm

| Page 33: [40] Formatted | Williams, Jason (KNMI) | 13/12/2016 15:21:00 |

Indent: Left: -0.46 cm, Right: -0.19 cm

| Page 33: [41] Formatted | Williams, Jason (KNMI) | 13/12/2016 15:21:00 |

Indent: Left: -0.19 cm

| Page 33: [42] Formatted | Williams, Jason (KNMI) | 13/12/2016 15:21:00 |

Indent: Left: -0.21 cm

| Page 33: [64] Formatted | Williams, Jason (KNMI) | 13/12/2016 15:21:00 |
|---|---|---|

Indent: Left: -0.21 cm

| Page 33: [65] Formatted | Williams, Jason (KNMI) | 13/12/2016 15:21:00 |
|---|---|---|

Indent: Left: -0.22 cm

| Page 33: [66] Formatted | Williams, Jason (KNMI) | 13/12/2016 15:21:00 |
|---|---|---|

Indent: Left: -0.19 cm

| Page 33: [67] Formatted | Williams, Jason (KNMI) | 13/12/2016 15:21:00 |
|---|---|---|

Indent: Left: -0.19 cm

| Page 33: [68] Formatted | Williams, Jason (KNMI) | 13/12/2016 15:21:00 |
|---|---|---|

Indent: Left: -0.19 cm, Right: -0.19 cm

| Page 33: [69] Formatted | Williams, Jason (KNMI) | 13/12/2016 15:21:00 |
|---|---|---|

Indent: Left: -0.46 cm, Right: -0.19 cm

| Page 33: [70] Formatted | Williams, Jason (KNMI) | 13/12/2016 15:21:00 |
|---|---|---|

Position: Horizontal: 0.69 cm, Relative to: Margin

| Page 33: [71] Formatted Table | Williams, Jason (KNMI) | 13/12/2016 15:21:00 |
|---|---|---|

Formatted Table

| Page 33: [72] Formatted | Williams, Jason (KNMI) | 13/12/2016 15:21:00 |
|---|---|---|

Indent: Left: -0.37 cm, Hanging: 0.19 cm, Position: Horizontal: 0.69 cm, Relative to: Margin

| Page 33: [73] Formatted | Williams, Jason (KNMI) | 13/12/2016 15:21:00 |
|---|---|---|

Indent: Left: -0.19 cm, Position: Horizontal: 0.69 cm, Relative to: Margin

| Page 33: [74] Formatted | Williams, Jason (KNMI) | 13/12/2016 15:21:00 |
|---|---|---|

Indent: Left: -0.19 cm, Position: Horizontal: 0.69 cm, Relative to: Margin

| Page 33: [75] Formatted | Williams, Jason (KNMI) | 13/12/2016 15:21:00 |
|---|---|---|

Justified, Indent: Left: -0.23 cm, Position: Horizontal: 0.69 cm, Relative to: Margin

| Page 33: [76] Formatted | Williams, Jason (KNMI) | 13/12/2016 15:21:00 |
|---|---|---|

Indent: Left: -0.25 cm, Position: Horizontal: 0.69 cm, Relative to: Margin

| Page 33: [77] Formatted | Williams, Jason (KNMI) | 13/12/2016 15:21:00 |
|---|---|---|

Position: Horizontal: 0.69 cm, Relative to: Margin

| Page 33: [78] Formatted | Williams, Jason (KNMI) | 13/12/2016 15:21:00 |
|---|---|---|

Indent: Left: -0.19 cm, Position: Horizontal: 0.69 cm, Relative to: Margin

| Page 33: [79] Formatted | Williams, Jason (KNMI) | 13/12/2016 15:21:00 |
|---|---|---|

Position: Horizontal: 0.69 cm, Relative to: Margin

| Page 33: [80] Formatted | Williams, Jason (KNMI) | 13/12/2016 15:21:00 |
|---|---|---|

Indent: Left: -0.19 cm, Position: Horizontal: 0.69 cm, Relative to: Margin

| Page 33: [81] Formatted | Williams, Jason (KNMI) | 13/12/2016 15:21:00 |
|---|---|---|

Indent: Left: -0.19 cm, Position: Horizontal: 0.69 cm, Relative to: Margin

| Page 33: [82] Formatted | Williams, Jason (KNMI) | 13/12/2016 15:21:00 |
|---|---|---|

Indent: Left: -0.19 cm, Position: Horizontal: 0.69 cm, Relative to: Margin

| Page 33: [83] Formatted | Williams, Jason (KNMI) | 13/12/2016 15:21:00 |
|---|---|---|

Indent: Left: -0.25 cm, Right: -0.18 cm, Position: Horizontal: 0.69 cm, Relative to: Margin

| Page 33: [84] Formatted | Williams, Jason (KNMI) | 13/12/2016 15:21:00 |
|---|---|---|

Position: Horizontal:  0.69 cm, Relative to: Margin

Indent: Left:  -0.19 cm, Position: Horizontal:  0.69 cm, Relative to: Margin

Position: Horizontal:  0.69 cm, Relative to: Margin

Indent: Left:  -0.19 cm, Position: Horizontal:  0.69 cm, Relative to: Margin

Indent: Left:  -0.19 cm, Position: Horizontal:  0.69 cm, Relative to: Margin

Indent: Left:  -0.19 cm, Position: Horizontal:  0.69 cm, Relative to: Margin

Indent: Left:  -0.25 cm, Right:  -0.18 cm, Position: Horizontal:  0.69 cm, Relative to: Margin

Position: Horizontal:  0.69 cm, Relative to: Margin

Indent: Left:  -0.19 cm, Position: Horizontal:  0.69 cm, Relative to: Margin

Position: Horizontal:  0.69 cm, Relative to: Margin

Indent: Left:  -0.19 cm, Position: Horizontal:  0.69 cm, Relative to: Margin

Indent: Left:  -0.19 cm, Position: Horizontal:  0.69 cm, Relative to: Margin

Indent: Left:  -0.19 cm, Position: Horizontal:  0.69 cm, Relative to: Margin

Indent: Left:  -0.25 cm, Right:  -0.18 cm, Position: Horizontal:  0.69 cm, Relative to: Margin

Position: Horizontal:  0.69 cm, Relative to: Margin

Indent: Left:  -0.19 cm, Position: Horizontal:  0.69 cm, Relative to: Margin

Position: Horizontal:  0.69 cm, Relative to: Margin

Indent: Left:  -0.19 cm, Position: Horizontal:  0.69 cm, Relative to: Margin

Indent: Left:  -0.19 cm, Position: Horizontal:  0.69 cm, Relative to: Margin

Indent: Left:  -0.19 cm, Position: Horizontal:  0.69 cm, Relative to: Margin

Indent: Left:  -0.25 cm, Right:  -0.18 cm, Position: Horizontal:  0.69 cm, Relative to: Margin

Position: Horizontal:  0.69 cm, Relative to: Margin

| Page 33: [106] Formatted | Williams, Jason (KNMI) | 13/12/2016 15:21:00 |
|---|---|---|

Indent: Left:  -0.19 cm, Position: Horizontal:  0.69 cm, Relative to: Margin

| Page 33: [107] Formatted | Williams, Jason (KNMI) | 13/12/2016 15:21:00 |
|---|---|---|

Position: Horizontal:  0.69 cm, Relative to: Margin

| Page 33: [108] Formatted | Williams, Jason (KNMI) | 13/12/2016 15:21:00 |
|---|---|---|

Indent: Left:  -0.19 cm, Position: Horizontal:  0.69 cm, Relative to: Margin

| Page 33: [109] Formatted | Williams, Jason (KNMI) | 13/12/2016 15:21:00 |
|---|---|---|

Indent: Left:  -0.19 cm, Position: Horizontal:  0.69 cm, Relative to: Margin

| Page 33: [110] Formatted | Williams, Jason (KNMI) | 13/12/2016 15:21:00 |
|---|---|---|

Indent: Left:  -0.19 cm, Position: Horizontal:  0.69 cm, Relative to: Margin

| Page 33: [111] Formatted | Williams, Jason (KNMI) | 13/12/2016 15:21:00 |
|---|---|---|

Indent: Left:  -0.25 cm, Right:  -0.18 cm, Position: Horizontal:  0.69 cm, Relative to: Margin

| Page 33: [112] Formatted | Williams, Jason (KNMI) | 13/12/2016 15:21:00 |
|---|---|---|

Position: Horizontal:  0.69 cm, Relative to: Margin

| Page 33: [113] Formatted | Williams, Jason (KNMI) | 13/12/2016 15:21:00 |
|---|---|---|

Indent: Left:  -0.19 cm, Position: Horizontal:  0.69 cm, Relative to: Margin

| Page 33: [114] Formatted | Williams, Jason (KNMI) | 13/12/2016 15:21:00 |
|---|---|---|

Position: Horizontal:  0.69 cm, Relative to: Margin

| Page 33: [115] Formatted | Williams, Jason (KNMI) | 13/12/2016 15:21:00 |
|---|---|---|

Indent: Left:  -0.19 cm, Position: Horizontal:  0.69 cm, Relative to: Margin

| Page 33: [116] Formatted | Williams, Jason (KNMI) | 13/12/2016 15:21:00 |
|---|---|---|

Indent: Left:  -0.19 cm, Position: Horizontal:  0.69 cm, Relative to: Margin

| Page 33: [117] Formatted | Williams, Jason (KNMI) | 13/12/2016 15:21:00 |
|---|---|---|

Indent: Left:  -0.19 cm, Position: Horizontal:  0.69 cm, Relative to: Margin

| Page 33: [118] Formatted | Williams, Jason (KNMI) | 13/12/2016 15:21:00 |
|---|---|---|

Indent: Left:  -0.25 cm, Right:  -0.18 cm, Position: Horizontal:  0.69 cm, Relative to: Margin